ELECTRON WAVE INSTABILITIES IN A MAGNETOPLASMA CAUSED BY ELECTRON-NEUTRAL COLLISIONS

by John Q. Howell

Langley Research Center
Hampton, Va. 23365

NATIONAL AERONAUTICS AND SPACE ADMINISTRATION • WASHINGTON, D. C. • SEPTEMBER 1971

1. Report No.	2. Government Accession No.	3. Recipient's Catalog No.
NASA TR R-363		

4. Title and Subtitle	5. Report Date
ELECTRON WAVE INSTABILITIES IN A MAGNETOPLASMA CAUSED BY ELECTRON-NEUTRAL COLLISIONS	September 1971
	6. Performing Organization Code
7. Author(s)	8. Performing Organization Report No.
John Q. Howell	L-7531
	10. Work Unit No.
9. Performing Organization Name and Address	115-21-00-00
NASA Langley Research Center Hampton, Va. 23365	11. Contract or Grant No.
	13. Type of Report and Period Covered
12. Sponsoring Agency Name and Address	Technical Report
National Aeronautics and Space Administration Washington, D.C. 20546	14. Sponsoring Agency Code

15. Supplementary Notes The information in this paper is largely based on a dissertation entitled "Collisional Effects on Waves in a Magnetoplasma" submitted in partial fulfillment of the requirements for the degree of Doctor of Philosophy in Applied Physics, Stanford University, Stanford, California, June 1970.

16. Abstract A new class of collision-dependent electron waves is found in a non-Maxwellian Lorentz magnetoplasma, and it is shown that electron-neutral collisions may cause these waves to become unstable. The Boltzmann equation with collision integral is solved while assuming propagation to be either parallel or perpendicular to the magnetic field. Both conductivity tensors are derived and put in a form that is useful for numerical calculations. The full set of Maxwell's equations is then used to derive the dispersion relations for both directions of propagation. The dispersion relations are initially solved for a monoenergetic electron distribution function and then an isotropic distribution with a peak of nonzero half-width is treated. Some consideration is also given to an isotropic Maxwellian distribution both with and without a bump on the tail. As an example of propagation parallel to the magnetic field, transverse electromagnetic or "whistler" waves in a nitrogen plasma are considered. A new collisional mode is found with real frequency near the electron cyclotron frequency, and under appropriate conditions it may be either convectively or absolutely unstable. Longitudinal or electrostatic waves propagating perpendicular to the magnetic field in a nitrogen plasma are also considered. A series of new collisional modes with real frequency near the electron cyclotron frequency and its harmonics are shown to be unstable under some conditions. For both directions of propagation, the electron waves can be unstable if a large fraction of plasma electrons have their velocity in a region where the electron-neutral collision frequency increases (or decreases) rapidly enough. The requirement on the electron-neutral collision frequency is easily met by nitrogen, mercury, and the Ramsauer gases.

17. Key Words (Suggested by Author(s))	18. Distribution Statement
Whistler waves Cyclotron waves Electron-neutral collisions Boltzmann equation Collision integral	Unclassified – Unlimited

19. Security Classif. (of this report)	20. Security Classif. (of this page)	21. No. of Pages	22. Price*
Unclassified	Unclassified	112	$3.00

*For sale by the National Technical Information Service, Springfield, Virginia 22151

CONTENTS

ELECTRON WAVE INSTABILITIES IN A MAGNETOPLASMA CAUSED BY ELECTRON-NEUTRAL COLLISIONS*

By John Q. Howell
Langley Research Center

SUMMARY

A new class of collision-dependent electron waves is found in a non-Maxwellian Lorentz magnetoplasma, and it is shown that electron-neutral collisions may cause these waves to become unstable. The Boltzmann equation with collision integral is solved while assuming propagation to be either parallel or perpendicular to the magnetic field. Both conductivity tensors are derived and put in a form useful for numerical calculations. The full set of Maxwell's equations is then used to derive the dispersion relations for both directions of propagation. The dispersion relations are initially solved for a monoenergetic electron distribution function and then an isotropic distribution with a peak of nonzero half-width is treated. Some consideration is also given to an isotropic Maxwellian distribution both with and without a bump on the tail.

An an example of propagation parallel to the magnetic field, transverse electromagnetic or "whistler" waves in a nitrogen plasma are considered. A new collisional mode is found with real frequency near the electron cyclotron frequency, and under appropriate conditions it may be either convectively or absolutely unstable. Longitudinal or electrostatic waves propagating perpendicular to the magnetic field in a nitrogen plasma are also considered. A series of new collisional modes with real frequency near the electron cyclotron frequency and its harmonics are shown to be unstable under some conditions. For both directions of propagation, the electron waves can be unstable if a large fraction of plasma electrons have their velocity in a region where the electron-neutral collision frequency increases (or decreases) rapidly enough. The requirement on the electron-neutral collision frequency is easily met by nitrogen, mercury, and the Ramsauer gases.

---

*The information in this paper is largely based on a dissertation entitled "Collisional Effects on Waves in a Magnetoplasma" submitted in partial fulfillment of the requirements for the degree of Doctor of Philosophy in Applied Physics, Stanford University, Stanford, California, June 1970.

INTRODUCTION

In recent years both experimental and theoretical investigations of collision-induced instabilities in a plasma have been undertaken. Most of this effort has been directed toward determining the effect of electron-neutral collisions on electron waves in a weakly ionized plasma where electron-electron and electron-ion collisions are negligible. It has been found that both convective and absolute instabilities are possible if (1) the electron distribution function is sufficiently non-Maxwellian and if (2) the electron-neutral collision cross section increases (or decreases) rapidly enough with electron energy. The purpose of this paper is to obtain dispersion relations for waves in a weakly ionized magnetoplasma by treating electron-neutral collisions in the most rigorous manner possible, and then to solve these dispersion relations for realistic plasma conditions. There may be electron-neutral attachment in plasmas of this type but the resulting negative ions will not affect the waves being considered because of their large mass.

Historical Review of Previous Work

To predict the effect of electron-neutral collisions on waves in a plasma, two approaches have been utilized. Some workers have considered the effective radiation temperature of the plasma whereas others have determined the stability of waves propagating in the plasma. The latter point of view is taken in this report.

In 1958 Twiss (ref. 1), while investigating the radiation spectra from a plasma, found that under some conditions a non-Maxwellian plasma could radiate more energy than it absorbs over a region of the spectrum. Then in 1961 Bekefi et al. (ref. 2) showed that electron-neutral collisions could be responsible for such enhanced emission. This phenomenon was investigated experimentally by Fields et al. (ref. 3) and they found a peak in the radiation spectra from some plasmas at the electron cyclotron frequency. Both their experimental and theoretical work showed that this condition occurred when the electron energy distribution was highly non-Maxwellian and when the electron-neutral collision cross section increased rapidly enough with velocity. The radiation temperature approach was also used in references 4 to 8 where more experimental results are reported and in references 9 to 12 where further theoretical work is given. Ďurček (ref. 12) used a purely quantum mechanical point of view and obtained results similar to those of other authors.

Of those authors treating the collisional effects on waves propagating in a plasma, only those analyzing electron-neutral collisions by means of a realistic velocity-dependent collision model are discussed here. In 1964 Drummond et al. (ref. 13) assumed that the electron-neutral collision cross section was isotropic but velocity dependent and derived

the dispersion relation for electrostatic waves in an unmagnetized plasma. They recovered the well-known Landau dispersion relation in the collisionless limit. Derfler (ref. 14), as did Drummond, assumed the electrons to be colliding with infinitely heavy neutrals but allowed for an angular dependence in the collision cross section. In the limit of isotropic collisions, his dispersion relation is identical to that of Drummond. Derfler solved the dispersion relation for a simple case and discovered a group of potentially unstable collision-dependent modes he called "pseudo-sound waves." Suzuki (ref. 15), Idehara and Sugaya (ref. 16), and Shimomura and Mitani (ref. 17) investigated the effects of electron-neutral collisions on waves in a magnetoplasma. They all assumed a Lorentz gas model (that is, infinitely heavy neutrals and ions) and allowed for an isotropic velocity-dependent collision cross section. Suzuki considered transverse electric waves propagating parallel to the applied magnetic field and found a new mode with real frequency near the cyclotron frequency. This mode was unstable under some conditions and vanished in the collisionless limit. Idehara and Sugaya considered waves propagating perpendicular to the magnetic field and investigated both the ordinary and the extraordinary waves. They assumed monoenergetic electrons and found that either mode may be unstable at frequencies near the electron cyclotron harmonics. However, their results are valid only in the near infinite wavelength limit. Shimomura and Mitani also considered ordinary waves propagating perpendicular to the magnetic field. Unfortunately, they made an error in solving the first-order Boltzmann equation and their conductivity tensor is incorrect. Their solution for the first-order electron distribution function does not satisfy the differential equation. The error is of such nature, however, that their σ_{33} term is correct, and hence their dispersion relation for the ordinary wave is correct. They also assumed monoenergetic electrons and found collision-induced instabilities.

Collision Models

When solving the Boltzmann equation

$$\frac{\partial f}{\partial t} + \vec{v} \cdot \frac{\partial f}{\partial \vec{r}} - \frac{e}{m}\left(\vec{E} + \vec{v} \times \vec{B}\right) \cdot \frac{\partial f}{\partial \vec{v}} = \left(\frac{\partial f}{\partial t}\right)_{coll} \tag{1}$$

for the electron distribution function $f\left(\vec{v},\vec{r},t\right)$, the collision model assumed is very important in determining how easily the solution will be obtained. The most common (and the simplest) approach merely ignores collisions altogether, that is,

$$\left(\frac{\partial f}{\partial t}\right)_{coll} = 0 \tag{2}$$

In this form the Boltzmann equation is usually called the Vlasov equation. On the other hand, for elastic binary collisions, the most exact collision term one can use (and the most difficult to work with) is the Boltzmann collision integral

$$\left(\frac{\partial f}{\partial t}\right)_{coll} = \int |\vec{v} - \vec{V}| \sigma \left[f(\vec{v}') \; F(\vec{V}') - f(\vec{v}) \; F(\vec{V}) \right] d\Omega \; d^3V \tag{3}$$

where σ is the collision cross section and $F(\vec{V})$ is the distribution function of the particles with which the electrons are colliding. The velocities of an electron before and after the collision are $\vec{v}$ and $\vec{v}'$, and the before and after velocities of the particle with which the electron collided are $\vec{V}$ and $\vec{V}'$. The differential solid angle in velocity space in the center of mass frame of reference is $d\Omega$. For electrons in a weakly ionized plasma, electron-neutral collisions are much more frequent than either electron-electron or electron-ion collisions. Hence, in this case $F(\vec{V})$ is the distribution function of the neutral background gas.

The Lorentz gas model assumes elastic collisions with neutrals that are infinitely heavy and stationary, that is,

$$F(\vec{V}) = N\delta(\vec{V}) \tag{4}$$

where N is the number density of the neutrals. Equation (3) then becomes

$$\left(\frac{\partial f}{\partial t}\right)_{coll} = N|\vec{v}| \int \sigma(\chi, |\vec{v}|) \left[f(\vec{v}') - f(\vec{v}) \right] d\Omega' \tag{5}$$

where χ is the angle between $\vec{v}$ and $\vec{v}'$ and $d\Omega'$ is the differential solid angle in $\vec{v}'$ space. This collision model was used by Derfler (ref. 14) to derive the dispersion relation for electrostatic waves in an unmagnetized plasma. Drummond, et al. (ref. 13), Suzuki (ref. 15), Idehara and Sugaya (ref. 16), and others have assumed that the collision cross section is isotropic, that is, σ is a function of $|\vec{v}|$ only. In this case equation (5) trivially becomes

$$\left(\frac{\partial f}{\partial t}\right)_{coll} = -\nu(v) \, f(\vec{v}) + \frac{\nu(v)}{4\pi} \int f(\vec{v}') \, d\Omega' \tag{6}$$

where $\nu(v) = 4\pi N v \sigma(v)$ is a velocity-dependent collision frequency.

Wilensky (ref. 18), in his work on electrostatic waves in an unmagnetized argon plasma, showed that the most important physics is in the energy dependence of the cross section and not in the angular dependence. He allowed for an angular-dependent cross

section and found that the wave dispersion differed very little from that given by the isotropic collision model. Consequently, ignoring the angular dependence as in equation (6) should be a very good approximation. In this report the collision models given by equations (5) and (6) are used exclusively.

In an attempt to put the Boltzmann equation in a more tractable form than the collision integral allows, a large number of approximate collision models have been used. Dougherty (ref. 19) in his investigation of the upper ionosphere used a model Fokker-Planck equation

$$\left(\frac{\partial f}{\partial t}\right)_{coll} = \nu \frac{\partial}{\partial \vec{v}} \cdot \left[(\vec{v} - \vec{c})f + \frac{\kappa T}{m} \frac{\partial f}{\partial \vec{v}}\right] \tag{7}$$

where ν is a constant electron collision frequency and $\vec{c}$ and T are a velocity and a temperature which Dougherty chose so that the generation-dissipation rates take on the proper values as discussed later. This collision model is more appropriately used when collisions result in only small changes in the velocity vector of the colliding particle and hence is most appropriately applied to coulomb collisions. This equation is derived in a more general form from equation (3) by Holt and Haskell (ref. 20). On the other hand, Bhatnager, Gross, and Krook (ref. 21) replaced Boltzmann's collision integral by a simple dissipation term

$$\left(\frac{\partial f}{\partial t}\right)_{coll} = \nu(f_m - f) \tag{8}$$

which describes the relaxation of electron velocities to a local Maxwellian distribution

$$f_m = \left(\pi v_0^2\right)^{-3/2} \exp \frac{(\vec{v} - \vec{c})^2}{v_0^2} \tag{9}$$

Similarly, Allis, Buchsbaum, and Bers (ref. 22) assumed relaxation to some as yet unspecified equilibrium distribution function f_0 and wrote

$$\left(\frac{\partial f}{\partial t}\right)_{coll} = \nu(f_0 - f) \tag{10}$$

Note that the last three models all contain an average collision frequency ν which must be specified, and equations (7) and (8) have other unspecified parameters. These unknown parameters should in practice be specified so that the principle of detailed balancing is obeyed. This procedure involves taking the following generation-dissipation rates of particles, momentum, and energy:

$$I = \int \left(\frac{\partial f}{\partial t}\right)_{coll} d^3v \tag{11}$$

$$\vec{G} = m \int \vec{v} \left(\frac{\partial f}{\partial t}\right)_{coll} d^3v \tag{12}$$

$$H = \frac{m}{2} \int v^2 \left(\frac{\partial f}{\partial t}\right)_{coll} d^3v \tag{13}$$

and choosing the unknown parameters so that these rates take on their proper values. For example, I should be chosen equal to zero if no particles are generated by the collision process. If the collisions are between particles of the same species, then the choice $\vec{G} = H = 0$ should be made as Dougherty did, whereas for the Lorentz gas model described earlier H should be equal to zero but $\vec{G}$ not equal to zero. Achieving the correct generation-dissipation rates is not a problem with the collision models expressed by equations (3), (5), and (6) as they automatically take on the correct rates to all orders, and not just to the first three expressed by equations (11) to (13).

Outline of the Present Analysis

As mentioned earlier, the collision models expressed by equations (5) and (6) are used exclusively in this report. Waves proportional to $\exp\left(i\omega t - i\vec{k} \cdot \vec{r}\right)$ are assumed and the Boltzmann equation with equation (6) is solved for the general wavenumber $\vec{k}$. The solution is then specialized to $\vec{k}$ perpendicular to the magnetic field $\vec{B}$, and the conductivity tensor and dispersion relations are obtained. The stability and dispersion of the longitudinal or electrostatic waves are investigated by numerically solving the appropriate dispersion relation. The stability character of the waves is determined by mapping the real wavenumber axis into the complex frequency plane by means of the dispersion relation and then applying Derfler's frequency cusp criterion (refs. 23 to 26). In a somewhat simplified form sufficient for use here, if the mapping in the complex frequency plane is above the real frequency axis, the plasma is stable. If it goes below the axis, the plasma is at least convectively unstable. It is absolutely unstable only if a branch point can be located either on the mapping but below the real frequency axis or in a closed region above the mapping but below the real frequency axis. The Boltzmann equation with equation (5) is solved and the dispersion relations and conductivity tensor for $\vec{k}$ parallel to the magnetic field are obtained. The dispersion relation representing the transverse electromagnetic waves is numerically solved, and solutions of the dispersion relations for various isotropic electron distribution functions are given. For propagation both parallel and perpendicular to the magnetic field, a monoenergetic electron

distribution is treated first and then a peaked energy distribution function having a peak of nonzero half-width is considered. Consideration is also given to a Maxwellian distribution function and to a Maxwellian with a bump on the tail. It is assumed that electrons collide with nitrogen neutrals, but similar results would be obtained for any gas having a steep slope in its electron-neutral collision cross-section curve. In particular, the Ramsauer gases (argon, xenon, and krypton) would be appropriate because of their rapidly increasing collision frequency near the Ramsauer minimum.

SYMBOLS

A	defined by equation (H5)
$A(\vec{v})$	defined by equations (27)
$A_j(\vec{v})$	defined by equation (37)
a_l	parameter used in equation (E13)
B	defined by equation (H6)
$\vec{B}$	magnetic field vector
$\vec{B}_0, B_0$	zero-order magnetic field vector and magnitude
$\vec{B}_1$	first-order magnetic field vector
$B_l(x)$	Bernoulli polynomials (eq. (H9))
C_G	number of electrons gaining energy
C_L	number of electrons losing energy
C_m	constant, (eq. (78))
C_s	constant in peaked electron distribution (eqs. (73) and (78))
$C(\tau)$	dummy function (eq. (B8))
c	velocity of light

$\vec{c}$ velocity parameter in equation (7)

$D, D_1, D_2, D_E, D_\pm$ dispersion relations

$\overline{D}, D_{ij}$ defined by equation (29)

$d\Omega$ element of solid angle in $\vec{v}$ space

$d\Omega'$ element of solid angle in $\vec{v}'$ space

d^3r differential volume

$\vec{E}$ electric field vector

$\vec{E}_1$ first-order electric field vector

E_x, E_y components of $\vec{E}_1$ along x and y directions

$E_\pm$ symbolic for $E_x \pm iE_y$ and represents right- and left-hand polarized waves (eq. (122))

e unsigned charge of electron

$\hat{e}_1, \hat{e}_3$ unit vectors along X axis and Z axis

$\hat{e}_x, \hat{e}_y, \hat{e}_z$ unit vectors along x, y, and z directions

$F(\vec{V})$ particle distribution function (eq. (3))

${}_pF_q, {}_2F_3$ generalized hypergeometric function

$F(z)$ dummy function (eq. (I1))

$F(\varphi)$ dummy function (eq. (E8))

f electron distribution function

f_H homogeneous part of electron distribution function (eq. (B5))

$f_{\ell,m}$ expansion variable of first-order electron distribution function (eq. (84))

f_m Maxwellian electron distribution (eq. (9))

f_s peaked electron distribution function

f_0 zero-order electron distribution function

f_1 first-order electron distribution function

$f_\pm$ components of first-order electron distribution function (eq. (M5))

$\hat{f}_1$ transform of first-order distribution function

$\vec{G}$ momentum generation rate (eq. (12))

$G(v)$ defined by equations (36) and (52)

g_s defined by equation (97)

$g_\pm$ defined by equation (109)

H energy generation rate (eq. (13))

H_ℓ defined by equation (H10)

h collisional frequency slope parameter used in equation (67)

$h(\vec{v})$ defined by equation (21)

h_α defined by equation (H7)

I particle generation-dissipation rate (eq. (11))

$\bar{I}$ unit tensor

$I_\ell(z)$ modified Bessel function

I_1, I_2, I_3 convenient symbols denoting specific integral used in appendix E

Im( )	imaginary part of variable
i	$\sqrt{-1}$
$\vec{j}$	current density (eq. (33))
$\vec{j}_{ext}$	driving current (eq. (121))
j_x, j_y	components of current density along X axis and Y axis (eq. (121))
$j_0( ), j_1( ), j_2( ), \ldots, j_n( )$	spherical Bessel functions of first kind
$j_\pm$	symbolic for $j_x \pm i j_y$ (eq. (122))
$\vec{k}, k$	wavenumber vector and magnitude
$\overline{L}, L_{ij}$	defined by equation (30)
l, m	indices of summation
m	mass of electron
N	neutral particle density; electron number
N_G	number of electrons gaining energy
N_L	number of electrons losing energy
n	electron density
$\vec{n}$	unit vector along $\vec{B}$
n_i, n_j, n_k	components of vector $\vec{n}$
$\vec{P}$	polarization vector
P_c	probability of collision
$P_l( )$	Legendre polynomials

$P_l^m(\ )$	associated Legendre polynomials
p	pressure in equation (71); dummy variable in equation (H2)
$Q_{l,m}$	defined by equation (86)
Q_l	transfer collision cross section (eq. (87))
Re( )	real part of variable
$\vec{r}$	space position vector
$S(a_l)$	symbolic notation given in equation (41)
s	parameter in peaked electron distribution (eq. (73))
T	temperature
$T_{r,s}$	defined by equation (91)
t	time variable; dummy variable (eq. (B17))
t'	dummy variable (eq. (B17))
$\vec{V}$	velocity vector (eq. (3))
V_l	defined by equation (H9)
$\vec{v},\vec{v}'$	velocity vectors
v_i	component of velocity vector
v_0	thermal speed; velocity at maximum of peaked distribution function
v_1	thermal speed (eq. (78))
v_2	location of peak in peaked distribution (eq. (78))
v_3	component of velocity along Z axis

w_l weights of Gauss quadrature rule (eq. (G2))

w'_l weights of Gauss quadrature rule along contour (eq. (I8))

X,Y,Z coordinate axes

x_l nodes of Gauss quadrature rule (eq. (G2))

x_m, y_m parameters in complex contour (eqs. (I2) and (I3))

$Y_{l,m}(\theta,\varphi)$ spherical harmonic

$Z(\ )$ defined by equation (N8)

$Z_F(\ )$ Fried function

z_l nodes of Gauss quadrature rule along contour (eq. (I7))

α proportion of electron distribution function that is Maxwellian (eq. (78))

$\alpha_1, \alpha_2, \ldots, \alpha_{10}$ collision frequency function parameters (eq. (70))

β_s defined by equation (98)

$\Gamma(\ )$ gamma function

γ parameter in complex contour (eq. (I3))

$\delta(v)$ Dirac delta function

$\delta_{r,s}$ Kronecker delta

ϵ_{ijk} permutation tensor

ϵ_0 free-space dielectric constant

η normalized frequency, ω_ν/ω_c

θ, θ' spherical coordinate angles in velocity space

κ Boltzmann's constant

λ defined by equation (55)

$\lambda_{n,s}$ defined by equation (99)

λ_0 defined after equation (N4)

$\lambda_\pm$ defined by equation (117)

μ_0 permeability of free space

ν collision frequency (eq. (6))

ν_l transfer collision frequency (eq. (88))

ν_∞ collision frequency at infinite electron velocity

$\langle\nu\rangle$ average collision frequency (eq. (77))

ξ dummy variable (eq. (59))

$\bar{\pi},\pi_{ij}$ polarization tensor (eq. (C11)) and its components

ρ charge density

$\sigma(\chi,v)$ collision cross section

$\sigma_n(v)$ expansion constant of collision cross section (eq. (J2))

$\bar{\sigma},\sigma_{ij}$ conductivity tensor

$\tau,\tau',\tau'',\tau_1,\tau_0$ dummy variables (appendix B)

φ spherical coordinate angle in velocity space; also a dummy integration variable

$\Phi(\varphi,\vec{v})$ defined by equation (28)

χ	scattering angle
ω	frequency angle
$\vec{\omega}_c, \omega_c$	cyclotron frequency (eq. (22))
ω_H	hybrid frequency, $\sqrt{\omega_c^2 + \omega_p^2}$
ω_p	plasma frequency, $\left(ne^2/m\epsilon_0\right)^{1/2}$
ω_ν	abbreviated notation for $\omega - i\nu$ (eq. (23))

Subscript:

coll	collision

Vector symbols without arrows denote the magnitude. An asterisk denotes a complex conjugate and a circumflex denotes a transform.

THEORY OF WAVES PROPAGATING PERPENDICULAR TO THE MAGNETIC FIELD

In this section dispersion relations for waves propagating perpendicular to an applied magnetic field $\vec{B}_0$ are derived. A Lorentz gas model is assumed, and the electron-neutral collision cross section is assumed to be isotropic. The first order distribution function is derived and from it the conductivity tensor for the general case of $\vec{k}$ at any angle to $\vec{B}_0$ is obtained. This tensor is then specialized to propagation perpendicular to the magnetic field, and the dispersion relations are obtained. A discussion of some of the analytic properties of the dispersion relation that describes electrostatic or longitudinal waves is given.

Conductivity Tensor for General $\vec{k}$ With Isotropic Collisions

In the Introduction it was stated that the Boltzmann equation for electrons colliding elastically and isotropically with infinitely heavy neutrals is

$$\frac{\partial f}{\partial t} + \vec{v} \cdot \frac{\partial f}{\partial \vec{r}} - \frac{e}{m}\left(\vec{E} + \vec{v} \times \vec{B}\right) \cdot \frac{\partial f}{\partial \vec{v}} = -\nu(v) f(\vec{v}) + \frac{\nu(v)}{4\pi} \int f(\vec{v}')\, d\Omega' \tag{14}$$

where $d\Omega'$ is an element of solid angle in $\vec{v}'$ space. This equation is linearized by making the "ansatz" (initial assumption)

$$\left.\begin{aligned} f(\vec{v}) &= f_0(\vec{v}) + f_1(\vec{v}) \\ \vec{E} &= 0 + \vec{E}_1 \\ \vec{B} &= \vec{B}_0 + \vec{B}_1 \end{aligned}\right\} \tag{15}$$

and in the usual manner consider the first-order terms (subscript 1) to be small perturbations about the much larger zero-order terms (subscript 0). Then obtain the zero-order equation

$$-\frac{e}{m}\left(\vec{v} \times \vec{B}_0\right) \cdot \frac{\partial f_0}{\partial \vec{v}} = -\nu f_0 + \frac{\nu}{4\pi}\int f_0(\vec{v}')d\Omega' \tag{16}$$

and the first-order equation

$$\frac{\partial f_1}{\partial t} + \vec{v} \cdot \frac{\partial f_1}{\partial \vec{r}} - \frac{e}{m}\left(\vec{v} \times \vec{B}_0\right) \cdot \frac{\partial f_1}{\partial \vec{v}} = \frac{e}{m}\left(\vec{E}_1 + \vec{v} \times \vec{B}_1\right) \cdot \frac{\partial f_0}{\partial \vec{v}} - \nu f_1 + \frac{\nu}{4\pi}\int f_1(\vec{v}')d\Omega' \tag{17}$$

In appendix A the solution of the zero-order equation is found to be any isotropic distribution function $f_0(v)$ and hence the term $\left(\vec{v} \times \vec{B}_1\right) \cdot \partial f_0/\partial \vec{v}$ in the first-order equation is identically zero. To solve equation (17), use is made of a Fourier transform in space defined by

$$\hat{f}\left(\vec{v},\vec{k},t\right) = \int f\left(\vec{v},\vec{r},t\right)e^{i\vec{k}\cdot\vec{r}}d^3r \tag{18}$$

and a Laplace transform in time defined by

$$\hat{f}\left(\vec{v},\vec{r},\omega\right) = \int_0^\infty f\left(\vec{v},\vec{r},t\right)e^{-st}dt \tag{19}$$

where s is chosen equal to $i\omega$. Applying these transforms to equation (17) or equivalently assuming that all the variables are proportional to $\exp\left(i\omega t - i\vec{k} \cdot \vec{r}\right)$ yields

$$i\left(\omega_\nu - \vec{k} \cdot \vec{v}\right)\hat{f}_1 - \left(\vec{v} \times \vec{\omega}_c\right) \cdot \frac{\partial \hat{f}_1}{\partial \vec{v}} = h(\vec{v}) \tag{20}$$

where

$$h(\vec{v}) = \frac{e}{m}\vec{E}_1 \cdot \frac{\partial f_0}{\partial \vec{v}} + \frac{\nu}{4\pi}\int f_1(\vec{v}')d\Omega' \tag{21}$$

$$\vec{\omega}_c = \frac{e\vec{B}_0}{m} = \omega_c \frac{\vec{B}_0}{B_0} \tag{22}$$

$$\omega_\nu = \omega - i\nu(v) \tag{23}$$

The Laplace transform analysis was used so that the rules of the inverse Laplace transform could be used later to define the dispersion relations properly. Even though no initial conditions are allowed for, the dispersion relations that are derived will properly describe any waves that are excited and will predict the onset of wave instabilities.

Equation (20) is solved by the method of characteristics in a manner similar to that used by Omura (ref. 27). A parameter τ is introduced so that $\vec{v} = \vec{v}(\tau)$. The characteristic equations then become

$$\frac{d\vec{v}(\tau)}{d\tau} = -\left(\vec{v} \times \vec{\omega}_c\right) \tag{24}$$

$$i\left(\omega_\nu - \vec{k} \cdot \vec{v}\right)\hat{f}_1 + \frac{d\hat{f}_1}{d\tau} = h(\vec{v}) \tag{25}$$

In appendix B these equations are solved and the solution is found to be

$$\hat{f}_1 = \frac{e}{m\omega_c}\left[A(\vec{v}) + \frac{\frac{\nu}{4\pi\omega_c}\int A(\vec{v}')d\Omega' \int_0^\infty e^{-\Phi(\varphi,\vec{v})}d\varphi}{1 - \frac{\nu}{4\pi\omega_c}\int\int_0^\infty e^{-\Phi(\varphi,\vec{v}')}d\varphi\, d\Omega'}\right] \tag{26}$$

where

$$\left.\begin{aligned} A(\vec{v}) &= \int_0^\infty e^{-\Phi(\varphi,\vec{v})}\vec{E}_1 \cdot \overline{D}(\varphi) \cdot \vec{v}\,\frac{f_0'}{v}\,d\varphi \\ f_0' &= \frac{\partial f_0}{\partial v} \end{aligned}\right\} \tag{27}$$

$$\Phi(\varphi,\vec{v}) = i\,\frac{\varphi(\omega - i\nu) - \vec{k}\cdot\bar{\bar{L}}(\varphi)\cdot\vec{v}}{\omega_c} \tag{28}$$

$$\left[\bar{\bar{D}}\right]_{ij} = D_{ij} = n_i n_j + \left(\delta_{ij} - n_i n_j\right)\cos\varphi + \epsilon_{ijk} n_k \sin\varphi \tag{29}$$

$$\left[\bar{\bar{L}}\right]_{ij} = L_{ij} = n_i n_j \varphi + \left(\delta_{ij} - n_i n_j\right)\sin\varphi - \epsilon_{ijk} n_k (\cos\varphi - 1) \tag{30}$$

$$\vec{\omega}_c = \frac{e}{m}\vec{B}_0 = \omega_c \frac{\vec{B}_0}{B_0} = \omega_c \vec{n} \tag{31}$$

By direct substitution of equation (26) into equation (20), one can show that the solution has been obtained.

Equation (26) was also obtained by Idehara and Sugaya (ref. 16) in a somewhat more complicated form. However, they were unable to simplify it to obtain relatively simple dispersion relations of wide validity, as will be done here.

In the collisionless limit equation (26) yields

$$\hat{f}_1 = \frac{e}{m\omega_c} A(\vec{v}) \tag{32}$$

This result was obtained by Omura (ref. 27) and others and can be used to derive Bernstein's (refs. 28 and 29) dispersion relation describing the propagation of cyclotron waves in the Vlasov limit.

In appendix C, Maxwell's equations are stated and the general dispersion relation is derived for a conductivity tensor $\bar{\sigma}$ defined by

$$\vec{j} = \bar{\sigma}\cdot\vec{E} = -en\int \vec{v}\,\hat{f}_1(\vec{v})\,d^3v \tag{33}$$

Using equation (33) and taking $\vec{B} = B\hat{e}_3$ in equation (26) yields

$$\sigma_{ij} = -\frac{\omega_p^2 \epsilon_0}{\omega_c}\int_0^\infty v f_0'(v)\left[\int v_i A_j(\vec{v})\,d\Omega\right]dv$$
$$-\frac{\omega_p^2 \epsilon_0}{4\pi\omega_c^2}\int_0^\infty v\nu(v)\,f_0'(v)\left[\frac{\int A_j(\vec{v})\,d\Omega\int\int_0^\infty v_i e^{-\Phi(\varphi,\vec{v})}\,d\varphi\,d\Omega}{1 + \frac{i\nu(v)}{\omega}G(v)}\right]dv \tag{34}$$

where

$$\omega_p^2 = \frac{ne^2}{m\epsilon_0} \tag{35}$$

$$G(v) = \frac{i\omega}{4\pi\omega_c} \int \int_0^\infty e^{-\Phi(\varphi,\vec{v})} d\varphi \, d\Omega \tag{36}$$

$$A_j(\vec{v}) = \int_0^\infty e^{-\Phi(\varphi,\vec{v})} D_{jk} v_k \, d\varphi \tag{37}$$

$$\Phi(\varphi,\vec{v}) = i \frac{\varphi\omega_\nu - \vec{k} \cdot \overline{L} \cdot \vec{v}}{\omega_c} \tag{38}$$

$$\overline{L} = \begin{bmatrix} \sin\varphi & (1 - \cos\varphi) & 0 \\ -(1 - \cos\varphi) & \sin\varphi & 0 \\ 0 & 0 & \varphi \end{bmatrix} \tag{39}$$

$$\overline{D} = \begin{bmatrix} \cos\varphi & \sin\varphi & 0 \\ -\sin\varphi & \cos\varphi & 0 \\ 0 & 0 & 1 \end{bmatrix} \tag{40}$$

This tensor is the exact conductivity tensor appropriate to the model assumed. In the next section this tensor is put in a usable form after assuming $\vec{k} \perp \vec{B}$, and the wave dispersion relations are then obtained from Maxwell's equations. In a later section $\vec{k} \parallel \vec{B}$ is assumed and again the simplified conductivity tensor and wave dispersion relations are obtained.

Conductivity Tensor and Dispersion Relations for $\vec{k} \perp \vec{B}$

In this section the conductivity tensor given by equation (34) is simplified by considering propagation strictly perpendicular to the magnetic field, for example, $\vec{k} = k\hat{e}_1$. For convenience, the symbolic notation

$$S(a_l) \equiv \sum_{l=1}^{\infty} \frac{(kv/\omega_c)^{2l} a_l}{(\eta^2 - 1) \ldots (\eta^2 - l^2)} \tag{41}$$

where $\eta = \omega_\nu/\omega_c$ will be used.

In appendixes D and E after much algebraic manipulation, the conductivity tensor is given by

$$\bar{\sigma} = \begin{bmatrix} \sigma_{11} & \sigma_{12} & 0 \\ -\sigma_{12} & \sigma_{22} & 0 \\ 0 & 0 & \sigma_{33} \end{bmatrix} \tag{42}$$

where

$$\sigma_{11} = \frac{4\pi i\omega\epsilon_0\omega_p^2}{k^2} \int_0^\infty \frac{vf_0'\omega_\nu S\left(\frac{1}{2l+1}\right)}{\omega + i\nu S\left(\frac{1}{2l+1}\right)} dv \tag{43}$$

$$\sigma_{12} = -\frac{4\pi\omega\epsilon_0\omega_p^2\omega_c}{k^2} \int_0^\infty \frac{vf_0' S\left(\frac{l}{2l+1}\right)}{\omega + i\nu S\left(\frac{1}{2l+1}\right)} dv \tag{44}$$

$$\sigma_{22} = 4\pi i\omega_p^2\epsilon_0 \int_0^\infty \frac{v^3 f_0'}{\omega_\nu} \left\{ \frac{1}{3} + S\left[\frac{1}{(2l+1)(2l+3)}\right] + \left(\frac{\omega_c}{kv}\right)^2 \left[S\left(\frac{l^2}{2l+1}\right) - \frac{i\nu S^2\left(\frac{l}{2l+1}\right)}{\omega + i\nu S\left(\frac{1}{2l+1}\right)} \right] \right\} dv \tag{45}$$

$$\sigma_{33} = 4\pi i\omega_p^2\epsilon_0 \int_0^\infty \frac{v^3 f_0'}{\omega_\nu} \left\{ \frac{1}{3} + S\left[\frac{1}{(2l+1)(2l+3)}\right] \right\} dv \tag{46}$$

Equations (42) to (46) give the conductivity tensor in a form suitable for computations. Shimomura and Mitani (ref. 17) attempted to derive this tensor also, but they made an error in solving the first-order Boltzmann equation given here by equation (20). Their error was of such a nature, however, that they still obtained the correct expression for σ_{33}. It agrees with equation (46) when allowances are made for differences in notation.

To obtain the dispersion relations, assume $\vec{k} = k\hat{e}_1$ in equation (C17), and use equation (42) to obtain

$$D(\omega,k) \equiv \begin{vmatrix} 1 + \frac{\sigma_{11}}{i\omega\epsilon_0} & \frac{\sigma_{12}}{i\omega\epsilon_0} & 0 \\ -\frac{\sigma_{12}}{i\omega\epsilon_0} & 1 + \frac{\sigma_{22}}{i\omega\epsilon_0} - \left(\frac{kc}{\omega}\right)^2 & 0 \\ 0 & 0 & 1 + \frac{\sigma_{33}}{i\omega\epsilon_0} - \left(\frac{kc}{\omega}\right)^2 \end{vmatrix} = 0 \tag{47}$$

By expanding the determinant, two uncoupled dispersion relations are obtained:

$$D_1(\omega,k) \equiv 1 + \frac{\sigma_{33}}{i\omega\epsilon_0} - \left(\frac{kc}{\omega}\right)^2 = 0 \tag{48}$$

and

$$D_2(\omega,k) \equiv \left(1 + \frac{\sigma_{11}}{i\omega\epsilon_0}\right)\left[1 + \frac{\sigma_{22}}{i\omega\epsilon_0} - \left(\frac{kc}{\omega}\right)^2\right] + \left(\frac{\sigma_{12}}{i\omega\epsilon_0}\right)^2 = 0 \tag{49}$$

The waves described by $D_1(\omega,k)$ are characterized by $\vec{E}_1 \parallel \vec{B}_0$ and are usually called ordinary waves, since they are unaffected by the magnetic field in the cold plasma limit. This same dispersion relation was derived in an approximate form and discussed by Idehara and Sugaya (ref. 16) for a monoenergetic electron distribution. Shimomura and Mitani (ref. 17) also obtained equations (48) and (46) and found that a monoenergetic distribution function leads to collisional instabilities if the electron-neutral collision frequency increases rapidly enough with velocity. This dispersion relation is not discussed further in this report.

In the limit of very small phase velocity, that is, $kc/\omega >>> 1$, equation (49) yields

$$D_2(\omega,k) \approx 1 + \frac{\sigma_{11}}{i\omega\epsilon_0} = 0 \tag{50}$$

Using equation (43) and dropping the subscript 2 on D then yields

$$D(\omega,k) = 1 + 4\pi\left(\frac{\omega_p}{k}\right)^2 \int_0^\infty \frac{vf_0'\omega_\nu G(v)}{\omega + i\nu G(v)}\, dv = 0 \tag{51}$$

where

$$G(v) = \sum_{l=1}^{\infty} \frac{\left(kv/\omega_c\right)^{2l}}{(2l+1)(\eta^2 - 1)\ldots(\eta^2 - l^2)} \tag{52}$$

The waves described by this equation are characterized by $\vec{E}_1 \parallel \vec{k}$ and in the collisionless limit have been variously called extraordinary, longitudinal, electrostatic, cyclotron, or Bernstein waves. They were discussed in a review paper by Crawford (ref. 30) in 1967. The dispersion relation describing these waves is generally derived in a much simpler manner by using the electrostatic approximation ab initio. This derivation has been made in appendix F where equation (51) is obtained more directly. This dispersion relation is discussed further in the next section and is later solved for several interesting cases.

Discussion of Electrostatic Dispersion Relation

In the preceding section, the dispersion relations for waves propagating perpendicular to an applied magnetic field in a Lorentz gas plasma were derived. These dispersion relations were exact in the framework of the collision model assumed, that is, an isotropic velocity-dependent electron-neutral collision cross section. The quasi-static approximation was then made to obtain the dispersion relation for cyclotron or Bernstein waves. The properties of this dispersion relation will now be discussed.

From the series expansion given by equation (52), G(v) can be written alternatively as a generalized hypergeometric function

$$G(v) = -1 + {}_2F_3\left[1,\ 1/2;\ 3/2,\ 1 - \eta,\ 1 + \eta;\ -\left(\frac{kv}{\omega_c}\right)^2\right] \tag{53}$$

Consequently, the theory of asymptotic expansions of hypergeometric functions can be used to help evaluate G(v) (ref. 31).

In the limit of zero magnetic field, that is, $\omega_c \to 0$, equation (51) reduces to

$$D(\omega,k) = 1 - 4\pi\left(\frac{\omega_p}{k}\right)^2 \int_0^\infty \frac{vf_0'\left(1 - \lambda \coth^{-1}\lambda\right)}{1 + \frac{i\nu}{kv}\coth^{-1}\lambda}\, dv = 0 \tag{54}$$

where

$$\lambda = \frac{\omega_\nu}{kv} \tag{55}$$

This dispersion relation was obtained by Drummond et al. (ref. 13) and Derfler (ref. 14) and represents electrostatic waves in an isotropic Lorentz gas plasma. Hence, equation (51) has the correct form in the limit of a vanishing magnetic field.

On the other hand, in the presence of a magnetic field, but in the limit of zero collisions, equation (51) yields

$$D(\omega,k) = 1 + 4\pi\left(\frac{\omega_p}{k}\right)^2 \int_0^\infty v f_0' G(v)\, dv = 0 \tag{56}$$

If f_0 is taken to be Maxwellian, that is,

$$f_0(v) = \frac{\exp\left(-v^2/v_0^2\right)}{\pi^{3/2} v_0^3} \tag{57}$$

then equation (56) yields

$$D(\omega,k) = 1 - 2\left(\frac{\omega_p}{kv_0}\right)^2 \sum_{l=1}^{\infty} \frac{\left(kv_0/\omega_c\right)^{2l} 1\cdot 3\cdot 5 \ldots (2l-1)}{2^l\left(\eta^2 - 1\right) \ldots \left(\eta^2 - l^2\right)} = 0 \tag{58}$$

where

$$\eta = \frac{\omega - i\nu}{\omega_c}$$

This relation can be shown to be equivalent to Bernstein's dispersion relation (refs. 28 and 29), given by

$$D(\omega,k) = 1 + \left(\frac{2\omega_p}{kv_0}\right)^2 e^{-\xi} \sum_{l=1}^{\infty} \frac{I_l(\xi)\, l^2}{l^2 - \eta^2} = 0 \tag{59}$$

where

$$\xi = \frac{1}{2}\left(\frac{kv_0}{\omega_c}\right)^2$$

However in practice, equation (58) has proven to be much more efficient for computation. The collisionless electrostatic dispersion relation, given by either equation (58) or equation (59), is characterized by undamped pass bands at frequencies just above each electron cyclotron harmonic separated by bands that are very heavily damped. In the limit of zero magnetic field, neither of these equations predict Landau damping since the infinite series in both equations represents only the contribution from an integral along the real axis in velocity space. However, in this limit the electrostatic waves are damped as Landau (ref. 32) and others (ref.33) have shown. To recover Landau damping properly it is necessary to indent the velocity contour around a singularity that crosses the real axis as the magnetic field vanishes. Baldwin and Rowlands (ref. 34) have shown how Landau damping can be recovered by rewriting equation (59) in an integral form and eventually obtain the Landau dispersion relation

$$D(\omega,k) = 1 - \left(\frac{\omega_p}{kv_0}\right)^2 Z'\left(\frac{\omega}{kv_0}\right) = 0 \tag{60}$$

where Z' is the derivative of the Hilbert transform of the Gaussian as tabulated by Fried and Conte (ref. 35). However, the theory given here quite easily yields equation (60) from either equation (56) as the magnetic field vanishes or from equation (54) as collisions vanish, if it is assumed, of course, that f_0 is chosen to be Maxwellian. When doing this, one must keep in mind that the dispersion relations are defined for k real and ω on a Laplace integral path. For other k and ω values, the appropriate analytic continuation must be taken by choosing the correct contour in velocity space.

The dispersion relation given by equation (51) is considerably different from those given by cruder collision models. Use of the simple constant collision frequency model of Allis et al. (ref. 22), that is,

$$\left(\frac{\partial f}{\partial t}\right)_{coll} = \nu(f_0 - f) \tag{61}$$

has the effect of replacing ω by $\omega - i\nu$ in the collisionless equation. In an attempt to improve on this collision model, a variation of the Bhatnagar-Gross-Krook (BGK) collision model has been used (ref. 36),

$$\left(\frac{\partial f}{\partial t}\right)_{coll} = \nu\left[f_0\left(1 + \frac{n_1}{n_0}\right) - f\right] \tag{62}$$

where n_0 is the zero-order electron density and n_1 is the first-order electron density. In addition to the replacement of ω by $\omega - i\nu$, this model also replaces ω_p^2

by $\left[1 - i(\nu/\omega)\right]\omega_p^2$ in the collisionless equation. Note that neither of these collision models correctly produces the denominator in the integrand of equation (51). This denominator is of major importance in determining the characteristics of the solutions of the dispersion relation as it tends to cancel the resonance effect of the integrand when the frequency is near a multiple of the cyclotron frequency. Hence one must conclude that the collision models expressed by equations (61) and (62) can only be applied in the near-collisionless and off-resonance limit.

Next note that equation (51) contains only even powers of k, and hence the following symmetry relation holds:

$$D(\omega,k) = D(\omega,-k) \tag{63}$$

Consequently, the roots of $D(\omega,0) = 0$ are branch points in the mapping of k into the complex frequency plane. The location of these points is of prime importance in determining the stability character of the waves (refs. 23 to 26). From equation (51) also obtain the symmetry relation

$$D(\omega,k) = D^*(-\omega^*,-k^*) \tag{64}$$

This relation is, of course, a statement of the Kramers-Kronig (ref. 37) relationship and is a direct consequence of the causality principle which was built into this theory by using the Laplace transform analysis in time.

Combining equations (63) and (64) yields then for k real

$$D(\omega,k) = D^*(-\omega^*,k) \tag{65}$$

Hence, only complex frequency solutions need to be determined in, for example, the right half-plane. These properties are important when the dispersion relation (eq. (51)) is solved for several different electron distribution functions in the next section.

SOLUTIONS OF THE ELECTROSTATIC DISPERSION RELATION FOR PROPAGATION PERPENDICULAR TO THE MAGNETIC FIELD

In this section the dispersion relation is solved for electrostatic waves propagating perpendicular to the magnetic field for several isotropic electron distribution functions. A series of new collisional modes are found that depend for their existence on both a highly non-Maxwellian electron distribution function and a velocity-dependent collision frequency. Both convective and absolute instabilities are discovered when the electron

distribution function is monoenergetic. A Lorentz gas plasma with nitrogen neutrals is also considered and instabilities are again found when a peaked electron distribution function is assumed. When a Maxwellian electron distribution function is chosen, it is found that the wave dispersion predicted by the isotropic collision frequency model is very close to that predicted by a constant-collision-frequency BGK model. Also an electron distribution function consisting of both peaked and Maxwellian components is briefly considered and the stabilizing influence of the Maxwellian population is demonstrated.

Monoenergetic Electron Distribution

For the initial analysis of the dispersion relation (eq. (51)) it is assumed that the zero-order electron distribution function is monoenergetic, that is,

$$f_0(v) = \frac{\delta(v - v_0)}{4\pi v_0^2} \tag{66}$$

Substituting this relation into equation (51) leads to the dispersion relation

$$D(\omega,k) \equiv 1 - \left(\frac{\omega_p}{kv_0}\right)^2 \left\{ \frac{\omega\left[(\omega - i\nu)\left(G + v_0 G'\right) + i\nu G(G - hG - h)\right] + \nu^2 G^2}{(\omega + i\nu G)^2} \right\} = 0 \tag{67}$$

where

$$h = \left(\frac{v}{\nu}\frac{d\nu}{dv}\right)_{v=v_0}$$

$$G = \sum_{l=1}^{\infty} \frac{\left(kv_0/\omega_c\right)^{2l}}{(2l + 1)(\eta^2 - 1) \ldots (\eta^2 - l^2)}$$

$$G' = \left[\frac{dG(v)}{dv}\right]_{v=v_0} = \frac{2}{v_0} \sum_{l=1}^{\infty} \frac{\left(kv_0/\omega_c\right)^{2l}}{(2l + 1)(\eta^2 - 1) \ldots (\eta^2 - l^2)} \left(l + \frac{\eta i h \nu}{\omega_c} \sum_{j=1}^{l} \frac{1}{\eta^2 - j^2} \right)$$

$$\eta = \frac{\omega - i\nu}{\omega_c}$$

$$\nu = \nu(v_0)$$

The series representations given for G and G' were found to converge very rapidly; thus, equation (67) was easily solvable by numerical methods.

Idehara and Sugaya (ref. 16) considered the same problem but they did not derive the relatively simple dispersion relation given by equation (67). They instead made approximations that are valid only for very small wavenumbers (or large wavelengths).

Before solving equation (67) the roots of $D(\omega,0) = 0$ are investigated, since from a preceding section, these roots are known to correspond to branch points in the complex frequency plane. By expanding G and G' in equation (67) and keeping only terms to lowest order in k, the dispersion relation yields

$$\omega^5 + \omega^4\left(-4i\nu\right) + \omega^3\left(-6\nu^2 - 2\omega_c^2 - \omega_p^2\right) + \omega^2\left[4i\nu\left(\nu^2 + \omega_c^2\right) + i\nu\omega_p^2(3 - h/3)\right]$$
$$+ \omega\left[\left(\nu^2 + \omega_c^2\right)^2 + \omega_p^2\left(3\nu^2 + \omega_c^2 - 2h\nu^2/3\right)\right] + i\nu\omega_p^2\left[\nu^2(h/3 - 1) - \omega_c^2(1 + h/3)\right] = 0 \qquad (68)$$

This equation, being a complex fifth-order polynomial in ω, has five complex roots. However, because of the symmetry relations expressed by equation (65), there can be only three independent solutions. One root must have a zero real part, and each pair of the other four must be related by $\omega_A = -\omega_B^*$ where ω_A and ω_B denote one pair of the four remaining roots. One of these pairs has a real part near the hybrid frequency $\omega_H = \sqrt{\omega_c^2 + \omega_p^2}$ and the other has a real part near the cyclotron frequency. The precise location of these roots will, of course, depend on the plasma parameters chosen. If these roots lie below the real axis, then an absolute instability is indicated, whereas if they are above the axis, there is no absolute instability but there may or may not be a convective instability (refs. 23 to 26). By solving equation (68) for various values of the slope parameter h, it is found that the root with the real part near the cyclotron frequency leads to an absolute instability for large positive values of h, for example, $h > 3$. However, for large negative values of h, the roots with real parts zero and near the hybrid frequency both lead to an absolute instability. In addition to these solutions, one can show analytically that as $k \to 0$, equation (67) is solved by $\omega = 0$ and $\omega = \pm n\omega_c + i\nu$ where $n = 2,3,4,\ldots$.

With the help of these solutions, it is possible to numerically solve the dispersion relation (eq. (67)) with k real and greater than zero to obtain the desired complex frequency solutions in the right half-plane. This procedure leads to the mappings of the real wavenumber axis into the complex frequency plane shown in figures 1 to 4.

In figure 1 for $h = 4$, an absolute instability at $\mathrm{Re}(\omega) \approx \omega_c$ is predicted since one of the branch points (indicated by the small circles) is in the lower half-plane. In this figure only the first three terms of an infinite series of modes are plotted. The modes

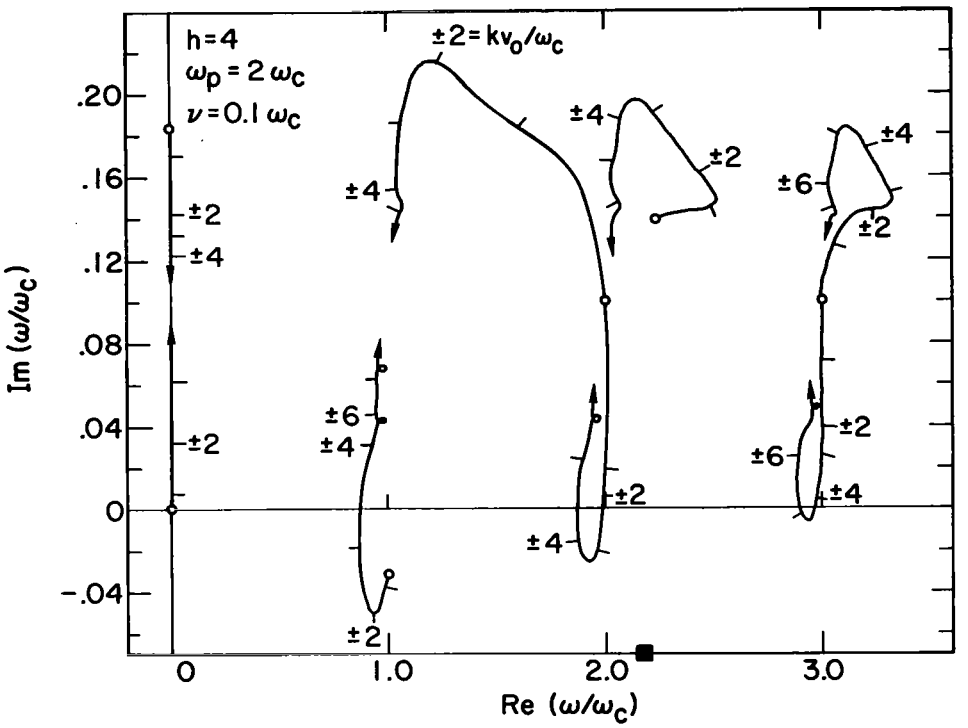

Figure 1.- Real wavenumber axis mapped into complex frequency plane with a positive slope parameter. The branch point (indicated by a small circle) below the real ω axis indicates an absolute instability. The upper set of modes are the modified collisionless modes. The bottom set are the collisional modes. The hybrid frequency is indicated by the solid square symbol on the real ω axis.

near higher cyclotron harmonics are similar to the two near $\omega = 3\omega_c$ in figure 1. The two modes with $\mathrm{Re}(\omega) = 0$ are collision-dependent modes and in the collisionless limit they both coalesce to the point $\omega = 0$. They are not of much interest here since in a real plasma they would be masked by ion effects. The three upper modes in figure 1 are modified collisionless modes. In the collisionless limit, these modes have ω real solutions and would hence map into lines on the real frequency axis. The three lower modes in this figure are collision-dependent modes, and in the collisionless limit they coalesce into the points $\omega = \pm n\omega_c$ $(n = 1,2,3,\ldots)$. Note particularly the absolutely unstable mode with $\mathrm{Re}(\omega) \approx \omega_c$. The location of the branch point associated with this mode is given by one of the roots of the fifth-order polynomial (eq. (68)). If either $\nu = 0$ or $h = 0$, the order of this equation is reduced by two as can be seen by reobtaining the new equation from equation (67). The roots that vanish have real parts near $\pm\omega_c$ and hence it is concluded that these modes are introduced by collisions. The branch points associated with the other collisional modes (and with the set of modified collisionless modes also) are located at $\omega = \pm n\omega_c + i\nu$ $(n = 2,3,4,\ldots)$. One can show analytically that if either h or ν goes to zero, the collisional modes vanish and the branch points are then

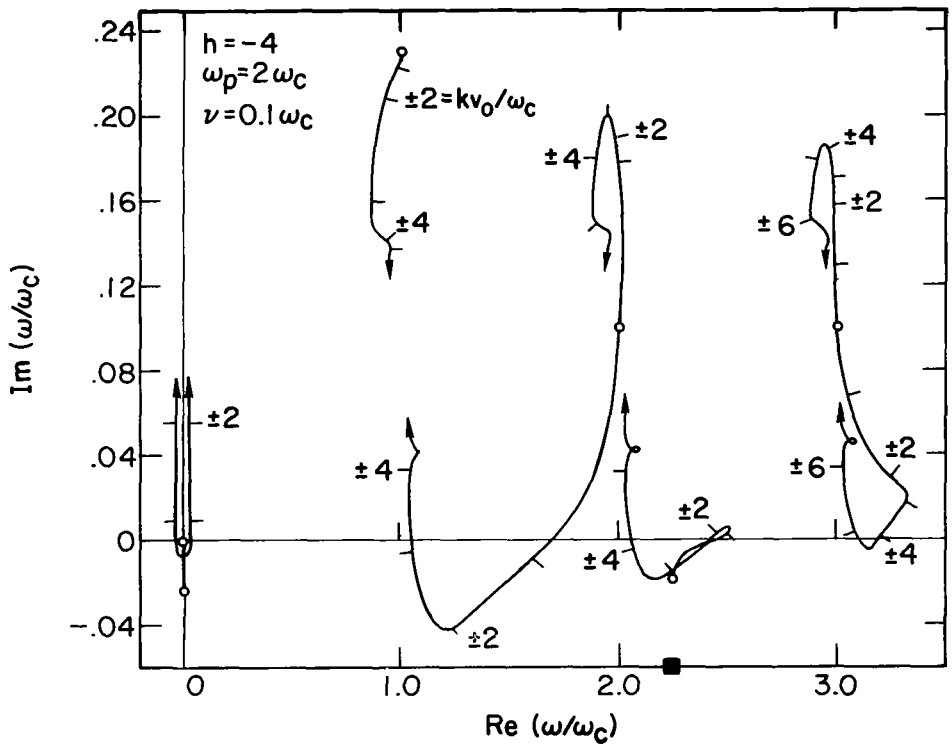

Figure 2.- Real wavenumber axis mapped into complex frequency plane with a negative slope parameter. The branch point at the hybrid frequency is in the lower complex frequency plane so that the plasma is absolutely unstable. Note that the modified collisionless modes are below the collisional modes rather than above as in figure 1. Hybrid frequency is indicated by a solid square symbol. Small circles denote branch points.

associated only with the collisionless modes. These branch points cannot lead to absolute instabilities for any set of plasma parameters. At most, these modes may be convectively unstable unless there is another branch point below the real frequency axis but above the mapping of the real k axis. No branch points of this type were found. Any other branch points in the lower frequency plane may be shown to be ignorable. For large k, the mappings appear to approach the points $\omega = n\omega_c + i\nu$ (n = 1,2,3,. . .), but this result was not shown conclusively. It is not expected, however, that anything of physical interest occurs at k values larger than those shown.

In figure 2 it is seen that for h = -4, there are two branch points in the lower half plane. Note that the position of the modes has reversed. The modified collisionless modes are on the bottom, and the collisional modes are on the top. The unstable modes are hence the modified collisionless modes, and there is an absolute instability at the hybrid frequency. The modes near $\mathrm{Re}(\omega) = 0$ are also shown here, but as before, are of only minor interest. Henceforth, they will not be considered.

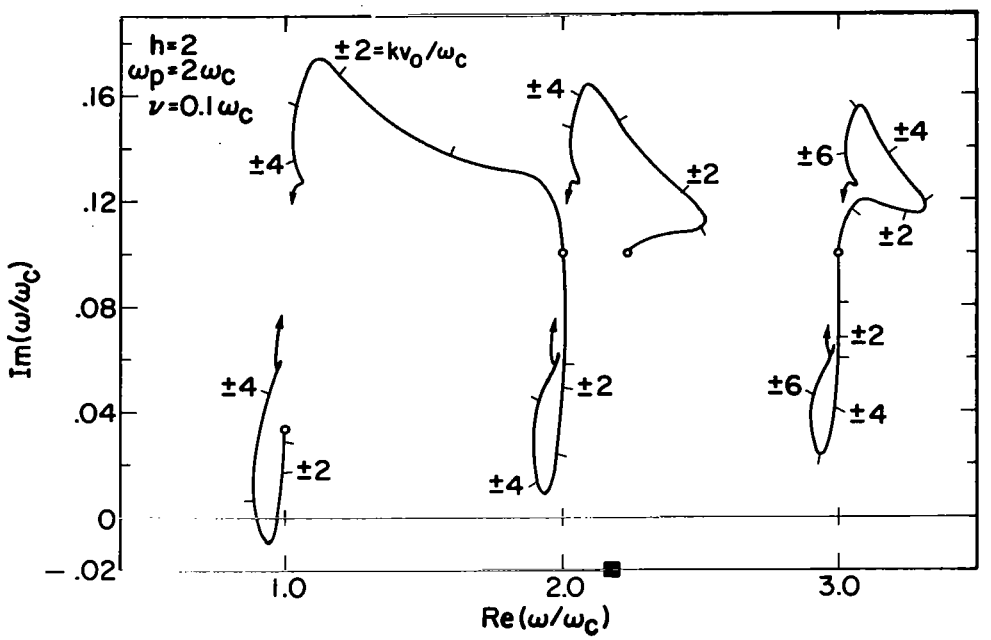

Figure 3.- Real wavenumber axis mapped into the complex frequency plane. The branch points are all above the real ω axis but the mapping does dip below this axis and indicates a convective instability. Hybrid frequency denoted by a solid square symbol; branch points are denoted by small circles.

In figures 3 and 4, cases that are convectively unstable are shown. Note that the branch points all lie above the real frequency axis so that there is no absolute instability. However, the mapping of the real wavenumber axis dips below the real frequency axis and indicates a convective instability. The unstable modes in both of these figures are collision dependent and vanish in the collisionless limit where the waves supported by the plasma are known to be stable (ref. 36). Furthermore, for large collision frequencies a damping effect is evident as shown by the fact that the $\nu = 0.05\omega_c$ case in figure 4 is more unstable than the $\nu = 0.1\omega_c$ case in figure 3. Hence there must be some intermediate collision frequency (and hence neutral gas density) for which the growth rate $Im(\omega)$ would reach a maximum. Note also that figures 3 and 4 are for $h = 2$. Values of the slope parameter in this range are common in gases that are used in laboratory discharge plasmas. For this reason it appears that this theory will find important applications in predicting cyclotron wave propagation through plasmas. More realistic electron distributions are treated in subsequent sections.

It should be pointed out at this point that a spherical shell distribution as considered here is unstable even in the collisionless limit for some ranges of the plasma parameters (ref. 36). However, for the cases investigated here and in the remaining part of this section, the collisionless limit predicts only stable or evanescent waves. Hence, one can

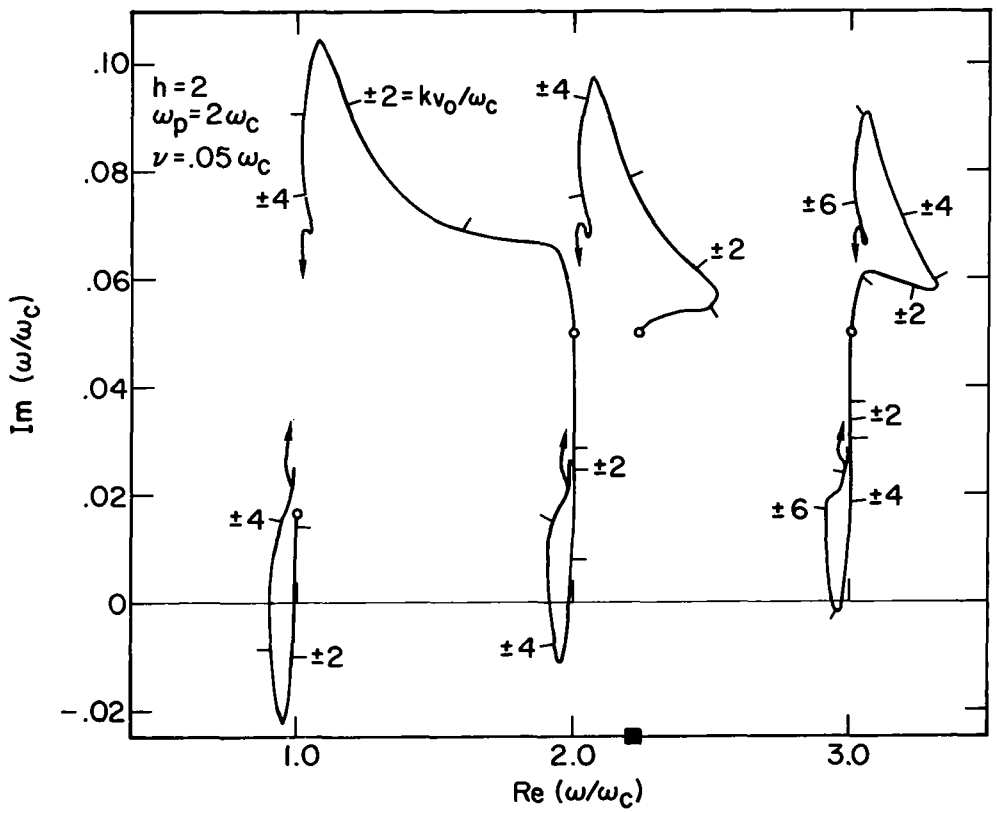

Figure 4.- Real wavenumber axis mapped into the complex frequency plane for a convectively unstable case. Hybrid frequency indicated by a solid square symbol; branch points are denoted by small circles.

truly say that the electron-neutral collision process is responsible for the predicted instabilities.

Peaked Electron Distribution

In a previous section equation (51) is solved for a monoenergetic electron distribution function and collision-induced instabilities are found for some ranges of the slope parameter

$$h = \frac{v}{\nu}\frac{d\nu}{dv} \tag{69}$$

In particular, unstable modes near the cyclotron harmonics are found for values of h near 2 and above. For h negative, unstable modes with real frequency near zero and near the hybrid frequency are found. Hence it seems likely that collisional instabilities of this type should be found in a plasma if there were present (1) a background of neutrals for which $h \gtrless 2$ over some region or regions of velocity space, and (2) a sharply peaked

electron distribution function centered in one of these regions. In the remainder of this section it is shown that this is indeed possible.

The measured electron-neutral collision frequency for nitrogen exhibits a sharp peak (refs. 38 and 39) as shown in figure 5. The parameter h ranges up to 5; thus criterion (1) is met. To use the experimental values in the dispersion relation, first fit a rational polynomial

$$P_c = \alpha_1 \left[\frac{\left(v^2 + \alpha_2 v + \alpha_4\right)\left(v^2 + \alpha_6 v + \alpha_8\right)}{\left(v^2 + \alpha_3 v + \alpha_5\right)\left(v^2 + \alpha_7 v + \alpha_9\right)\left(v - \alpha_{10}\right)} \right] \tag{70}$$

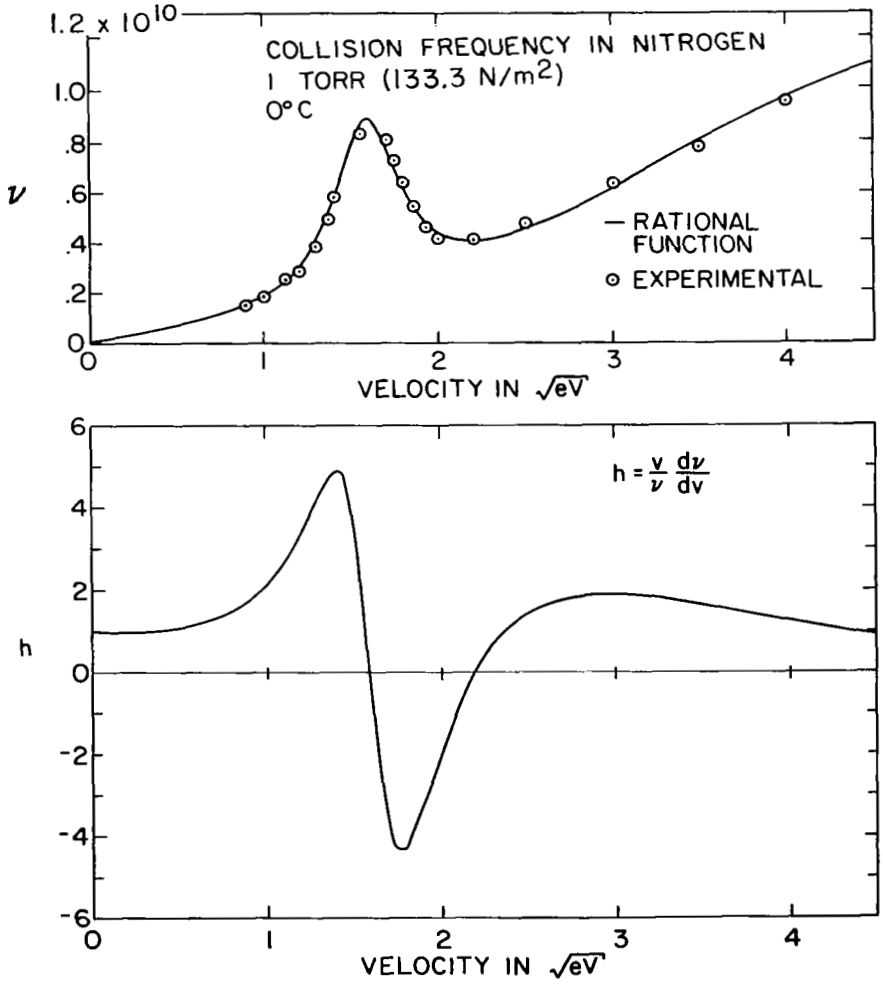

Figure 5.- Rational function fit to experimental electron-neutral collision frequency for nitrogen (ref. 38) and slope parameter from rational function.

to the experimental probability of collision for nitrogen measured by Brode (ref. 38). Then obtain the collision frequency (ref. 39) from

$$\nu(v) = \frac{273}{T} pP_c v \tag{71}$$

where p and T are, respectively, the pressure in torrs and the temperature in ^{o}K of the nitrogen. Note that since p is proportional to T, only the neutral particle number density is a parameter in the collision frequency function. Instead of number density, however, the collision frequency at infinite electron velocity ν_∞ defined by

$$\nu(v) = \frac{\nu_\infty v P_c}{\alpha_1} \tag{72}$$

will be used. A least-squares fit of equation (70) to the experimental probability of collision for nitrogen (and mercury) (refs. 38 and 40) led to the parameters given in table I. The quality of the fit for nitrogen can be seen in figure 5.

TABLE I.- LEAST SQUARES FIT TO EXPERIMENTAL PROBABILITY OF COLLISION FOR NITROGEN AND MERCURY*

$$\left[P_c = \alpha_1 \frac{\left(v^2 + \alpha_2 v + \alpha_4\right)\left(v^2 + \alpha_6 v + \alpha_8\right)}{\left(v^2 + \alpha_3 v + \alpha_5\right)\left(v^2 + \alpha_7 v + \alpha_9\right)\left(v - \alpha_{10}\right)} \right.$$

$$\left. \text{where } P_c \text{ is in } cm^2 \text{ and } v \text{ is in } \sqrt{eV} \right]$$

	Nitrogen	Mercury
α_1	274.304	381.030
α_2	-2.58343	.531224
α_3	-3.16090	-.107263
α_4	4.28551	.516368
α_5	2.55450	.475607
α_6	-3.35392	-.717384
α_7	-5.25412	-.840921
α_8	3.09938	.132412
α_9	12.5096	.180940
α_{10}	-4.55542	-7.01816

*References 38 to 40.

To meet criterion (2), the distribution function,

$$f_0(v) = f_s(v) = \frac{C_s}{2\pi v_0^3}\left(\frac{v}{v_0}\right)^s e^{-\frac{s}{2}(v/v_0)^2} \tag{73}$$

where

$$C_s = \frac{\left(\frac{s}{2}\right)^{(s+3)/2}}{\Gamma\left(\frac{s+3}{2}\right)}$$

is used. This distribution function has a peak at v_0 and is shown plotted in figure 6. The half-width of the peak is a transcendental function of s and is not conveniently used as a parameter. However, the half-width increases (1) proportionally with v_0 and/or (2) as s becomes smaller. The electron distribution function (eq. (73)) is normalized according to

$$\int f_0(v) d^3v = 1 \tag{74}$$

Once the distribution function $f_0(v)$ and the collision frequency function $\nu(v)$ are specified, the dispersion relation in equation (51) can be solved. It is necessary to evaluate the velocity integral numerically but this is easily done by using a Gauss quadrature rule. The details of this integration procedure are given in appendix G. When

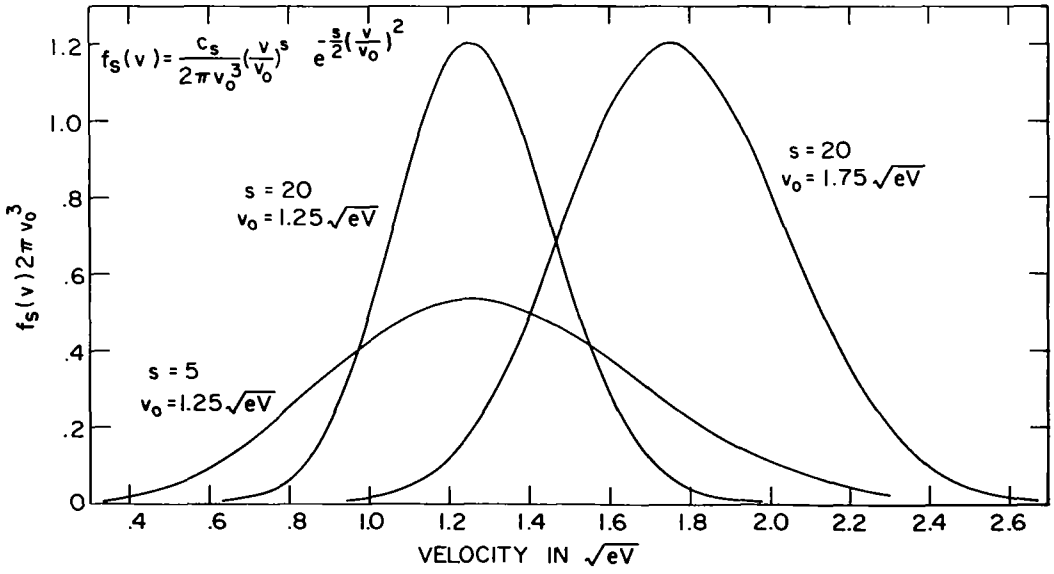

Figure 6.- Normalized peaked distribution function.

carrying out this integration, it was necessary at times to use an asymptotic expansion for G(v). Since G(v) was known to be a hypergeometric function (see eq. (53)), it was possible to utilize the asymptotic expansions of generalized hypergeometric functions given by Meijer (ref. 31). This expansion is given in appendix H. Note also that the integrand in equation (51) will have poles wherever the denominator is zero. Once the poles are located in velocity space, it is necessary to determine the correct integration contour before trying to solve the dispersion relation. This determination is made by recalling that equation (51) is defined for k real and ω on a Laplace integral path (LIP). Usually, the real velocity axis proved to be a valid contour, but occasionally, it was necessary to integrate along a deformed contour as described in appendix I. The scheme described worked very well but is only one of many that could be used.

To determine the stability of the waves predicted by equation (51) for the case being considered in this section, it was decided to map the real wavenumber axis into the

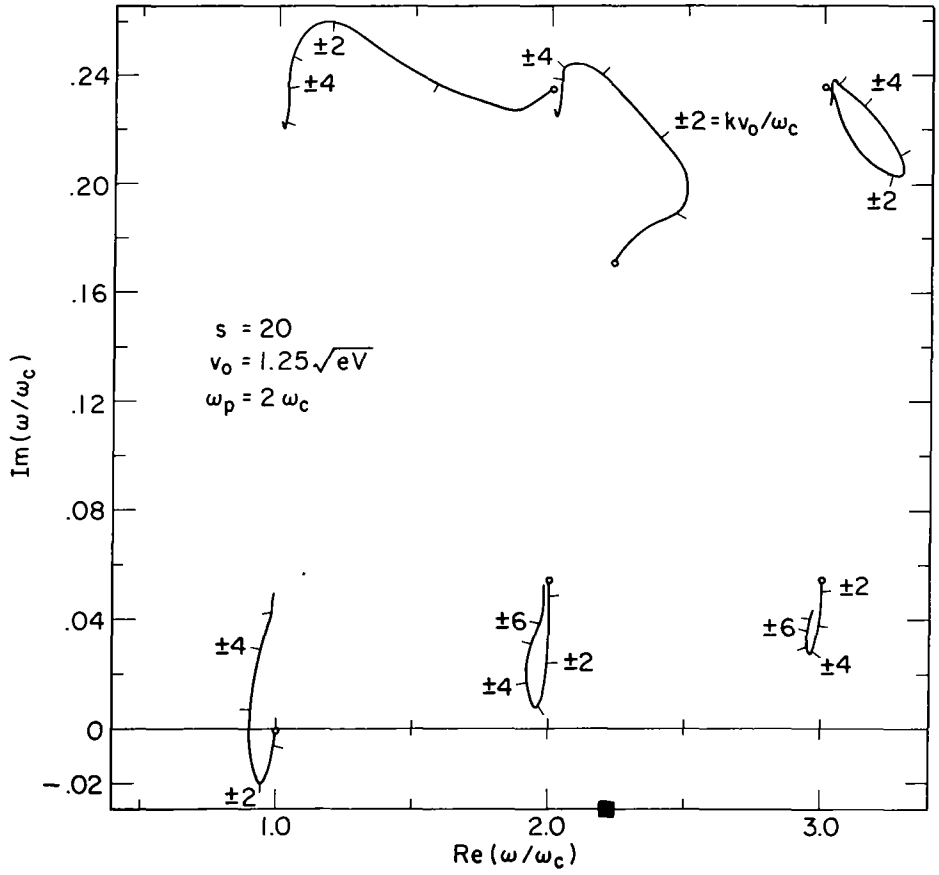

(a) $\nu_\infty = 0.5\omega_c$.

Figure 7.- Mapping of real wavenumber k into the complex frequency plane. Plot shows absolutely unstable waves. Hybrid frequency is indicated by a solid square symbol; branch points are denoted by small circles.

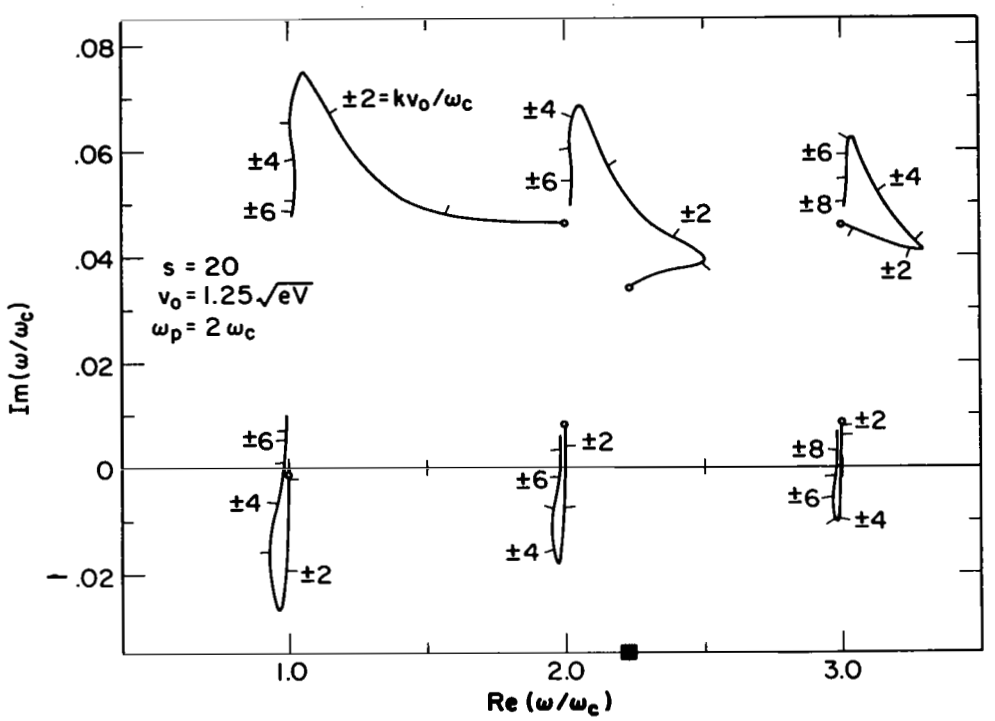

(b) $\nu_\infty = 0.1\omega_c$.

Figure 7.- Concluded.

complex frequency plane. If instabilities of an unknown nature are present, this method seems to be a more useful approach than, for example, mapping from the frequency plane into the wavenumber plane.

Figures 7 to 9 show the results of such a mapping. Because of the symmetry relations expressed by equations (63) and (65), it is necessary only to consider $k > 0$ and to look for roots in the right half frequency plane. Figure 7(a) shows a case that is absolutely unstable because of the branch point at $\omega \approx \omega_c$. The electron distribution function peak is at $v_0 = 1.25\sqrt{eV}$ and from figure 5 it can be seen that this point is the approximate location of the most positive slope of the collision frequency function. The three lower modes in figure 7(a) represent the new collisional modes described earlier and vanish as the collisionless limit is approached. The three upper modes are modifications of the collisionless modes but are damped here unlike in the collisionless limit. It is interesting to note that the modes shown in figure 7(a) all come from their own branch points at $k = 0$, whereas in the monoenergetic electron distribution case, there were sometimes two modes arising from a single branch point.

The case shown in figure 7(b) is identical to that shown in figure 7(a) except for a lower collision frequency. Note that there are now more unstable modes; thus, it appears that high collision frequencies tend to damp even the collisional modes. Since

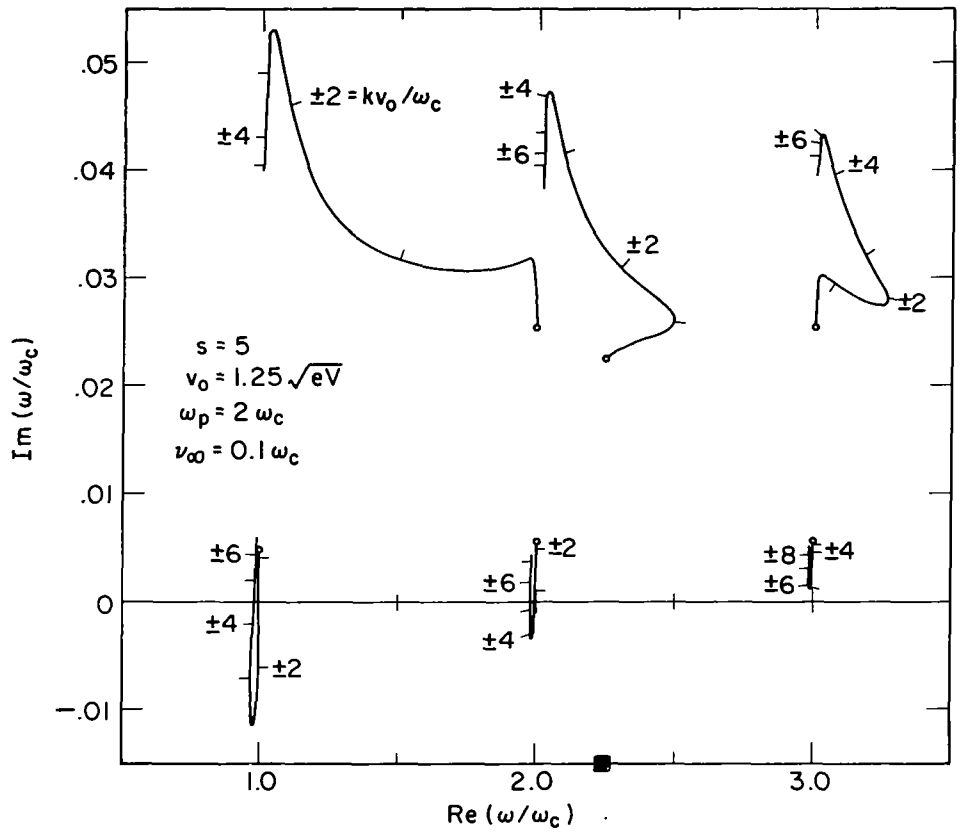

Figure 8.- Mapping of real wavenumber k into the complex frequency plane. Plot shows convectively unstable waves. Hybrid frequency is indicated by a solid square symbol; branch points are denoted by small circles.

these modes also vanish at zero collision frequency, there is a particular collision frequency, and hence a particular neutral gas pressure, at which the collisional cyclotron waves are most unstable.

In figure 8 is shown a case where the electron distribution function half-width is approximately twice that shown in figure 7(b). (See fig. 6.) Note that the first mode has changed from absolutely unstable to convectively unstable and the third mode has become stable. Hence, electron distribution functions with wider peaks tend to be more stable than those with narrow peaks.

In figure 9 a case with the electron distribution function peak located on the negative slope of the collision frequency curve is considered. As in the case of the monoenergetic distribution function, the location of the modes is reversed and the collisional modes are very heavily damped. However, the case in figure 9 is a stable situation unlike the one presented in figure 2. Consequently, if the peaks were made sufficiently narrow, the case given in figure 9 would become absolutely unstable because of the branch point with real frequency near the hybrid frequency. However, the case of a positive slope parameter

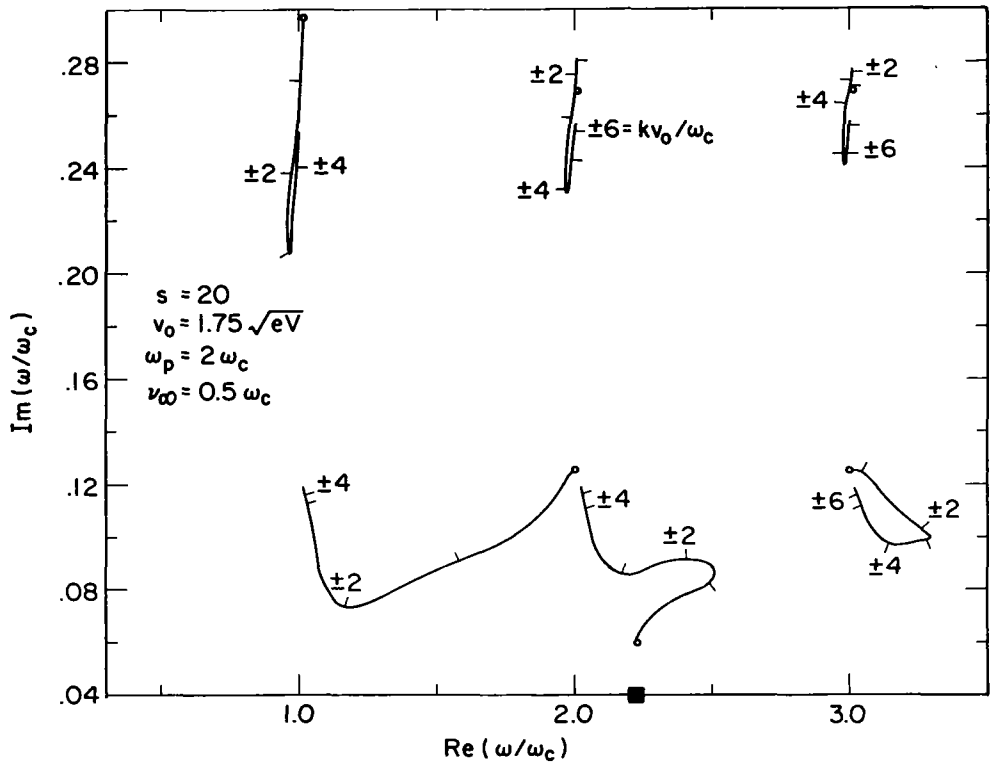

Figure 9.- Mapping of real wavenumber k into the complex frequency plane. Plot shows stable waves. Hybrid frequency is indicated by a solid square symbol; branch points are denoted by small circles.

seems to be of more physical interest because of the large number of gases having regions of positive slope in their collision frequency curves. Consequently, the negative slope case will not be investigated further here. A case with large half-width, $s = 1$ and $v_0 = 1.05\sqrt{eV}$, was also considered briefly. It was found that the collisional mode with real frequency near the cyclotron frequency was convectively unstable but that all other modes were stable.

Earlier it has been shown that collisional instabilities are possible in a plasma if a large percentage of the electrons are in a region in velocity space where the collision frequency increases (or decreases) rapidly with velocity. If the collision frequency slope is positive, there may be an absolute instability at the cyclotron frequency and convective instabilities at the higher harmonics. If the collision frequency slope is negative, there may be an absolute instability at the hybrid frequency and convective instabilities at frequencies between the cyclotron harmonics. The occurrence and strength of these instabilities depend very strongly on (1) the width of the peak in the electron distribution function and (2) the slope of the collision frequency in the region of the peak. It is difficult to give more precise statements about the occurrence of these collisional instabilities; thus it is necessary to consider each case separately.

Maxwellian Electron Distribution

In this section equation (51) is solved with the same collision frequency function as in the last section, that is, equation (72), but instead of a peaked electron energy distribution function a Maxwellian distribution function

$$f_0(v) = \frac{e^{-\left(v^2/v_0^2\right)}}{\pi^{3/2}\, v_0^3} \tag{75}$$

is used.

In figure 10 the real wavenumber axis is mapped into the complex frequency plane and the modes shown are of the modified collisionless type. These modes cannot be unstable since a Maxwellian plasma must be stable. As k becomes large, the mappings apparently approach the points $\omega = n\omega_c$ (n = 1,2,3,. . .). This statement, however, was not shown conclusively either by numerical or analytical means. The collisional modes, that were often unstable for the peaked electron distribution function, were not found in a Maxwellian plasma. Apparently, these collisional modes are present only if the electron

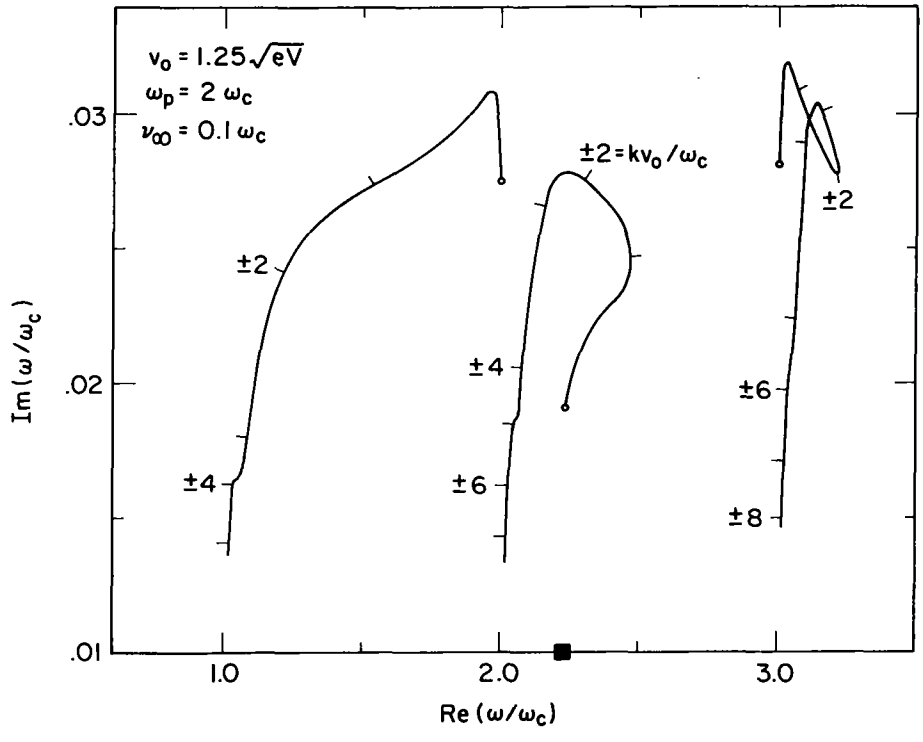

Figure 10.- Mapping of real wavenumber k into the complex frequency plane for a Maxwellian electron distribution. Hybrid frequency is denoted by a solid square symbol; branch points are denoted by small circles.

distribution function has a region of positive slope. To investigate the disappearance of these modes further, the isotropic distribution function given by

$$f_0(v) = \begin{cases} 3/\left(4\pi v_0^3\right) & (v < v_0) \\ 0 & (v > v_0) \end{cases} \tag{76}$$

was briefly considered and it was found analytically that the collisional mode did not exist. In support of this argument, Bekefi et al. (ref. 41) found that, in general, there must be a region where $\partial f_0/\partial v > 0$ for collisional instabilities to exist. However, they used a radiation temperature approach and could not say anything about the existence or nonexistence of the actual collisional mode.

Since the waves present in a Maxwellian plasma are stable, the complex k roots for real ω may be interpreted, according to established practice, as spatially damped or growing waves. This representation is relevant to laboratory experiments since one often excites the plasma at some real frequency and measures the complex and real parts of the wavenumber. The results of such a mapping are shown in figure 11. The case shown here was solved also by Tataronis (ref. 36) by using a constant collision frequency BGK model, that is, equation (62). Because of the presence of the velocity-dependent collision frequency in equation (51), the temperature of the Maxwellian electron distribution function did not normalize out as in his case, and so a thermal speed of $v_0 = 1.5\sqrt{eV}$ was chosen as representative of values found in a laboratory plasma. For the collision frequency parameter ν_∞, a value was chosen so that the average collision frequency given by

$$\langle \nu \rangle = \int_0^\infty \nu(v)\, f_0(v)\, 4\pi v^2\, dv \tag{77}$$

was the same as the constant collision frequency used by Tataronis. From figure 11 it is seen that the two models differ but not substantially. There appear to be no important differences, unlike in the case of the peaked distribution function where the collisional modes do not exist for other collision models. Hence, it would seem that for a Maxwellian plasma, it is not necessary to use the exact collisional model considered here unless very precise results are desired.

Sum of Maxwellian and Peaked Electron Distributions

Since it was found that a peaked distribution function could lead to collision-induced instabilities, one might wonder what portion of the distribution function must be

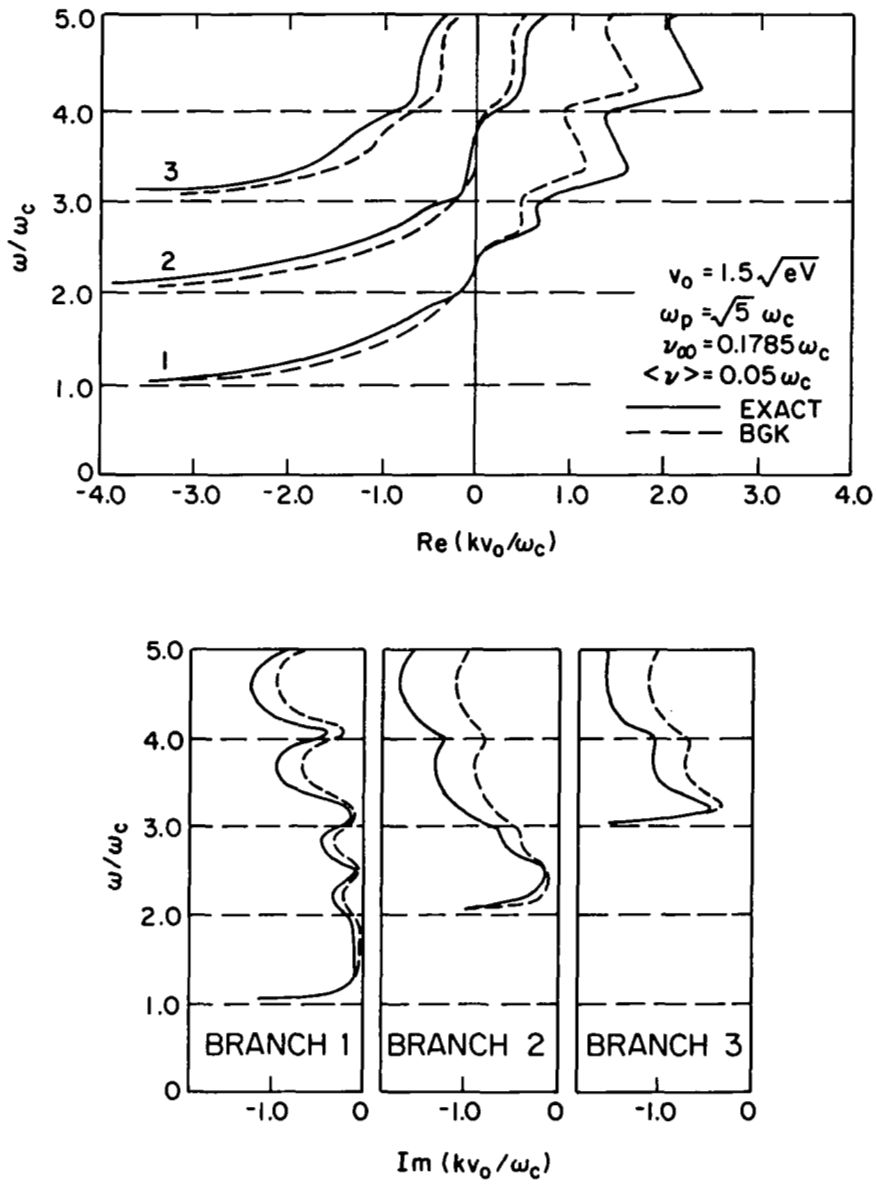

Figure 11.- Brillouin diagram giving Re(k) and Im(k) as functions of ω real for Maxwellian electron distribution. Bhatnagar-Gross-Krook (BGK) curves from reference 32.

Maxwellian before the waves become stable. To answer this question, the electron distribution function is chosen to be

$$f_0(v) = \alpha C_m e^{-v^2/v_1^2} + (1 - \alpha) C_s \left(\frac{v}{v_2}\right)^s e^{-\frac{s}{2}(v/v_2)^2} \tag{78}$$

where

$$C_m = \left(\sqrt{\pi} v_1\right)^{-3}$$

$$C_s = \frac{\left(\frac{s}{2}\right)^{(s+3)/2}}{2\pi v_2^3 \, \Gamma\left(\frac{s+3}{2}\right)}$$

Note that α gives the proportion of the total electron population that is Maxwellian. This distribution function also obeys the normalization criterion (eq. (74)).

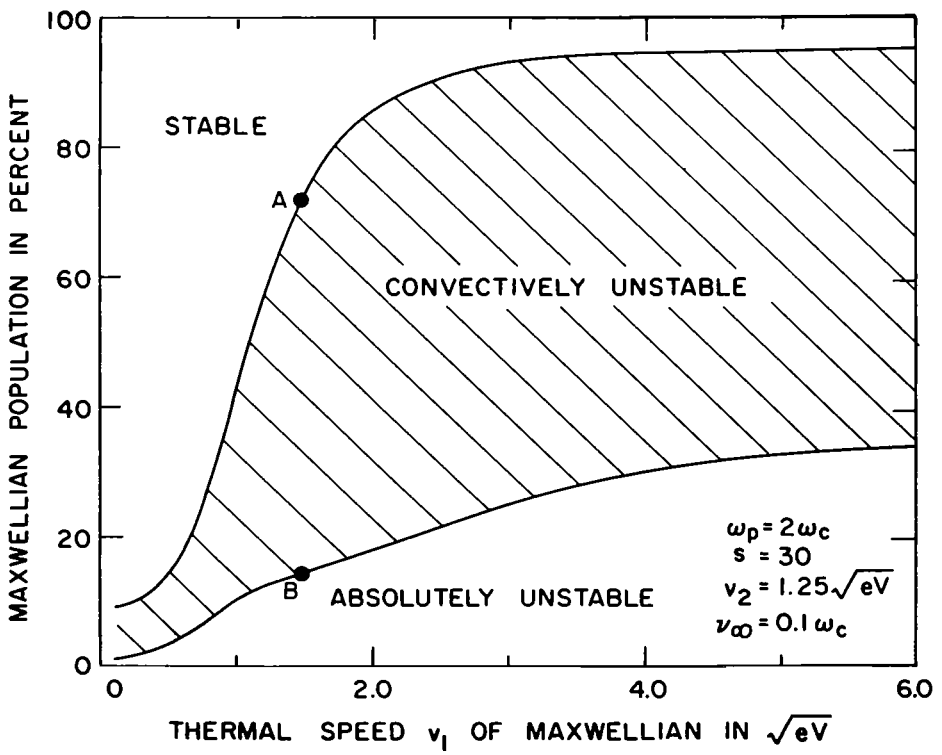

Figure 12.- Stability plot for Maxwellian plus peaked distribution function. Mode with $\mathrm{Re}(\omega) \approx \omega_c$.

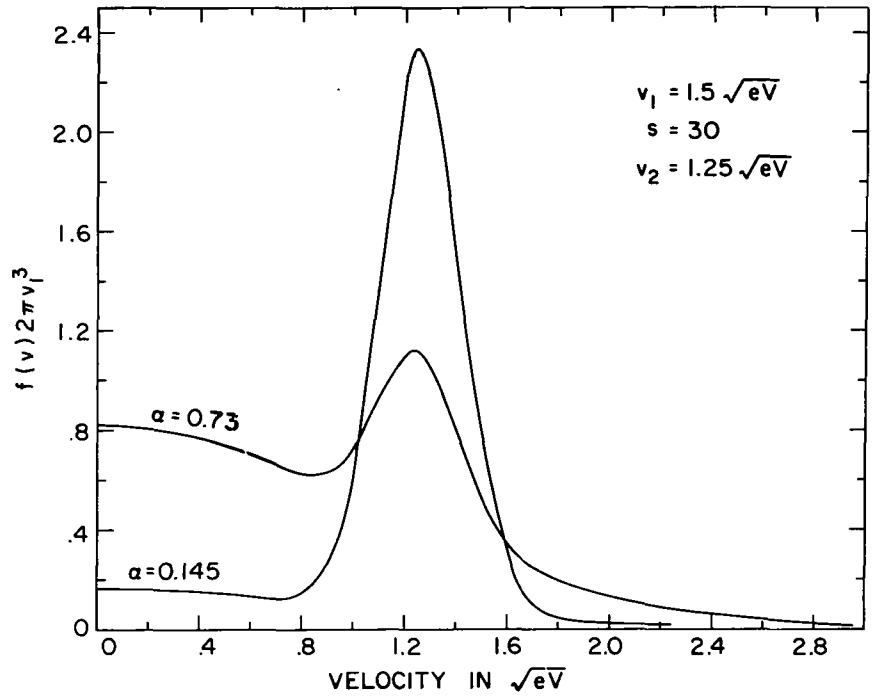

Figure 13.- Normalized distribution function consisting of peaked and Maxwellian components (eq. (78)). Points A and B in figure 12.

Parameters were then chosen that were known to be absolutely unstable, that is, $s = 30$, $v_2 = 1.25\sqrt{eV}$, and $\nu_\infty = 0.1\omega_c$. The dispersion relation was solved for various values of α and v_1 to obtain the instability boundaries in the α, v_1 plane shown in figure 12. The mode considered here was the collisional mode that has $\mathrm{Re}(\omega) \approx \omega_c$. On the lower curve in figure 12, $k = 0$ since the branch point in the complex frequency plane is given by the root of $D(\omega,0) = 0$. On the upper curve the mapping of the real k axis into the frequency plane dips down and just barely touches the real frequency axis but does not go below it. At the point of contact it was found that $k \approx 2.5\omega_c/v_2$.

Since an absolute instability occurs at zero group velocity ($\partial\omega/\partial k = 0$), it is not too surprising to find that low-temperature Maxwellians affect the waves a great deal since there would be proportionally more electrons near zero velocity. However, at higher temperatures it is somewhat surprising to see that as much as 95 percent Maxwellian is required to stabilize the unstable collisional mode. In figure 13 is shown a plot of the distribution function (eq. (78)) for a case on each of the boundary lines in figure 12 (points A and B). Even though there are appreciable numbers of Maxwellian electrons, the distribution function is still highly non-Maxwellian.

Synopsis of Numerical Results

Briefly, it has been found that a rigorous treatment of electron-neutral collisions in a non-Maxwellian Lorentz magnetoplasma predicts a new series of electrostatic modes that vanish both in the collisionless and Maxwellian limits. Solutions of the wave-dispersion relation show that these modes may be unstable for some plasma parameters. Both convective and absolute instabilities were found near the cyclotron frequency whereas only convective instabilities were found at the cyclotron harmonics. In addition, it was found that there could be present an absolute instability near the hybrid frequency and convective instabilities at frequencies between the cyclotron harmonics. It is well known that cyclotron harmonic waves may be unstable in the collisionless limit for some of the electron distribution functions considered in this section. However, all cases investigated here are stable or evanescent in the collisionless limit; therefore, the electron-neutral collision process is indeed responsible for the predicted instabilities.

THEORY OF WAVES PROPAGATING PARALLEL TO THE MAGNETIC FIELD

In this section waves propagating along the direction of the applied magnetic field are considered for both isotropic and anisotropic collision models. The general case of anisotropic collisions is considered initially and the first-order distribution function is written in terms of a set of inhomogeneous partial difference equations. After specializing to waves propagating parallel to the magnetic field, these equations are solved and the conductivity tensor and dispersion relations are obtained. The isotropic collision model is then considered and the conductivity tensor and dispersion relations are again derived. It is shown that in the limit of isotropic collisions, the dispersion relations found from the anisotropic collision frequency model are equivalent to those found when collisions are assumed to be isotropic in the beginning. Some of the analytic properties of the dispersion relations are discussed and comparison is made with other collision models.

First-Order Distribution Function With Anisotropic Collisions

In the Lorentz gas model it is assumed that the ions and neutrals are infinitely heavy and that the plasma is weakly ionized so that electron-neutral collisions are much more frequent than either electron-electron or electron-ion collisions. The Boltzmann equation for electrons can be written as

$$\frac{\partial f}{\partial t} + \vec{v} \cdot \frac{\partial f}{\partial \vec{r}} - \frac{e}{m}\left(\vec{E} + \vec{v} \times \vec{B}\right) \cdot \frac{\partial f}{\partial \vec{v}} = N|\vec{v}| \int \sigma(v,\chi) \left[f(\vec{v}') - f(\vec{v})\right] d\Omega' \tag{79}$$

where χ is the angle between $\vec{v}$ and $\vec{v}'$. The number density of the neutrals is N, and $\sigma(v,\chi)$ is the differential scattering cross section describing the electron-neutral collision process. This equation is linearized by making the ansatz

$$\left.\begin{aligned} f(\vec{v}) &= f_0(\vec{v}) + f_1(\vec{v}) \\ \vec{E} &= 0 + \vec{E}_1 \\ \vec{B} &= \vec{B}_0 + \vec{B}_1 \end{aligned}\right\} \tag{80}$$

The zero-order equation

$$\left(\vec{v} \times \vec{\omega}_c\right) \cdot \frac{\partial f_0}{\partial \vec{v}} = N|\vec{v}| \int \sigma(v,\chi) \left[f_0(\vec{v}') - f_0(\vec{v})\right] d\Omega' \tag{81}$$

and the first-order equation

$$\frac{\partial f_1}{\partial t} + \vec{v} \cdot \frac{\partial f_1}{\partial \vec{r}} - \left(\vec{v} \times \vec{\omega}_c\right) \cdot \frac{\partial f_1}{\partial \vec{v}} = \frac{e}{m}\left(\vec{E}_1 + \vec{v} \times \vec{B}_1\right) \cdot \frac{\partial f_0}{\partial \vec{v}} + N|\vec{v}| \int \sigma(v,\chi) \left[f_1(\vec{v}') - f_1(\vec{v})\right] d\Omega' \tag{82}$$

where $\vec{\omega}_c = e\vec{B}_0/m$ are then obtained. The solution of the zero-order equation (appendix A) is any isotropic distribution function $f_0(v)$ and hence the term $\left(\vec{v} \times \vec{B}_1\right) \cdot \partial f_0/\partial \vec{v}$ in the first-order equation is identically zero. As done previously, the Fourier transform in space and the Laplace transform, in time, corresponding to the wave representation $\exp(i\omega t - i\vec{k} \cdot \vec{r})$ are taken to obtain

$$i(\omega - \vec{v} \cdot \vec{k})\hat{f}_1 - \left(\vec{v} \times \vec{\omega}_c\right) \cdot \frac{\partial \hat{f}_1}{\partial \vec{v}} = \frac{e}{m} \vec{E}_1 \cdot \frac{\partial f_0}{\partial \vec{v}} + N|\vec{v}| \int \sigma(v,\chi) \left[\hat{f}_1(\vec{v}') - \hat{f}_1(\vec{v})\right] d\Omega' \tag{83}$$

Expanding $\hat{f}_1(\omega,\vec{k},\vec{v})$ in spherical harmonics in velocity space yields

$$\hat{f}_1(\omega,\vec{k},\vec{v}) = \sum_{l=0}^{\infty} \sum_{m=-l}^{l} f_{l,m}(\omega,\vec{k},v)\, Y_{l,m}(\theta,\varphi) \tag{84}$$

where $Y_{l,m}(\theta,\varphi) = \left[\frac{(2l+1)(l-m)!}{4\pi(l+m)!}\right]^{1/2} P_l^m(\cos\theta)e^{im\varphi}$. Substituting this relation into equation (83) yields

$$\sum_{l,m} i\left(\omega - \vec{v}\cdot\vec{k} + m\omega_c\right)f_{l,m}Y_{l,m} = \frac{e}{m}\vec{E}_1\cdot\frac{\partial f_0}{\partial\vec{v}} - N|\vec{v}|\sum_{l,m} f_{l,m}Y_{l,m}Q_{l,m} \tag{85}$$

where

$$Q_{l,m} \equiv \int \sigma(v,\chi)\left[1 - \frac{Y_{l,m}(\theta',\varphi')}{Y_{l,m}(\theta,\varphi)}\right]d\Omega' \tag{86}$$

In appendix J it is shown that for all m,

$$Q_{l,m} = Q_l \equiv 2\pi\int_0^\pi \sigma(v,\chi)\left[1 - P_l(\cos\chi)\right]\sin\chi\, d\chi \tag{87}$$

where $P_l(\cos\chi)$ is the Legendre function of degree l. Then by following Allis (ref. 42) and Derfler (ref. 14), the transfer collision frequencies are defined as

$$\nu_l(v) = N|\vec{v}|Q_l \tag{88}$$

and equation (85) then yields

$$\sum_{l,m} i\left(\omega - i\nu_l - \vec{v}\cdot\vec{k} + m\omega_c\right)f_{l,m}Y_{l,m} = \frac{e}{m}\vec{E}_1\cdot\frac{\partial f_0}{\partial\vec{v}} \tag{89}$$

Multiplying this equation by $Y^*_{r,s}(\theta,\varphi)$ and performing an integration over the solid angle $d\Omega = \sin\theta\, d\theta\, d\varphi$, an inhomogeneous difference equation is obtained

$$i\left(\omega - i\nu_r + s\omega_c\right)f_{r,s} - i\sum_{l,m} f_{l,m}\int \vec{v}\cdot\vec{k}Y_{l,m}(\theta,\varphi)\,Y^*_{r,s}(\theta,\varphi)\,d\Omega = T_{r,s} \tag{90}$$

where

$$T_{r,s} = \frac{e}{m}f_0'\left(\frac{2\pi}{3}\right)^{1/2}\delta_{r,1}\left[\delta_{s,1}\left(-E_x + iE_y\right) + \delta_{s,-1}\left(E_x + iE_y\right) + \delta_{s,0}\sqrt{2}\,E_z\right] \tag{91}$$

The integral can be easily evaluated for general k to give a partial difference equation for $f_{r,s}$, but instead it will be specialized to the case of k parallel to the magnetic

field. For this case, $\vec{v} \cdot \vec{k} = vk \cos\theta$ and the integral becomes

$$vk \int \cos\theta \, Y_{l,m}(\theta,\varphi) \, Y^*_{r,s}(\theta,\varphi) \, d\Omega = \frac{vk\delta_{m,s}}{\sqrt{2r+1}} \left\{ \left[\frac{(r+s+1)(r-s+1)}{2r+3} \right]^{1/2} \delta_{l,r+1} + \left[\frac{(r+s)(r-s)}{2r-1} \right]^{1/2} \delta_{l,r-1} \right\} \tag{92}$$

From equation (90) the difference equation

$$i(\omega - i\nu_r + s\omega_c) f_{r,s} - \frac{ivk}{\sqrt{2r+1}} \left\{ f_{r+1,s} \left[\frac{(r+s+1)(r-s+1)}{2r+3} \right]^{1/2} + f_{r-1,s} \left[\frac{(r+s)(r-s)}{2r-1} \right]^{1/2} \right\} = T_{r,s} \tag{93}$$

is obtained. Note that this equation is an ordinary difference equation in the index r at constant s and is readily solvable by use of standard techniques. This equation is solved later in this section to obtain the conductivity tensor and dispersion relation.

For the case $\vec{k} \perp \vec{B}$, equation (90) would lead to a partial difference equation, that is, one in which both the indices change. This type of equation is not readily solvable by using standard techniques and is not considered in this report. Note, however, that the isotropic collision model for $\vec{k} \perp \vec{B}$ was treated earlier.

Conductivity Tensor and Dispersion Relations for $\vec{k} \parallel \vec{B}$ With Anisotropic Collisions

The conductivity tensor for the case of propagation parallel to the magnetic field will now be sought. Equation (84) is substituted into the current equation

$$\vec{j} = \bar{\sigma} \cdot \vec{E} = -en \int \vec{v} \hat{f}_1(\vec{v}) d^3v \tag{94}$$

to obtain

$$\vec{j} = \bar{\sigma} \cdot \vec{E} = e\left(\frac{2\pi}{3}\right)^{1/2} n \int_0^\infty v^3 \left[\hat{e}_x (f_{1,1} - f_{1,-1}) + \hat{e}_y i (f_{1,1} + f_{1,-1}) - \hat{e}_z \sqrt{2} f_{1,0} \right] dv \tag{95}$$

Note that only $f_{1,-1}$, $f_{1,0}$, and $f_{1,1}$ are needed to find the conductivity tensor $\bar{\sigma}$, and with this in mind the solution of equation (93) is expressed in terms of a continued fraction as

$$f_{1,s} = g_s T_{1,s} \tag{96}$$

where

$$g_s = \frac{3/ikv}{\beta_s + 3\lambda_{1,s}} - \frac{4 - s^2}{5\lambda_{2,s}} - \frac{9 - s^2}{7\lambda_{3,s}} - \frac{16 - s^2}{9\lambda_{4,s}} - \cdots - \frac{n^2 - s^2}{(2n+1)\lambda_{n,s}} - \cdots \tag{97}$$

$$\beta_s = \begin{cases} 0 & (s = \pm 1) \\ -\frac{kv}{\omega} & (s = 0) \end{cases} \tag{98}$$

and

$$\lambda_{n,s} = \frac{\omega - i\nu_n + s\omega_c}{kv} \tag{99}$$

$s = 0, +1, -1$

The continued fraction notation used here is defined in references 43 and 44. By combining equations (95) and (96), the conductivity tensor may be written as

$$\tilde{\sigma} = \begin{pmatrix} \sigma_{11} & \sigma_{12} & 0 \\ -\sigma_{12} & \sigma_{11} & 0 \\ 0 & 0 & \sigma_{33} \end{pmatrix} \tag{100}$$

where

$$\sigma_{11} = -\epsilon_0 \omega_p^2 \frac{2\pi}{3} \int_0^\infty v^3 f_0' (g_1 + g_{-1}) dv \tag{101}$$

$$\sigma_{12} = -\epsilon_0 \omega_p^2 \frac{2\pi}{3} \int_0^\infty v^3 f_0' i(g_{-1} - g_1) dv \tag{102}$$

$$\sigma_{33} = -\epsilon_0 \omega_p^2 \frac{4\pi}{3} \int_0^\infty v^3 f_0' g_0 \, dv \tag{103}$$

From appendix C, with $\vec{k} = k\hat{e}_3$ in equation (C17), the dispersion function is

$$D(\omega,k) = \begin{vmatrix} 1 + \left(\sigma_{11}/i\omega\epsilon_0\right) - (ck/\omega)^2 & \sigma_{12}/i\omega\epsilon_0 & 0 \\ -\sigma_{12}/i\omega\epsilon_0 & 1 + \left(\sigma_{11}/i\omega\epsilon_0\right) - (ck/\omega)^2 & 0 \\ 0 & 0 & 1 + \left(\sigma_{33}/i\omega\epsilon_0\right) \end{vmatrix} = 0 \tag{104}$$

Expansion of the determinant yields two uncoupled dispersion relations

$$D_E(\omega,k) \equiv 1 + \frac{\sigma_{33}}{i\omega\epsilon_0} = 0 \tag{105}$$

$$D_\pm(\omega,k) \equiv 1 - \left(\frac{ck}{\omega}\right)^2 + \frac{\sigma_{11} \pm i\sigma_{12}}{i\omega\epsilon_0} = 0 \tag{106}$$

By using equation (103) for σ_{33}, equation (105) becomes

$$D_E(\omega,k) = 1 + \frac{4\pi i}{3}\frac{\omega_p^2}{\omega}\int_0^\infty v^3 f_0' g_0 \, dv = 0 \tag{107}$$

This dispersion relation represents a purely longitudinal electrostatic wave that is not affected by the magnetic field. This same dispersion relation was found by Derfler (ref. 14) for an unmagnetized plasma and is not considered further here. Substituting for σ_{11} and σ_{12} in equation (106) yields

$$D_\pm(\omega,k) = 1 - \left(\frac{ck}{\omega}\right)^2 + \frac{2\pi\omega_p^2}{\omega k}\int_0^\infty g_\pm(v)\, v^2 f_0'(v) dv = 0 \tag{108}$$

where $g_\pm$ is the continued fraction

$$g_\pm(v) = \frac{2}{3\lambda_{1,\pm1} - \dfrac{3}{5\lambda_{2,\pm1} - \cdots - \dfrac{n^2 - 1}{(2n+1)\lambda_{n,\pm1} - \cdots}}} \tag{109}$$

This dispersion relation describes transverse electromagnetic waves propagating parallel to the applied magnetic field, that is, left- and right-hand circularly polarized waves.

The dispersion relations derived in this section (eqs. (107) and (108)) exactly describe the dispersion of waves propagating along the magnetic field in a Lorentz gas plasma. If an anisotropic electron-neutral collision cross section $\sigma(v,\chi)$ is given, one can obtain the transfer collision frequencies from equations (87) and (88) and then, in principle, solve the dispersion relations. Often, in practice, only the velocity dependence of the collision cross section is available and in this case the isotropic collision model is of more interest. This case is considered in the next section.

Conductivity Tensor and Dispersion Relations for $\vec{k} \parallel \vec{B}$ With Isotropic Collisions

In this section it is assumed from the beginning that the electron-neutral collision process is isotropic. This procedure was followed earlier for general k where the calculation started with the Boltzmann equation given by equation (14) and a conductivity tensor $\bar{\sigma}$ given by equation (34) was found. In appendix K this $\bar{\sigma}$ is specialized to propagation parallel to the magnetic field to obtain

$$\bar{\sigma} = \begin{pmatrix} \sigma_{11} & \sigma_{12} & 0 \\ -\sigma_{12} & \sigma_{11} & 0 \\ 0 & 0 & \sigma_{33} \end{pmatrix} \tag{110}$$

where

$$\sigma_{11} = -i\omega_p^2 \epsilon_0 \int \frac{f_0' v_1^2}{v} \frac{\omega_\nu - kv_3}{\omega_c^2 - (\omega_\nu - kv_3)^2} d^3v \tag{111}$$

$$\sigma_{12} = \omega_p^2 \epsilon_0 \int \frac{f_0' v_1^2}{v} \frac{\omega_c}{\omega_c^2 - (\omega_\nu - kv_3)^2} d^3v \tag{112}$$

$$\sigma_{33} = -\frac{4\pi i \omega_p^2 \epsilon_0 \omega}{k^2} \int_0^\infty v f_0' \left(\frac{1 - \lambda \coth^{-1}\lambda}{1 + \frac{i\nu}{kv} \coth^{-1}\lambda} \right) dv \tag{113}$$

$$\lambda = \frac{\omega_\nu}{kv}$$

$$\omega_\nu = \omega - i\nu(v)$$

After writing $d^3v = v^2 \sin\theta \, d\theta \, d\varphi \, dv$, the angular integrals in equations (111) and (112) can be evaluated exactly but it is easier here to leave them in their present form for now. Using equation (105) and σ_{33} from equation (113) yields

$$D_E(\omega,k) = 1 - 4\pi\left(\frac{\omega_p}{k}\right)^2 \int_0^\infty v f_0' \left(\frac{1 - \lambda \coth^{-1}\lambda}{1 + \frac{i\nu}{kv}\coth^{-1}\lambda}\right) dv = 0 \tag{114}$$

where

$$\lambda = \frac{\omega_\nu}{kv}$$

This equation describes a purely longitudinal electrostatic wave as does equation (107) and Derfler (ref. 14) has shown that in the limit of isotropic collisions, equation (107) reduces to equation (114).

From equations (106), (111), and (112), the following dispersion relation for transverse electromagnetic waves is obtained:

$$D_\pm(\omega,k) = 1 - \left(\frac{ck}{\omega}\right)^2 + \frac{\omega_p^2}{\omega}\frac{1}{2}\int \frac{f_0' v_\perp^2/v}{\omega_\nu - kv_3 \pm \omega_c} d^3v = 0 \tag{115}$$

Then since $d^3v = v^2 \sin\theta \, d\theta \, d\varphi \, dv$, the integrals over the angles can be evaluated to obtain

$$D_\pm(\omega,k) = 1 - \left(\frac{ck}{\omega}\right)^2 + \frac{2\pi\omega_p^2}{\omega k}\int_0^\infty v^2 f_0' \left[\lambda_\pm + \left(1 - \lambda_\pm^2\right)\coth^{-1}\lambda_\pm\right] dv = 0 \tag{116}$$

where

$$\lambda_\pm = \frac{\omega_\nu \pm \omega_c}{kv} \tag{117}$$

In appendix L it is shown that equation (108) is identical to equation (116) if isotropic collisions are assumed in the former. In appendix M equation (116) is derived in a much simpler but less rigorous manner. The dispersion relation expressed by equation (116) is discussed further in the next section and is solved subsequently.

Discussion of the Transverse Wave Dispersion Relation for $\vec{k} \parallel \vec{B}$

If one goes through the derivation of the dispersion relation (eq. (116)) carefully, it is apparent that the integral term in equation (14) has no contribution as was shown in reference 45. This condition is true only for an isotropic collision process and for transverse waves propagating parallel to the magnetic field. Hence, the collision model

$$\left(\frac{\partial f}{\partial t}\right)_{coll} = \nu(v)\left[f_0(\vec{v}) - f(\vec{v})\right] \tag{118}$$

will give the identical dispersion relation. If there is no velocity dependence of the collision frequency in equation (118), then the constant collision frequency model of Allis is obtained. Hence, the dispersion relation for constant collision frequency is obtained merely by setting ν equal to a constant in equation (116). This model is often used because of its relative simplicity both in derivation and solution. In the case of a Maxwellian electron distribution function, that is, equation (75), it is found in appendix N that this model yields the dispersion relation

$$D_{\pm}(\omega,k) = 1 - \left(\frac{ck}{\omega}\right)^2 + \frac{\omega_p^2}{\omega k v_0} Z\left(\frac{\omega_\nu \pm \omega_c}{k v_0}\right) = 0 \tag{119}$$

where $Z(\lambda_0)$ can be written in terms of the complex conjugate of the Fried function (ref. 35) (plasma dispersion function) by

$$Z(\lambda_0) = Z_F^*(\lambda_0^*) \tag{120}$$

This dispersion relation has been previously obtained by Scarf (ref. 46), Lee (ref. 47), and others.

In order to show how the dispersion relation given by equation (108) or (116) determines the propagation characteristics of waves, it may be assumed that there is present a localized driving force given by

$$\vec{j}_{ext} = \left[j_x(t)\,\hat{e}_x + j_y(t)\,\hat{e}_y\right]\delta(z) \tag{121}$$

Substituting this equation and equation (110) into Maxwell's equations and performing appropriate manipulations yields

$$E_{\pm}(\omega,k) = \frac{i j_{\pm}(\omega,k)}{\omega \epsilon_0 D_{\mp}(\omega,k)} \tag{122}$$

where

$$E_{\pm} = E_x \pm iE_y$$

and

$$j_{\pm} = j_x \pm ij_y$$

Hence, it is seen that $D_-(\omega,k)$ and $D_+(\omega,k)$ represent right- and left-hand polarized waves, respectively.

When solving the dispersion relation, it is important to keep in mind that equation (116) is defined for k real and ω on a Laplace integral path. For this case the real v-axis is the proper contour as indicated. If solutions for $k(\omega$ real) are desired, it is necessary to use the appropriate analytic continuation of $D(\omega,k)$ which is found by deforming the contour in complex velocity space so that no singularities cross the contour while ω is moved from the Laplace integral path (LIP) to real frequencies.

Note that the symmetry relation

$$D_+(\omega,k) \equiv D_-^*(-\omega^*,-k^*) \tag{123}$$

is satisfied, and hence it is sufficient to consider only one of the dispersion relations: $D_-(\omega,k) = 0$ or $D_+(\omega,k) = 0$. Also note that

$$D(\omega,k) = D(\omega,-k) \tag{124}$$

thus, $k = 0$ is a saddlepoint in the k plane, and hence the roots of $D(\omega,0) = 0$ will be branch points in the ω plane. The location of these branch points in the frequency plane is of prime importance in determining the stability character of the system (refs. 23 to 26). Details are given in the next section where solutions of the dispersion relation (eq. (116)) are found.

SOLUTIONS OF THE DISPERSION RELATION FOR TRANSVERSE WAVES PROPAGATING PARALLEL TO THE MAGNETIC FIELD

In this section the dispersion relation for propagation parallel to the magnetic field is solved for several different electron distribution functions. A new collisional mode is found to be unstable for some ranges of the plasma parameters. The wave considered is the transverse-electric, circularly polarized wave known in ionospheric work as the

"whistler" wave. In solid-state plasmas it is sometimes called a "helicon" wave. Both convective and absolute instabilities are found when the electron distribution function is monoenergetic. A Lorentz gas with nitrogen neutrals is then considered and instabilities are again found when a peaked electron distribution function is considered. A Maxwellian electron distribution function is then assumed, and it is found that the wave dispersion predicted by the isotropic collision model (ref. 48) is very close to that predicted by the constant collision frequency model of Allis. An electron distribution function consisting of both peaked and Maxwellian components is briefly considered, and the stabilizing influence of the Maxwellian population is demonstrated.

Monoenergetic Electron Distribution

For the initial analysis of the dispersion relation (eq. (116)) it is assumed that the zero-order electron distribution is monoenergetic and solutions of the dispersion relation are obtained. Substituting equation (66) into equation (116) where the negative sign is chosen so that the dispersion relation represents right-hand polarized waves yields

$$D(\omega,k) = 1 - \left(\frac{ck}{\omega}\right)^2 + \frac{\omega_p^2}{\omega k v_0}\left[\frac{ih\nu}{kv_0}\left(1 - \lambda \coth^{-1}\lambda\right) - \coth^{-1}\lambda\right] = 0 \tag{125}$$

where

$$h = \left(\frac{v}{\nu}\frac{d\nu}{dv}\right)_{v=v_0}$$

$$\lambda = \frac{\omega_\nu - \omega_c}{kv_0}$$

$$\nu = \nu(v_0)$$

This dispersion relation was also derived and solved by Suzuki (ref. 15) but here a somewhat more detailed analysis of the stability of the waves is given.

Note that $\coth^{-1}\lambda$ is a multivalued function of λ; therefore, equation (125) has an infinite set of roots. However, later it will be shown that only those roots on the principal sheet are of physical interest. As v_0 goes to zero, equation (125) approaches the familiar cold plasma dispersion relation

$$D(\omega,k) = 1 - \left(\frac{ck}{\omega}\right)^2 - \frac{\omega_p^2}{\omega(\omega - \omega_c)} = 0 \tag{126}$$

consisting of the upper and lower electromagnetic fast-wave branches and the slow-wave whistler mode.

The dispersion relation given by equation (125) has been solved under conditions approximating those in the ionosphere at an altitude of 80 km, that is, $\omega_p = 2\omega_c$ and $\nu = 0.06\omega_c$. Nitrogen exhibits a resonance scattering (ref. 39) such that $h \approx 5$ at $mv_0^2/2e = 1.5$ eV. By using these values, the results of figure 14 that show the real part of the complex frequency as a function of k real are obtained. The upper, lower, and whistler branches (U, L, and Wh1, respectively) deviate only slightly from their cold plasma values. The Wh2 mode is a new collisional mode not predicted by cold plasma theory and first recognized by Suzuki (ref. 15). It has a very small group velocity and hence represents a plasma resonance. When either h or v_0 approaches zero, this mode has the solution $\omega = \omega_c + i\nu$ for all k. The major difference between the solution in figure 14 and the cold plasma solution is the mapping of the roots, Wh1 and Wh2,

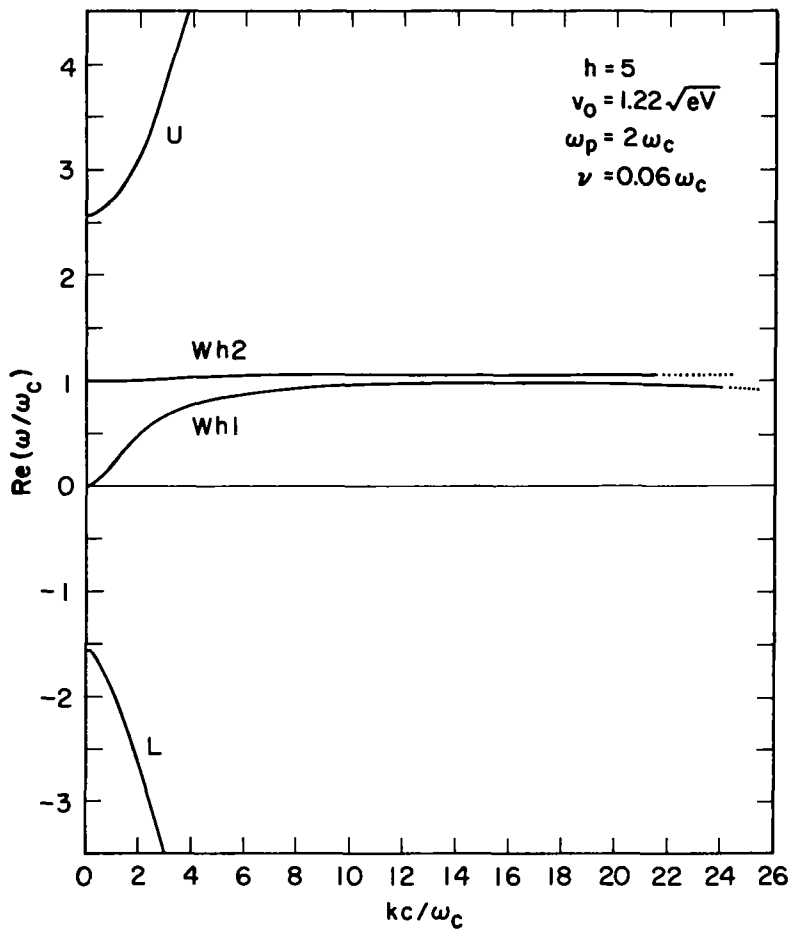

Figure 14.- Brillouin diagram, $Re(\omega)$ plotted against k real. Dotted line represents higher order sheet.

onto higher order Riemann sheets as k becomes sufficiently large. This mapping is shown for the mode Wh1 in figure 15 where the real k axis is mapped into the complex ω plane by the dispersion relation with $h = 0$. In order to understand the behavior of this root, note that $\coth^{-1}\lambda$ has a branch cut connecting the points at $\lambda = \pm 1$. If as k varies, the ω root moves in such a manner that λ crosses the real axis between +1 and -1, the appropriate analytic continuation of $\coth^{-1}\lambda$ must be used. By writing ω in terms of λ,

$$\omega = \omega_c + i\nu + \lambda k v_0 \tag{127}$$

and taking the branch cut to be on the real axis in the λ plane, it is seen that in the ω plane the cut for k real goes from $\mathrm{Re}(\omega) = \omega_c - kv_0$ to $\mathrm{Re}(\omega) = \omega_c + kv_0$ along the line $\mathrm{Im}(\omega) = \nu$. Hence, whenever the ω root crosses this line, λ must go onto another Riemann sheet. For the case shown in figure 15, it was found that the root oscillates with extremely small excursions about the branch line $\mathrm{Im}(\omega) = \nu$ and thereby goes onto successively higher order Riemann sheets. However, once the root leaves the principal sheet, it no longer needs to be considered explicitly, since in constructing a Green's function, this root would be taken into account by an integration around a branch cut. This phenomenon was explained in more detail by Derfler (ref. 14) for the case of electrostatic waves in an isotropic Lorentz gas.

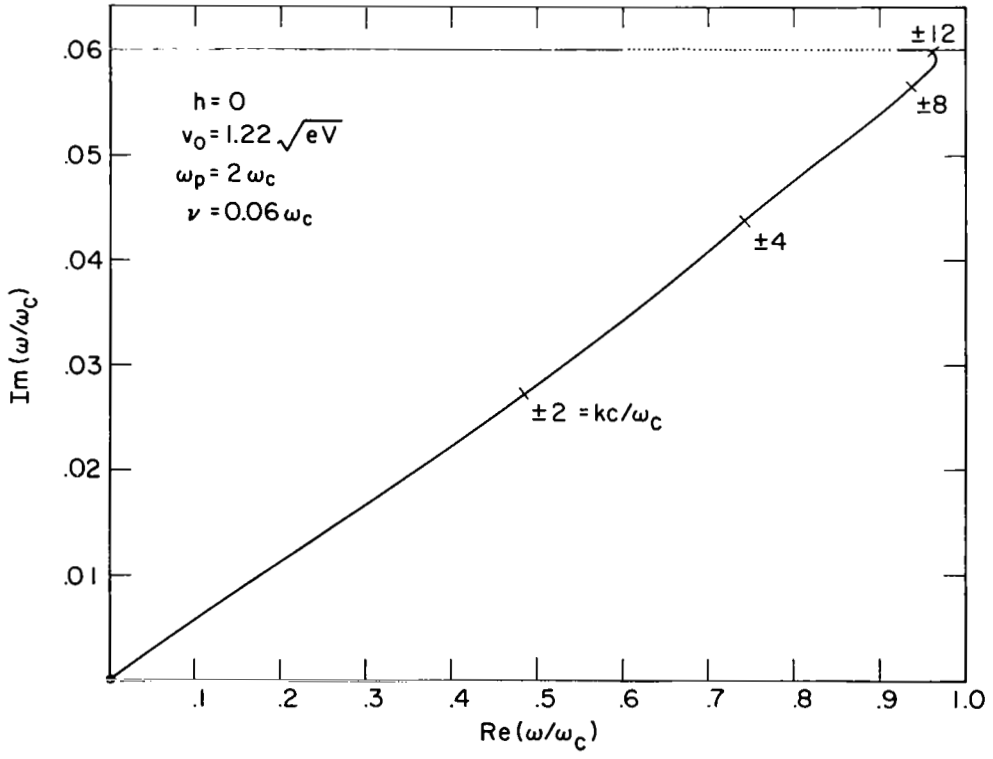

Figure 15.- Locus of real wavenumber k in the frequency plane for mode Wh1. Dotted line represents higher order sheets.

In figure 16, results are presented for the case $h = \pm 3$ and $h = \pm 5$ where the real k axis is mapped into the complex frequency plane for both the Whl and Wh2 modes.

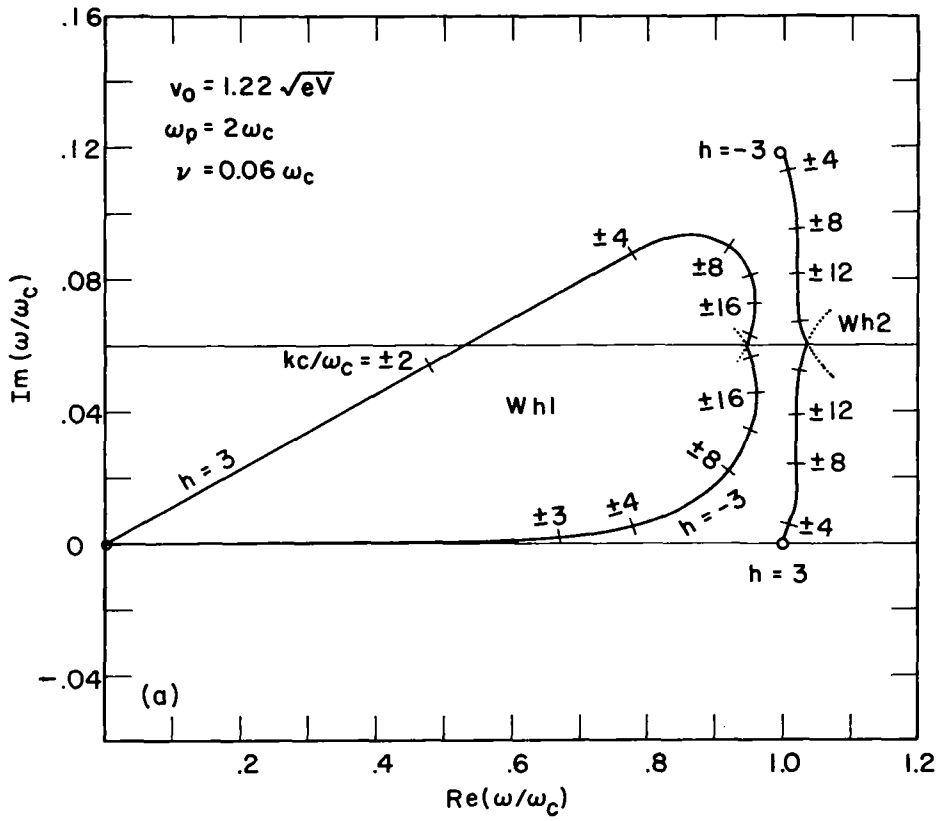

Figure 16.- Locus of real wavenumber k in the complex frequency plane for modes Whl and Wh2. Dotted line represents higher order sheets.

In figure 16(a) the roots never dip into the lower half plane; thus, it is concluded that no instabilities exist for that case. In figure 16(b) it is seen that for $h = 5$, the mode Wh2 has a branch point with $\mathrm{Re}(\omega) \approx \omega_c$ in the lower half plane and indicates an absolute instability, whereas for $h = -5$, the mode Whl dips into the negative half plane and indicates a convective instability (refs. 23 to 26). A similar mapping for the fast electromagnetic modes in figure 17 shows that both branches become absolutely unstable for $h \lessapprox -3$.

Negative values of h less than -3 are seldom realized in nature, and therefore, the new collisional mode Wh2 is considered more important for this analysis as it goes unstable for values of $h \gtrsim 3$. Since a value of $h = 5$ is characteristic of the resonance scattering peak near $mv_0^2/2e = 1.5$ eV in nitrogen, $h = 5$ was chosen to investigate the growth rate $\mathrm{Im}(\omega)$ of the Wh2 mode at $k = 0$. The growth rate is given by the

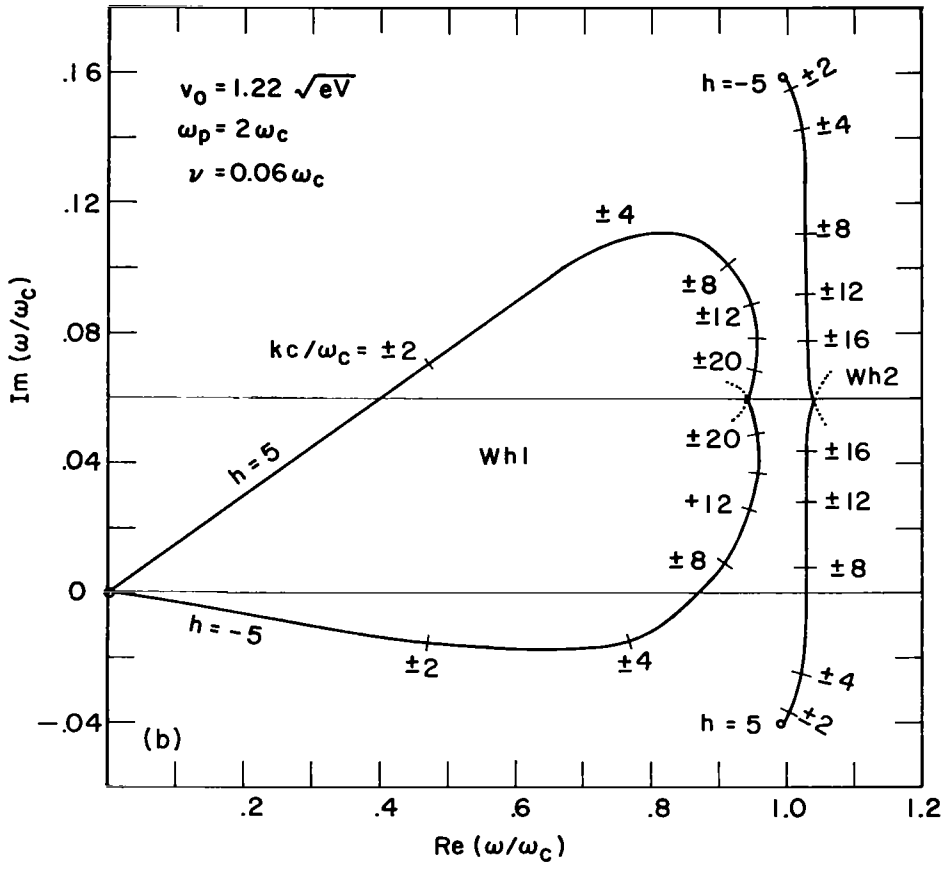

Figure 16.- Concluded.

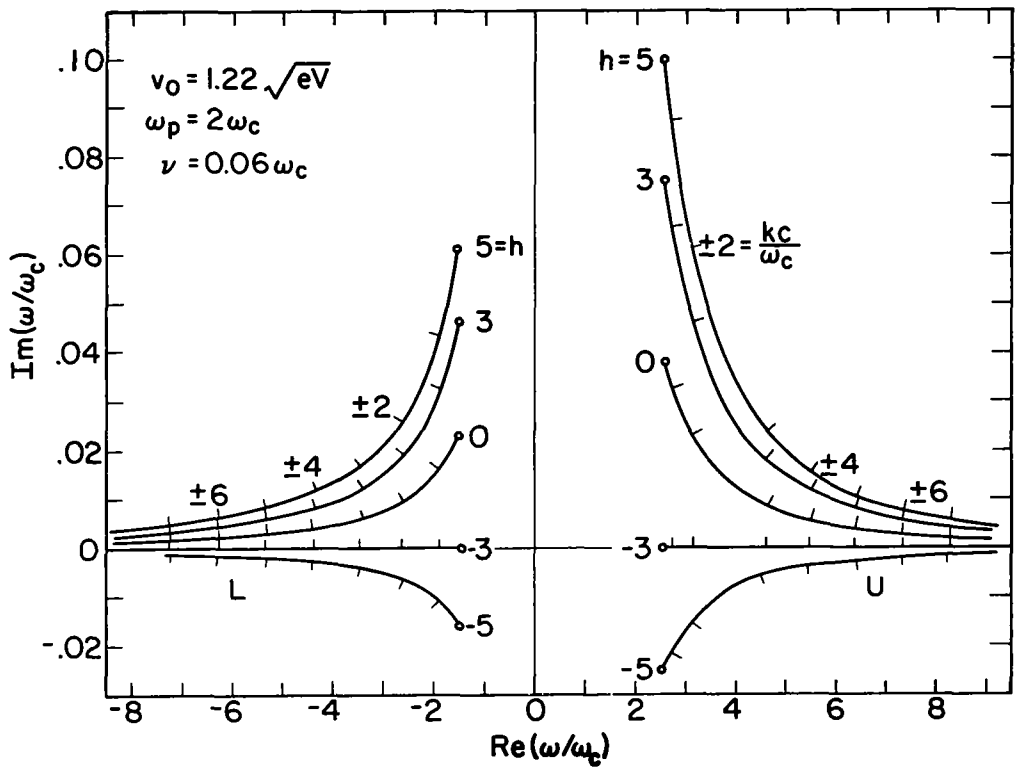

Figure 17.- Locus of real wavenumber k in the complex frequency plane for modes U and L.

solution of equation (125) with $k = 0$, that is, by

$$\omega - \omega_p^2(ih\nu/3)\left(\omega_\nu - \omega_c\right)^{-2} - \omega_p^2\left(\omega_\nu - \omega_c\right)^{-1} = 0 \tag{128}$$

In figure 18, the growth rate $\mathrm{Im}[\omega(k = 0)]$ is shown as a function of ν with ω_p as a parameter. Instabilities with an e-folding time of 1 cyclotron period are easily obtained with the parameters $\omega_p > \omega_c$ and $\nu > 0.2\omega_c$. Such values can be obtained in laboratory plasmas in the range of 0.1 to 10 mm Hg (13.33 to 1333 N/m^2). The lower left-hand corner of the diagram is typical of the conditions in the lower ionosphere in which deviations from a Maxwellian equilibrium are known to occur (refs. 49 and 50). It is therefore possible that collisional instabilities of this type arise in nature.

Equation (128) can be rearranged to yield a third-order polynomial in ω. The exact locations of the roots will depend on the plasma parameters chosen but for a large variety of cases it is found that the real parts on the roots were near ω_c and $\omega_c/2 \pm \left(\omega_c^2/4 + \omega_p^2\right)^{1/2}$. If either ν or h goes to zero, the order of equation (128) is reduced by 1. The root with real part near ω_c vanishes, and hence it is concluded that this mode was introduced by collisions.

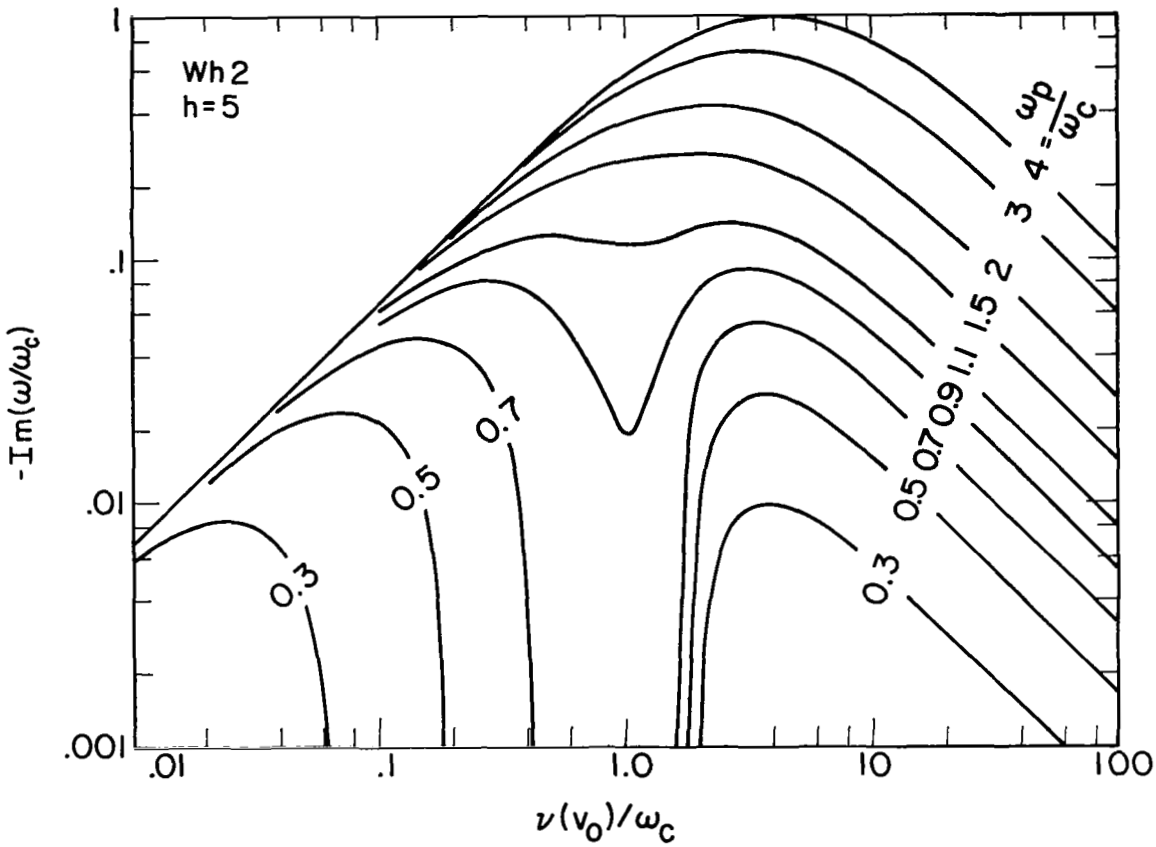

Figure 18.- Growth rate $Im(\omega)$ of Wh2 mode at infinite wavelength as a function of collision frequency ν. $Re(\omega) \approx \omega_c$.

Peaked Electron Distribution

Equation (116) was solved for a monoenergetic electron distribution function and instabilities were found for certain ranges of the slope parameter h. In particular, it was found that for $h \gtrsim 3$, there was an unstable mode (Wh2) with $\omega \approx \omega_c$. For $h \lesssim -3$ three unstable modes, a whistler mode (Wh1) and the two fast modes (U and L), were found. Hence, one concludes that collisional instabilities of this type will be found in a plasma if there are present (1) a background of neutrals that has $|h| > 3$ over a region or regions in velocity space and (2) a sharply peaked electron distribution function centered in one of these regions. As was done previously, the experimental electron-neutral collision cross section for nitrogen (eq. (72)) is used. To meet the second criterion, again the peaked distribution function described earlier and given by equation (73) was used.

A computer program was written to solve the dispersion relation (eq. (116)). The velocity integral was performed numerically by using a Gauss quadrature rule. (See appendix G). The integrand has a branch cut between the points $\lambda = 1$ and $\lambda = -1$, and

upon mapping this line into velocity space, six distinct branch cuts are found. The proper contour is found by requiring that the real v-axis from zero to infinity be a valid contour when k is real and when ω is on a Laplace integral path (LIP). Generally, the real v-axis from zero to infinity was found to be a valid contour for other ω and k, but occasionally it was necessary to deform the contour as described in appendix I.

The real k-axis was mapped into the complex frequency plane (fig. 19) to determine the locations and types of instabilities. As expected, the new collisional mode was unstable when s was sufficiently large, and when v_0 was located on the positive slope of the collision frequency curve. No instabilities were found when v_0 was located on the negative slope of the collision frequency curve, as numerical difficulties were encountered before the half-width of the distribution function could be made small enough. The instability of the mode with $\mathrm{Re}(\omega) \approx \omega_c$ was investigated more fully, and the curves in figure 20 giving the boundaries in the s,v_0 plane between the stable, convectively unstable, and absolutely unstable cases were obtained. For the points A and B in figure 20, the real k axis maps into the complex frequency plane as shown in figure 21. In figure 22 the electron distribution function is shown plotted for the points C and D in figure 20.

The value of the collision frequency chosen for these figures, that is, $\nu_\infty = 5.26\omega_c$, represents conditions in the lower ionosphere. Note that ν_∞ is the collision frequency

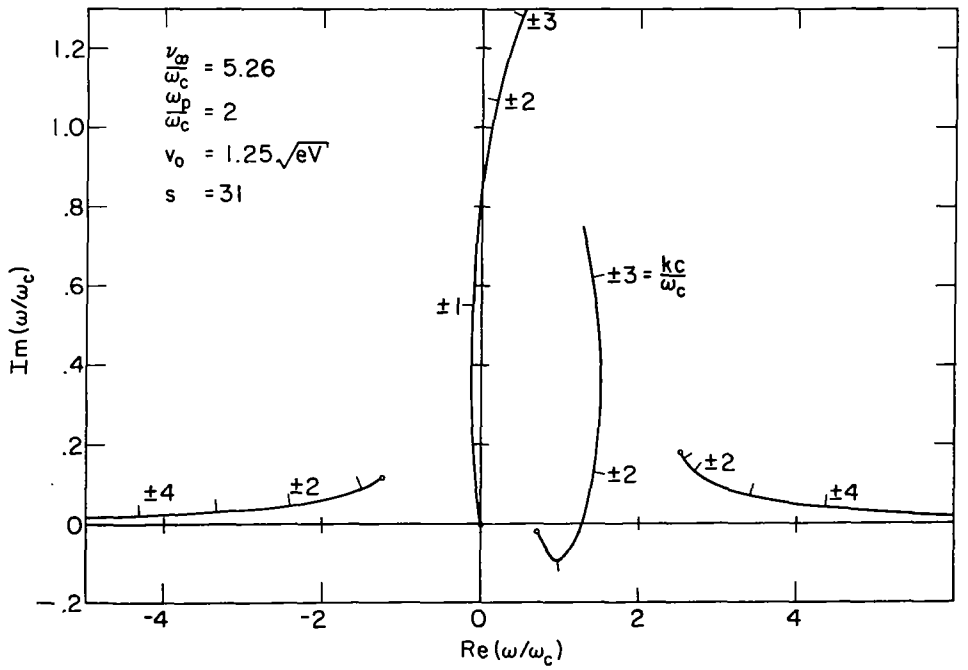

Figure 19.- Real k axis mapped into the complex frequency plane for peaked electron distribution. Plot shows absolutely unstable waves.

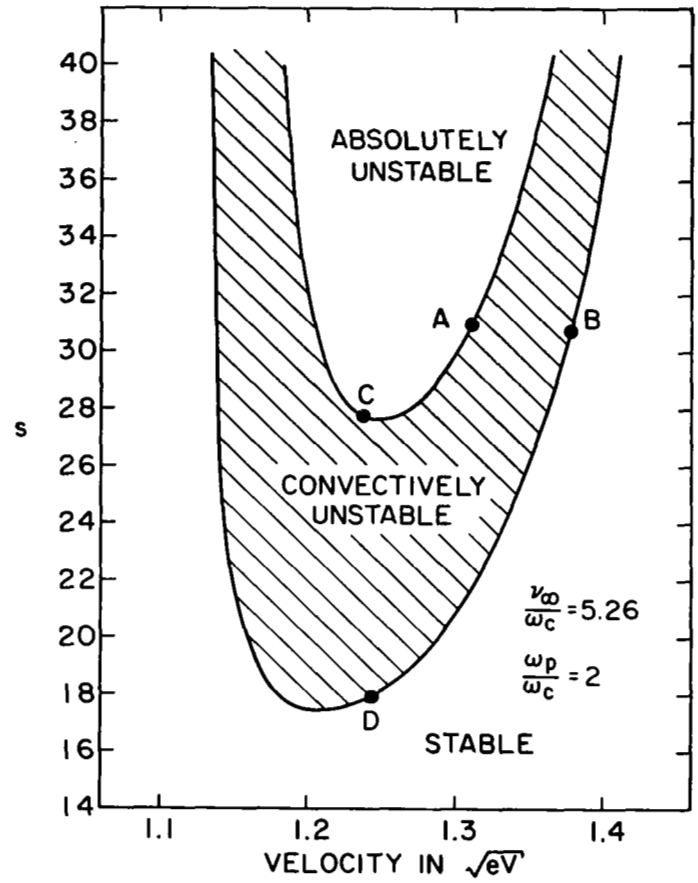

Figure 20.- Stability of Wh2 mode as a function of distribution function parameters.

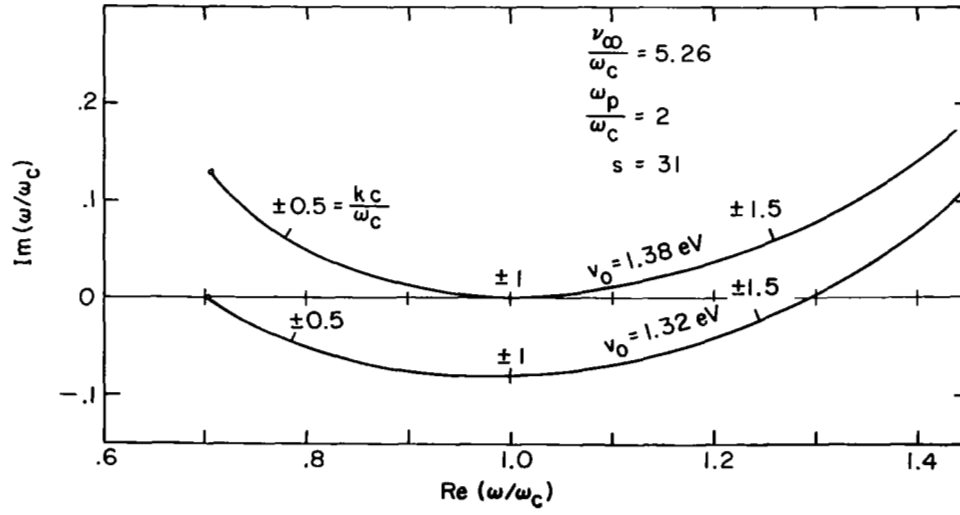

Figure 21.- Real wavenumber axis mapped into the complex frequency plane for distribution function parameters on boundaries of regions in figure 20. Points A and B.

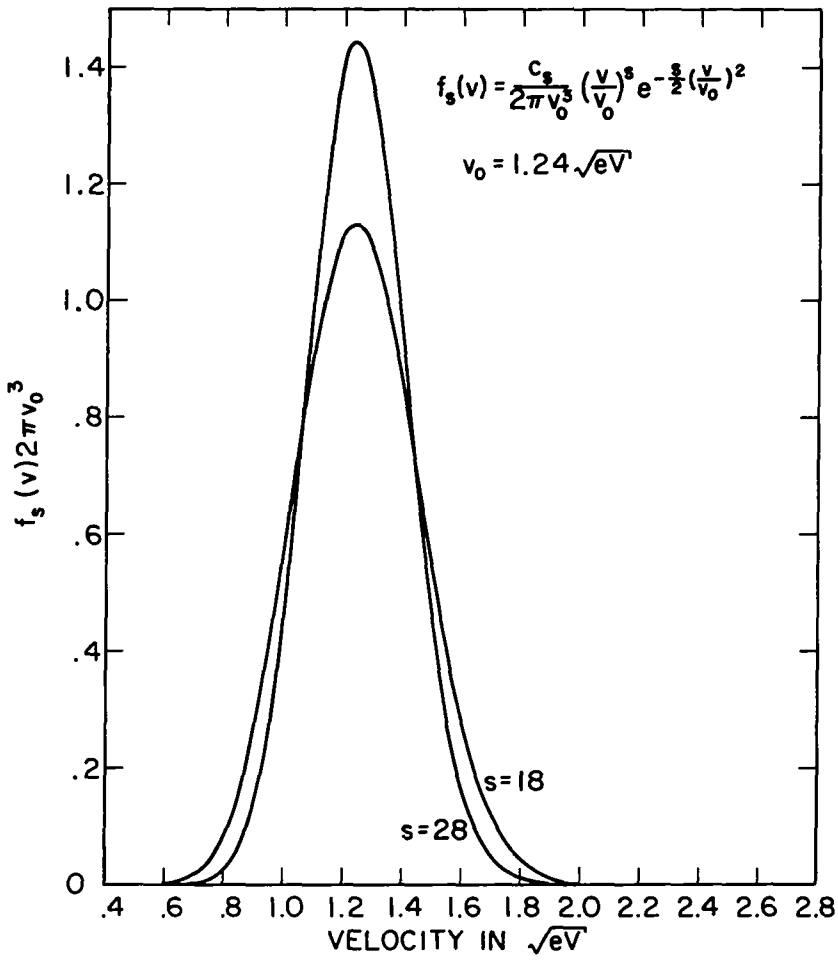

Figure 22.- Normalized peaked distribution function for points on boundaries of regions in figure 20. Points C and D.

at infinite electron velocity. If the collision frequency is averaged over a realistic electron distribution function, the average collision frequency will be on the order of $2\omega_c$. This value is perhaps on the high side of the range of values found in the ionosphere but lower values of ν_∞ will only change the strength of the instability and will not, for example, cause the case presented in figure 19 to become stable. It should be noted, however, that in the collisionless limit the collisional mode at $\omega \approx \omega_c$ in figure 19 vanishes, and the plasma is stable. Since the plasma is also stable in the collisional limit, there is some intermediate ν_∞ (and hence a neutral particle density) at which the collisional mode is most unstable.

For either stable or convectively unstable waves, the mapping of real ω into the wavenumber plane is of interest as this case is the steady-state situation often investigated in the laboratory. In figures 23 and 24, Brillouin diagrams that result from such mappings are shown. For comparison, the prediction of the constant collision frequency

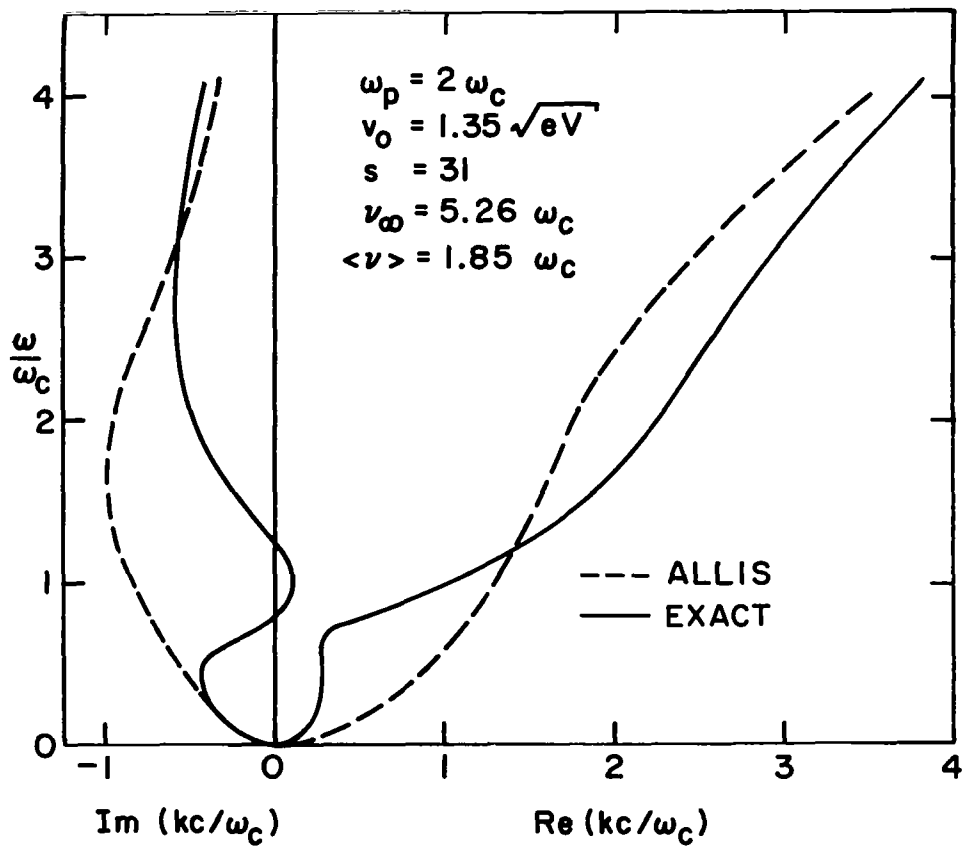

Figure 23.- Brillouin diagram giving Re(k) and Im(k) as a function of ω real for a convectively unstable case.

model of Allis obtained by using equation (10) for the collision term is also shown. The value of the collision frequency used in this model was the average over the distribution function, that is, equation (77). The exact theory predicts a convective instability for the case presented in figure 23 since Im(k) goes positive near $\omega = \omega_c$.

Figure 24(a) is a similar case that is stable because of the slightly higher v_0. Figures 24(b) and 24(c) are similar to figure 24(a) except that the collision frequencies are, respectively, one-fifth and one-tenth of those in figure 24(a). In figure 24(c) the collisionless limit is also shown and from the sequence figure 24(a) to figure 24(c) it is possible to see how the curves are approaching the proper collisionless limit.

Comparison of the Allis model and the exact theory shows that the discrepancies are rather large. Particularly near $\omega = \omega_c$, the exact theory predicts decreased damping and, in some cases, instabilities. Hence, it is seen that for non-Maxwellian electron distribution functions, it is necessary to treat collisions rigorously to obtain the correct wave dispersion.

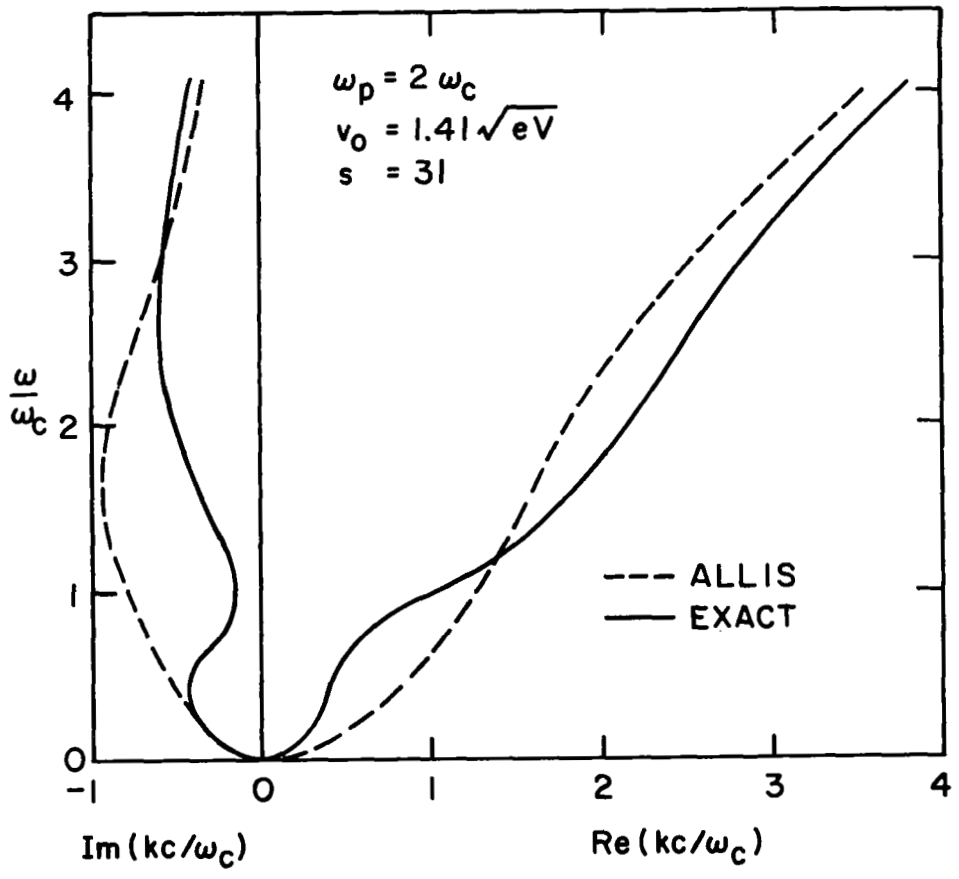

(a) $\nu_\infty = 5.26\omega_c$; $\langle\nu\rangle = 2.04\omega_c$.

Figure 24.- Brillouin diagram giving Re(k) and Im(k) as a function of ω real for a stable case.

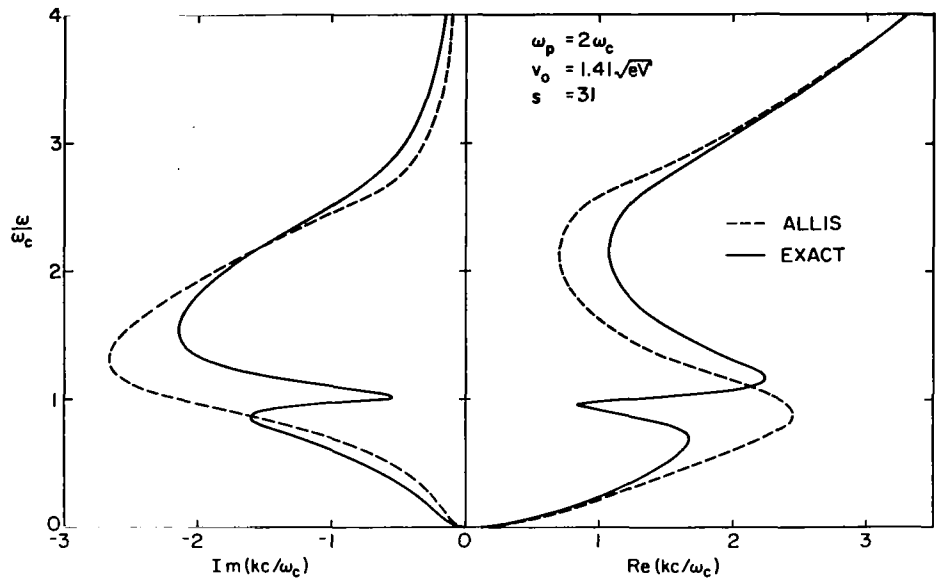

(b) $\nu_\infty = 1\omega_c$; $\langle\nu\rangle = 0.39\omega_c$.

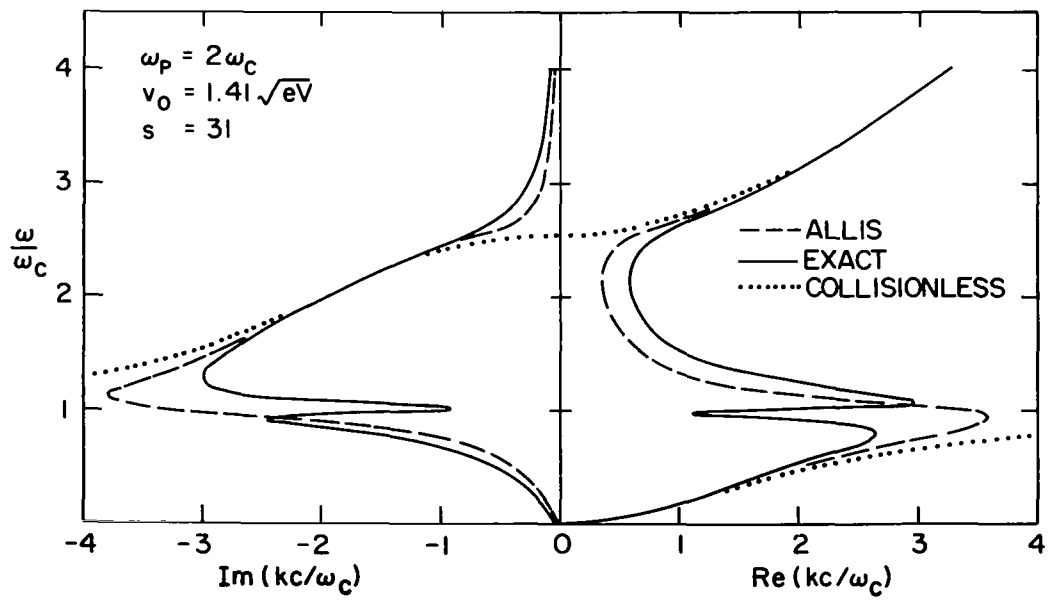

(c) $\nu_\infty = 0.5\omega_c$; $\langle\nu\rangle = 0.19\omega_c$.

Figure 24.- Concluded.

Maxwellian Electron Distribution

A Maxwellian electron distribution (eq. (75)) was then assumed and equation (116) was solved by use of the same collision frequency function. Since no instabilities were expected, the real frequency axis was immediately mapped into the wavenumber plane to obtain the Brillouin diagrams shown in figures 25(a) and 25(b). Again, the predictions of the constant-collision-frequency Allis model are shown for comparison purposes. The average of the velocity-dependent collision frequency as defined by equation (77) was used in this model.

The agreement between these two models is clearly good. Several other cases were calculated and the agreement between the two models was similar to the cases presented here. Hence, it would seem that if a Maxwellian electron plasma is being considered, the dispersion relation given by equation (119) should be satisfactory for most purposes. One could then use the very fast existing computer program for the plasma dispersion function developed by Derfler and Simonen (ref. 51).

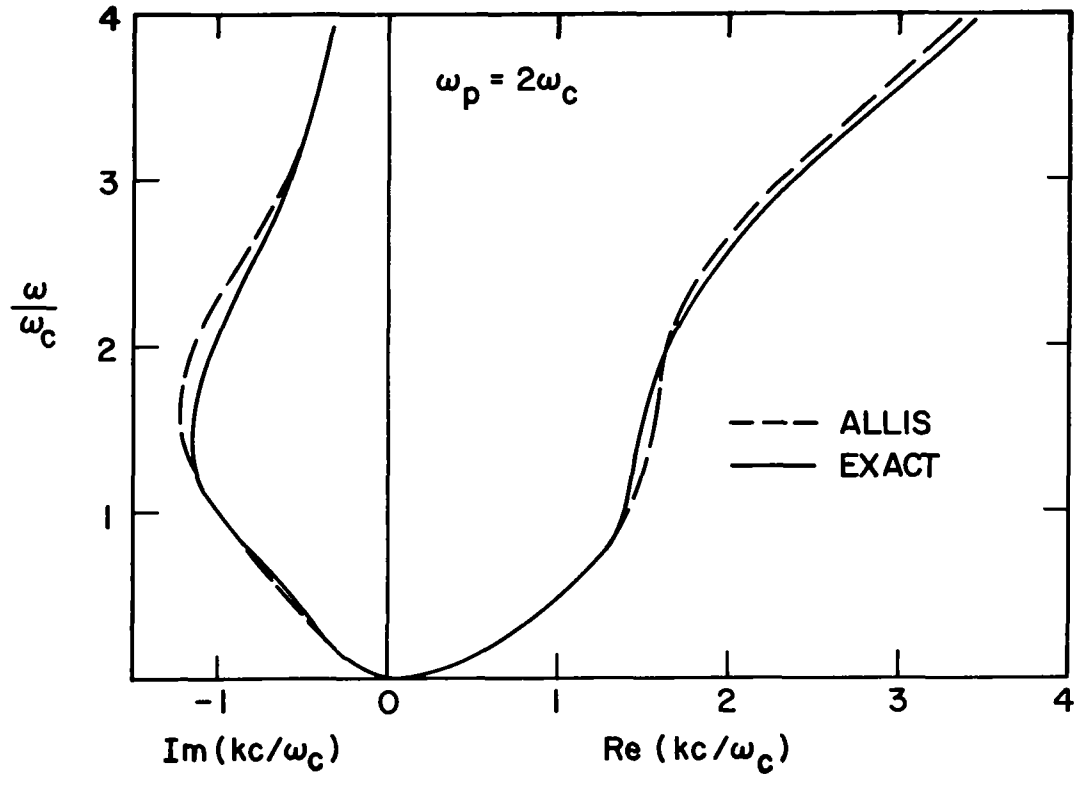

(a) $v_0 = 1.41\sqrt{eV}$; $\nu_\infty = 5.26\omega_c$; $\langle\nu\rangle = 1.42\omega_c$.

Figure 25.- Brillouin diagram giving Re(k) and Im(k) as a function of ω real for a Maxwellian electron distribution.

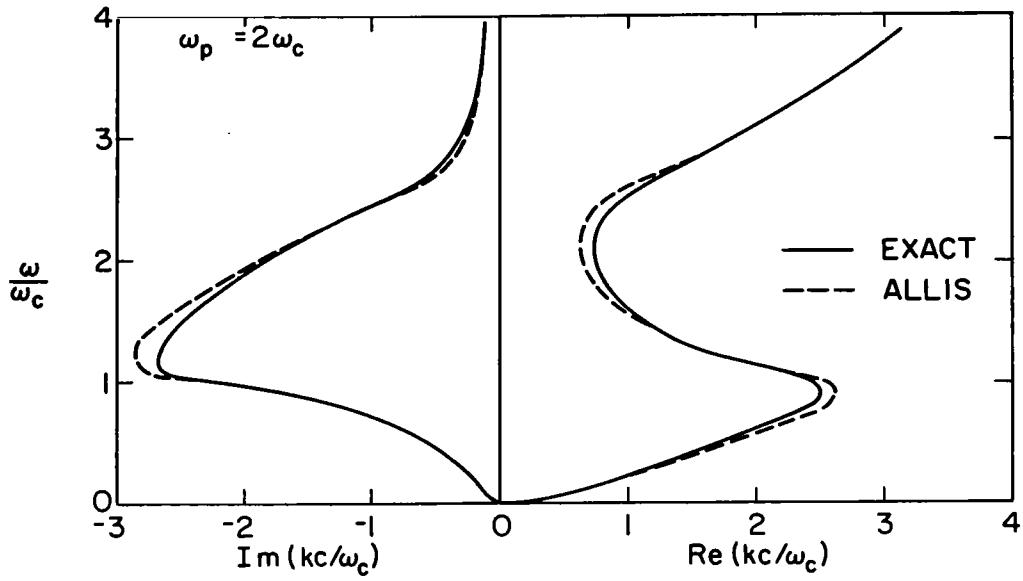

(b) $v_0 = 2\sqrt{eV}$; $\nu_\infty = 1\omega_c$; $\langle\nu\rangle = 0.34\omega_c$.

Figure 25.- Concluded.

Sum of Maxwellian and Peaked Electron Distributions

Since it was found that a peaked electron distribution may be unstable, one naturally wonders how great would be the stabilizing influence of a Maxwellian electron population when added to a peaked distribution. To answer this question, equation (78) was again used as the electron distribution function. For the peaked component, parameters were used that were known to lead to an absolute instability, that is, those used in figure 19. The stability of the waves at various values of α and v_1 was then investigated. The results are shown plotted in figure 26. From this figure it can be seen that the stabilizing influence of the Maxwellian population is critically dependent on the temperature of the Maxwellian. Since absolute instabilities occur at zero group velocity, that is, $\partial\omega/\partial k = 0$, it is not surprising to find that low-temperature Maxwellians have more of a stabilizing influence because of the larger number of low-velocity electrons. Comparison of figures 26 and 12 shows that the Maxwellian population required for stabilization is much less for transverse waves propagating parallel to the magnetic field than for longitudinal waves traveling perpendicular to the magnetic field. In figure 27 the electron distribution function for a case on each boundary in figure 26 (points A and B) has been plotted. Note that both cases are very much dominated by the peaked population of electrons.

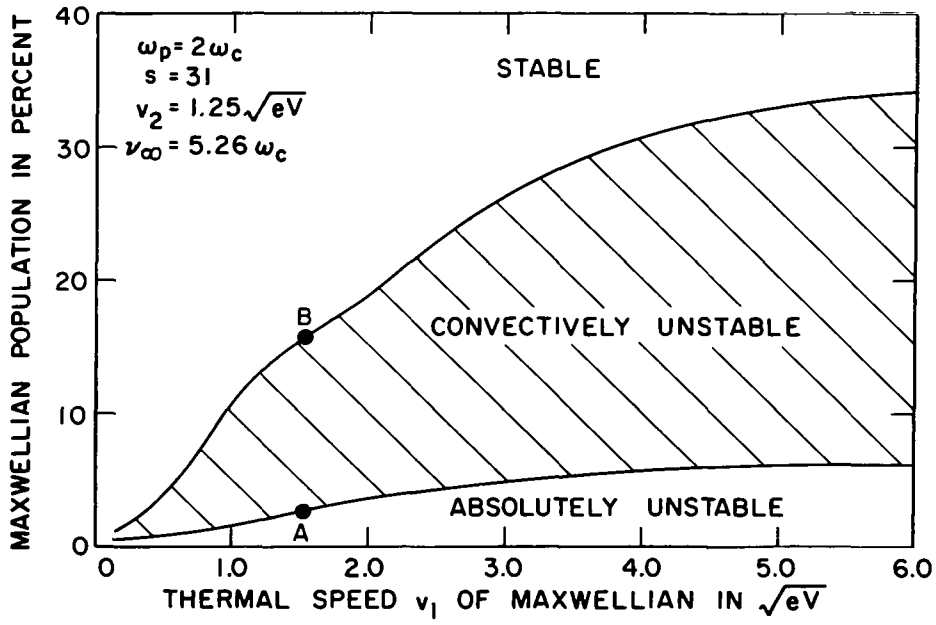

Figure 26.- Stability plot for peaked plus Maxwellian distribution function. Mode with $\mathrm{Re}(\omega) \approx \omega_c$.

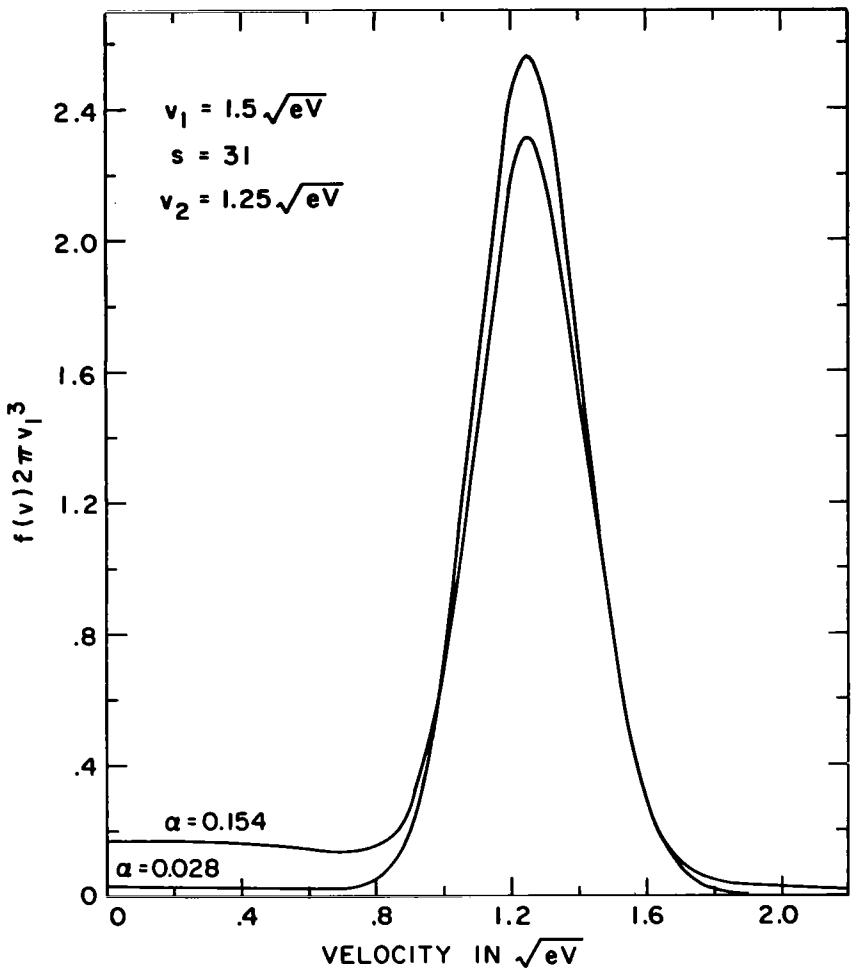

Figure 27.- Normalized distribution function consisting of peaked and Maxwellian components (eq. (78)). Points A and B in figure 26.

Synopsis of Numerical Results

Briefly, it has been found that a rigorous treatment of electron-neutral collisions in a non-Maxwellian Lorentz magnetoplasma predicts a new mode as well as the usual modified collisionless modes. This new mode vanishes both in the Maxwellian and collisionless limits and may cause the plasma to be unstable under some conditions. This instability may be either convective or absolute and occurs at frequencies near the cyclotron frequency. The modified collisionless modes were also found to be unstable for some plasma parameters. It is known (ref. 47) that in the collisionless limit the transverse electromagnetic waves considered in this section are stable; therefore, the instabilities investigated here are a result of the electron-neutral collision process.

DISCUSSION

The purpose of this report was to determine rigorously the effects of collisions on electron waves in a weakly ionized magnetoplasma. The waves were assumed to propagate in an electron plasma with infinitely heavy neutrals and ions. By using this model (usually called the Lorentz gas model), the linearized Boltzmann equation was solved with the collision integral and the conductivity tensor was derived. The dispersion relations for waves propagating both perpendicular and parallel to the magnetic field were then derived from Maxwell's equations and solved for a number of cases of general interest. It was found that the plasma supported a new class of collisional modes if (1) the collision frequency was velocity dependent, and if (2) the electron distribution function had a region in velocity space where $\partial f_0/\partial v > 0$. These new modes could be unstable if a large proportion ($\gtrsim$ 70 percent) of the electrons were located in a region in velocity space where the collision frequency increased (or decreased) rapidly.

For waves propagating perpendicular to the magnetic field, that is, $\vec{k} \perp \vec{B}$, the collision model assumed allows for an isotropic velocity-dependent electron-neutral collision cross section, and two uncoupled dispersion relations were derived. One described a modification of waves known in cold plasma theory as ordinary waves since they are unaffected by the magnetic field in that limit. The other described extraordinary waves and has slow wave solutions known variously as cyclotron, Bernstein, electrostatic, or longitudinal waves. In the collisionless limit, this dispersion relation yields an equation equivalent to that of Bernstein (ref. 29), whereas in the limit of zero magnetic field Drummond's results (ref. 13) are recovered. When both the collisions and the magnetic field vanish, Landau's dispersion relation is obtained (refs. 32 and 33).

The collisional dispersion relation for $\vec{k} \perp \vec{B}$ was solved for several electron distribution functions. One series of solutions were damped modes that were modifications of the undamped collisionless electrostatic modes. Under some conditions they could be driven unstable at frequencies near zero and the hybrid frequency. In addition, a series of new collisional waves were found with real frequencies near zero and near each cyclotron harmonic. Under the proper conditions, either absolute or convective instabilities were possible at the cyclotron frequency and convective instabilities were possible at the harmonics.

Waves propagating parallel to the magnetic field were also considered, and a collision model allowing a velocity and an angle-dependent electron-neutral collision cross section led to two uncoupled dispersion relations. One described an electrostatic or longitudinal wave that was not affected by the magnetic field. This same equation was derived by Derfler (ref. 14) for an unmagnetized plasma. The second dispersion relation described a transverse wave, one mode of which is commonly called a whistler wave in

ionospheric work. This dispersion relation was solved and a new collisional mode was found near the electron cyclotron frequency. It was found that this mode could be either absolutely or convectively unstable under some conditions.

The isotropic electron distribution functions used when solving the dispersion relations were of varying physical interest. The monoenergetic distribution function was of interest primarily because it gave relatively simple equations to solve. Furthermore, the solutions were very helpful in showing the type of results to expect when more realistic distributions were used. The peaked, Maxwellian, and Maxwellian with a bump on the tail were all of much more physcial interest since these distributions are quite possible in various types of plasmas.

To actually observe and measure the wave instabilities that this theory predicts, some means has to be devised to set up a known electron distribution function with a peak of the proper width and location. The plasma could then be excited at some frequency and the complex wavenumber measured. It would not be necessary, however, to actually observe an instability to show the validity of this theory, since it has been shown that for non-Maxwellian plasmas, the predicted wave dispersal may differ greatly from that predicted by simpler collision models. For example, experiments that have been previously done in the Vlasov limit might be redone in a regime where collisional effects are important. For the electrostatic waves with $\vec{k} \perp \vec{B}$, one should look for decreased damping at frequencies just below the cyclotron harmonics. For the transverse waves with $\vec{k} \parallel \vec{B}$, the decreased damping should occur precisely at the cyclotron frequency. If these effects are observed, it should be possible to assume some model for the electron distribution function, for example, equation (78), and vary the parameters to obtain the best fit to the experimental wave dispersion data. This procedure was followed by Fields et al. (ref. 3) using an equivalent temperature approach.

Most experimenters to date have merely observed the radiation from the plasma in an attempt to observe the collisional instabilities. Tanaka and Takayama (ref. 5) and Oddou (ref. 4) and others have observed anomalous emission at the cyclotron frequency in plasmas containing the three noble gases: argon, xenon, and krypton. These gases are generally called the Ramsauer gases, and they have a region where the electron collision frequency curve is very steep. No anomalous emission was observed from plasmas containing the other two noble gases: helium and neon. These gases have relatively flat collision frequency curves, and the theory given in this report would not predict any collisional instabilities. The emission from the Ramsauer gases was called anomalous since it had an intensity many orders of magnitude larger than could otherwise be explained. These experimenters observed also that the emission occurred in bursts that had a direct relationship to an oscillation of much lower frequency. It seems likely that the low-frequency oscillation was setting up the appropriate electron distribution function

necessary for the plasma to be unstable at the cyclotron frequency. It should be noted that the radiation was observed primarily at the electron cyclotron frequency. The theory presented here predicts an absolute instability at the cyclotron frequency but not at the higher harmonics. Hence, much stronger instabilities (and hence more radiation) would be expected at the cyclotron frequency than at the harmonics.

Wachtel and Hirshfield (ref. 8) have also performed an experiment demonstrating collisional instabilities. They introduced monoenergetic electrons into a microwave cavity containing xenon. They observed negative absorption at the cyclotron frequency when the speed of the electrons was in a region in velocity space where the collision frequency had a large positive slope. By negative absorption they mean that the electrons were giving up energy to the waves in the cavity, and hence the waves were unstable.

The collision-induced instabilities investigated quantitatively in this report can be understood qualitatively by considering a very simple model. Take a wave of frequency $\omega \approx \omega_c$ propagating in a magnetoplasma consisting of monoenergetic electrons. For the case of the transverse electromagnetic waves, right circularly polarized waves with $\vec{k} \parallel \vec{B}$ are assumed, and for the electrostatic waves one has $\vec{k} \perp \vec{B}$ with $\vec{E} \parallel \vec{k}$. Assume that there are N electrons in the plasma. A little thought will show that in the beginning for either direction of propagation, $N/2$ electrons will be gaining energy from the wave and $N/2$ electrons will deliver energy to the wave. After a given length of time, Δt, let C_G be the number of electrons that had a collision with a neutral while gaining energy. Of those electrons, $C_G/2$ will be gaining (or losing) energy after the collision since the collision will tend to randomize momenta. Likewise, let C_L be the number of electrons that have a collision while losing energy. After time Δt, the number of electrons that are gaining energy is

$$N_G = \left(\frac{N}{2} - C_G\right) + \frac{C_G}{2} + \frac{C_L}{2} = \frac{N}{2} + \frac{C_L}{2} - \frac{C_G}{2} \tag{129}$$

and the number of electrons that are losing energy is

$$N_L = \left(\frac{N}{2} - C_L\right) + \frac{C_G}{2} + \frac{C_L}{2} = \frac{N}{2} - \frac{C_L}{2} + \frac{C_G}{2} \tag{130}$$

If more electrons are losing energy, then the wave must be gaining energy and hence is unstable. Hence, assume that $N_L > N_G$; equations (129) and (130) then yield $C_G > C_L$. But the number of electrons that collide in a given time is proportional to the collision frequency, thus, $\nu(v + \Delta v) > \nu(v - \Delta v)$. Hence, the collision frequency must have a positive slope for the plasma to support an unstable wave at the cyclotron frequency. Earlier, it was found that these wave instabilities were indeed present only if the slope

parameter was positive and large enough. Because of the extreme simplicity of the model considered here, it is not surprising that the agreement is qualitative in nature and not quantitative. It is also interesting to note that this simple argument predicts instabilities for $\omega = \omega_c$ but not for $\omega = n\omega_c$ ($n = 2,3,4,\ldots$). It may be recalled that solutions of the dispersion found earlier sometimes predicted absolute instabilities at the cyclotron frequency but never at any of the harmonics.

The theory given in this report appears to be the most accurate and extensive to date concerning the effects of electron-neutral collisions on high frequency waves in a magnetoplasma. The model assumed is that of a plasma of electrons colliding only with infinitely heavy neutrals, and since all ion effects are ignored, this theory is valid for frequencies somewhat above the ion plasma and ion cyclotron frequencies. By using the techniques described in this report, it is possible to solve the dispersion relations for essentially any electron distribution function, and by working backward one might be able to calculate the electron distribution function or the collision frequency function when given the experimentally measured wave dispersion. The equations derived and the techniques described in this report should be particularly applicable to wave propagation through and radiation from plasmas containing especially the Ramsauer gases (Ar, Xe, and Kr) since the electron-neutral collision cross sections in these gases are such that large collisional effects on waves are both expected and observed.

CONCLUDING REMARKS

The Boltzmann equation with collision integral was solved and the wave dispersion relations for electron waves propagating both parallel and perpendicular to the magnetic field were obtained. A Lorentz gas magnetoplasma was the model assumed. This model requires (1) that the ions are infinitely heavy and (2) that the electrons are colliding only with infinitely heavy neutrals. Numerical solutions to the wave dispersion relations were obtained, and for both directions propagation the electron waves could be unstable if a large fraction of the electrons had a velocity in a region where the electron-neutral collision frequency increases (or decreases) rapidly enough.

Langley Research Center,
National Aeronautics and Space Administration,
Hampton, Va., May 4, 1971.

APPENDIX A

SOLUTION OF ZERO-ORDER BOLTZMANN EQUATION

In this appendix it is shown that any isotropic distribution $f_0(|\vec{v}|)$ is a solution of the zero-order Boltzmann equation (eq. (16)) which in spherical coordinates becomes

$$\omega_c \frac{\partial f_0(\vec{v})}{\partial \varphi} = -\nu f_0(\vec{v}) + \frac{\nu}{4\pi} \int f_0(\vec{v}') d\Omega' \tag{A1}$$

where $\vec{B}_0$ is taken equal to $B_0 \hat{e}_3$. Let us write $f_0(\vec{v})$ as a spherical harmonic expansion in velocity space

$$f_0(\vec{v}) = \sum_{l=0}^{\infty} \sum_{m=-l}^{l} f_{l,m}(v)\, Y_{l,m}(\theta,\varphi) \tag{A2}$$

Substituting equation (A2) into equation (A1) yields

$$\sum_{l,m} f_{l,m}(v)\, Y_{l,m}(\theta,\varphi)\left(im\omega_c + \nu\right) = \frac{\nu f_{0,0}}{\sqrt{4\pi}} \tag{A3}$$

For a nonzero ν, this relation is satisfied only by $f_{l,m} = 0$ for all l and m except $l = m = 0$. Hence, from equation (A2),

$$f_0(\vec{v}) = f_{0,0}(v) \tag{A4}$$

and the zero-order Boltzmann equation with isotropic collisions is satisfied by any isotropic distribution function. From equation (A3) if $\nu = 0$, one can also see that the solution then becomes $f_0(v_\parallel, v_\perp)$, but this case is not considered in this report. This same technique can be applied to the zero-order Boltzmann equation with anisotropic collisions (eq. (81)) to show that its solution is also any isotropic distribution function $f_0(|\vec{v}|)$.

APPENDIX B

DERIVATION OF FIRST-ORDER DISTRIBUTION FUNCTION FOR ISOTROPIC SCATTERING

In this appendix the equations

$$i\left(\omega_\nu - \vec{k} \cdot \vec{v}\right) f_1 + \frac{df_1}{d\tau} = h(\vec{v}) \tag{B1}$$

and

$$\frac{d\vec{v}(\tau)}{d\tau} = -\left(\vec{v} \times \vec{\omega}_c\right) \tag{B2}$$

are solved to obtain the solution given by equation (26). By direct substitution, it is easily shown that equation (B2) is satisfied by

$$\vec{v}(\tau) = \overline{D}\left[\omega_c\left(\tau_0 - \tau\right)\right] \cdot \vec{v}\left(\tau_0\right) \tag{B3}$$

where

$$D_{ij}(\varphi) = n_i n_j + \left(\delta_{ij} - n_i n_j\right)\cos\varphi + \epsilon_{ijk} n_k \sin\varphi \tag{B4}$$

To solve equation (B1), first find the solution of the homogeneous equation

$$i\left(\omega_\nu - \vec{k} \cdot \vec{v}\right) f_H + \frac{df_H}{d\tau} = 0 \tag{B5}$$

Rearranging yields

$$\frac{d \ln f_H}{d\tau} = -i\left(\omega_\nu - \vec{k} \cdot \vec{v}\right) \tag{B6}$$

and the solution of this equation is given by

$$f_H(\tau) = \exp\left[-i\omega_\nu \tau + i \int^\tau \vec{k} \cdot \vec{v}(\tau')d\tau'\right] \tag{B7}$$

Note that $|\vec{v}(\tau)|$ is not a function of τ as can be shown from equation (B3), and hence the term $\omega_\nu(v) = \omega - i\nu(v)$ may be extracted from the integral. Now by using the method of variation of parameter, it is assumed that

$$f_1\left[\vec{v}(\tau)\right] = C(\tau)\, f_H(\tau) \tag{B8}$$

is a solution of equation (B1) and, as a result,

$$f_H(\tau)\frac{dC(\tau)}{d\tau} = h\left[\vec{v}(\tau)\right] \tag{B9}$$

After integrating,

$$C(\tau) = \int^{\tau} \frac{h\left[\vec{v}(\tau')\right]}{f_H(\tau')}\, d\tau' + \text{Constant} \tag{B10}$$

and equation (B8) then becomes

$$f_1\left[\vec{v}(\tau)\right] = \left\{\text{Constant} + \int^{\tau} \frac{h\left[\vec{v}(\tau')\right]}{f_H(\tau')}\, d\tau'\right\} f_H(\tau) \tag{B11}$$

Let $\tau = \tau_0$, solve for the constant, and obtain

$$\text{Constant} = \frac{f_1(\tau_0)}{f_H(\tau_0)} - \int^{\tau_0} \frac{h\left[\vec{v}(\tau')\right]}{f_H(\tau')}\, d\tau' \tag{B12}$$

which when substituted back into equation (B11), yields

$$f_1 = f_1(\tau_0)\frac{f_H(\tau)}{f_H(\tau_0)} + \int_{\tau_0}^{\tau} h\left[\vec{v}(\tau')\right]\frac{f_H(\tau)}{f_H(\tau')}\, d\tau' \tag{B13}$$

Then using equation (B7) yields

$$\frac{f_H(\tau)}{f_H(\tau_1)} = \exp\left[-i\omega_\nu(\tau - \tau_1) + i\int_{\tau_1}^{\tau} \vec{k}\cdot\vec{v}(\tau')d\tau'\right] \tag{B14}$$

But τ_0 is arbitrary so let τ_0 be $-\infty$, and since ω is on a Laplace integral path, it can be seen from equation (B14) that

$$\frac{f_H(\tau)}{f_H(\tau_0)} \to 0 \tag{B15}$$

Equation (B13) then becomes

$$f_1 = \int_{-\infty}^{\tau} h\left[\vec{v}(\tau')\right] \exp\left[-i\omega_\nu(\tau - \tau') + i\int_{\tau'}^{\tau} \vec{k} \cdot \vec{v}(\tau'')d\tau''\right] d\tau' \tag{B16}$$

Let

$$\left.\begin{aligned} t &= \tau - \tau' \\ t' &= \tau - \tau'' \end{aligned}\right\} \tag{B17}$$

and from equation (B3)

$$\left.\begin{aligned} \vec{v}(\tau') &= \overline{D}\left(\omega_c t\right) \cdot \vec{v}(\tau) \\ \vec{v}(\tau'') &= \overline{D}\left(\omega_c t'\right) \cdot \vec{v}(\tau) \end{aligned}\right\} \tag{B18}$$

Equation (B16) then becomes

$$f_1 = \int_0^{\infty} h\left[\overline{D}\left(\omega_c t\right) \cdot \vec{v}\right] \exp\left[-i\omega_\nu t + i\int_0^{t} \vec{k} \cdot \overline{D}\left(\omega_c t'\right) \cdot \vec{v}\, dt'\right] dt \tag{B19}$$

The integral in the exponential is evaluated and a new tensor is obtained

$$L_{ij}\left(\omega_c t\right) \equiv \omega_c \int_0^{t} D_{ij}\left(\omega_c t'\right) dt' \equiv n_i n_j \omega_c t + \left(\delta_{ij} - n_i n_j\right) \sin \omega_c t - \epsilon_{ijk} n_k \left(\cos \omega_c t - 1\right) \tag{B20}$$

and then by defining $\varphi = \omega_c \tau$, equation (B19) becomes

$$f_1(\vec{v}) = \frac{1}{\omega_c} \int_0^{\infty} e^{-\Phi(\varphi,\vec{v})} h\left[\overline{D}(\varphi) \cdot \vec{v}\right] d\varphi \tag{B21}$$

where

$$\Phi(\varphi,\vec{v}) = i\,\frac{\omega_\nu \varphi - \vec{k} \cdot \overline{L} \cdot \vec{v}}{\omega_c}$$

From equation (21),

$$h(\vec{v}) = \frac{e}{m} \vec{E}_1 \cdot \frac{\partial f_0}{\partial \vec{v}} + \frac{\nu(v)}{4\pi} \int f_1(\vec{v}')d\Omega' \tag{B22}$$

and $h\left[\overline{D}(\varphi) \cdot \vec{v}\right]$ must now be found. The integral term is a function of $|\vec{v}|$ only and so is unchanged. Also, f_0 is a function of $|\vec{v}|$; thus,

$$\frac{\partial f_0(v)}{\partial \vec{v}} = \frac{\vec{v}}{v}\frac{\partial f_0}{\partial v} = \frac{\vec{v}}{v} f_0' \tag{B23}$$

Equation (B22) then becomes

$$h\left[\overline{D}(\varphi) \cdot \vec{v}\right] = \frac{e f_0'}{mv} \vec{E}_1 \cdot \overline{D} \cdot \vec{v} + \frac{\nu}{4\pi} \int f_1(\vec{v}')d\Omega' \tag{B24}$$

and substituting equation (B24)into equation (B21) yields

$$f_1(\vec{v}) = \frac{1}{\omega_c}\int_0^\infty e^{-\Phi(\varphi,\vec{v})} \frac{e}{m} \vec{E}_1 \cdot \overline{D} \cdot \vec{v} \frac{f_0'}{v} d\varphi + \frac{\nu}{4\pi\omega_c}\int_0^\infty e^{-\Phi(\varphi,\vec{v})} d\varphi \int f_1(\vec{v}')d\Omega' \tag{B25}$$

Taking the integral $\int d\Omega'$ of this equation and rearranging yields

$$\int f_1(\vec{v}')d\Omega' = \frac{e}{m\omega_c} \frac{\int A(\vec{v}')d\Omega'}{1 - \frac{\nu}{4\pi\omega_c}\int\int_0^\infty e^{-\Phi(\varphi,\vec{v}')} d\varphi\, d\Omega'} \tag{B26}$$

where

$$A(\vec{v}') = \int_0^\infty e^{-\Phi(\varphi,\vec{v}')} \vec{E}_1 \cdot \overline{D} \cdot \vec{v}' \frac{f_0'}{v} d\varphi$$

Substituting this equation back into equation (B25) leads to

$$f_1(\vec{v}) = \frac{e}{m\omega_c}\left[A(\vec{v}) + \frac{\frac{\nu}{4\pi\omega_c}\int A(\vec{v}')d\Omega' \int_0^\infty e^{-\Phi(\varphi,\vec{v})} d\varphi}{1 - \frac{\nu}{4\pi\omega_c}\int\int_0^\infty e^{-\Phi(\varphi,\vec{v}')} d\varphi\, d\Omega'}\right] \tag{B27}$$

Thus, equation (26) has been obtained as desired.

APPENDIX C

MAXWELL'S EQUATIONS AND WAVE DISPERSION RELATIONS

Maxwell's equations may be written

$$\epsilon_0 \nabla \cdot \vec{E} = \rho \tag{C1}$$

$$\nabla \cdot \vec{B} = 0 \tag{C2}$$

$$\nabla \times \vec{E} = -\frac{\partial \vec{B}}{\partial t} \tag{C3}$$

$$\frac{1}{\mu_0} \nabla \times \vec{B} = \vec{j} + \epsilon_0 \frac{\partial \vec{E}}{\partial t} \tag{C4}$$

The Fourier and Laplace transforms of these equations are taken as defined earlier and the following equations are obtained:

$$-i\vec{k} \cdot \vec{E} = \frac{\rho}{\epsilon_0} \tag{C5}$$

$$\vec{k} \cdot \vec{B} = 0 \tag{C6}$$

$$\vec{k} \times \vec{E} = \omega \vec{B} \tag{C7}$$

$$-i \frac{\vec{k} \times \vec{B}}{\mu_0} = \vec{j} + i\omega \vec{E} \epsilon_0 \tag{C8}$$

Electrostatic Approximation

First, consider what is commonly called the electrostatic approximation. This approximation is valid for waves whose electric field is very nearly parallel to the propagation vector $\vec{k}$. The dispersion relation can now be derived from equation (C5). The charge density in the plasma is given by

$$\rho = \rho_i + \rho_e - en \int f_1(\vec{v}) d^3v \tag{C9}$$

However, for the case being considered, the ion density ρ_i is exactly canceled by the zero-order electron density ρ_e. The part that remains is a polarization charge density

that can be written as the gradient of a polarization vector

$$\rho = -\nabla \cdot \vec{P} = -en \int f_1(\vec{v}) d^3v \tag{C10}$$

Now define a polarization tensor by $\vec{P} = \bar{\pi} \cdot \vec{E}$. Taking the transforms as defined earlier yields

$$i\vec{k} \cdot \bar{\pi} \cdot \vec{E} = \rho = -en \int \hat{f}_1(\vec{v}) d^3v \tag{C11}$$

and from this equation $\bar{\pi}$ may be obtained when given $\hat{f}_1$. Substitute equation (C11) into equation (C5) to obtain the dispersion relation

$$\vec{k} \cdot \left(\bar{I} + \frac{\bar{\pi}}{\epsilon_0} \right) \cdot \vec{E} = 0 \tag{C12}$$

where $\bar{I}$ is the unit tensor. It was assumed earlier that $\vec{k}$ and $\vec{E}$ were parallel and at this point it is further assumed, without loss of generality, that $\vec{k} = k\hat{e}_1$. Then,

$$D(\omega,k) = 1 + \frac{\pi_{11}}{\epsilon_0} = 0 \tag{C13}$$

This equation is the dispersion relation used to describe electrostatic or longitudinal waves. In a plasma Landau waves (without magnetic field) and cyclotron waves (with magnetic field) are in this class.

Electromagnetic Waves

For this case nothing is assumed about the $\vec{E}$ and $\vec{B}$ vectors of the waves. However, the perturbation distribution function $f_1(\vec{v})$ is still assumed to be known, and by using

$$\vec{j} = -en \int \vec{v} f_1(\vec{v}) d^3v \tag{C14}$$

an expression for the current density in the plasma is obtained. Then the conductivity tensor $\bar{\sigma}$ defined by

$$\vec{j} = \bar{\sigma} \cdot \vec{E} = -en \int \vec{v} f_1(\vec{v}) d^3v \tag{C15}$$

is obtained. Next combine equations (C7) and (C8) to obtain the equation

$$\left[\bar{\bar{I}} + \frac{\bar{\bar{\sigma}}}{i\omega\epsilon_0} + \left(\frac{c}{\omega}\right)^2\left(\vec{k}\,\vec{k} - k^2\bar{\bar{I}}\right)\right] \cdot \vec{E} = 0 \tag{C16}$$

But for this to be true, the equation

$$D(\omega,k) = \left|\bar{\bar{I}} + \frac{\bar{\bar{\sigma}}}{i\omega\epsilon_0} + \left(\frac{c}{\omega}\right)^2\left(\vec{k}\,\vec{k} - k^2\bar{\bar{I}}\right)\right| = 0 \tag{C17}$$

must first be satisfied. Equation (C17) gives the relationship between ω and k and is the wave dispersion relation describing the waves propagating in the medium whose conductivity tensor is $\bar{\bar{\sigma}}$.

APPENDIX D

SIMPLIFICATION OF CONDUCTIVITY TENSOR FOR $\vec{k} \perp \vec{B}$

In this appendix the general conductivity tensor given by equation (34) is reduced to the form given by equation (42). This result is exact and no approximations are made. The steps needed to obtain equation (42) necessarily involve large amounts of algebraic manipulations of a generally straightforward nature; thus only a brief outline of the procedure is given here. First, G(v) given by equation (36) is evaluated, and from appendix E

$$G(v) = \frac{\omega}{\omega_\nu}\left[1 + S\left(\frac{1}{2l+1}\right)\right] \tag{D1}$$

Equation (34) then becomes

$$\sigma_{ij} = -\frac{\omega_p^2 \epsilon_0}{\omega_c}\int_0^\infty v f_0'(v)\left[\int v_i A_j(\vec{v})\,d\Omega\right]dv$$

$$-\frac{\omega_p^2 \epsilon_0}{4\pi\omega_c^2}\int_0^\infty v\omega_\nu \nu f_0'(v)\left[\frac{\int A_j(\vec{v})\,d\Omega \int\int_0^\infty v_i e^{-\Phi}\,d\varphi\,d\Omega}{\omega + i\nu S\left(\frac{1}{2l+1}\right)}\right]dv \tag{D2}$$

Now consider each component of the tensor in turn. First $\sigma_{13} = \sigma_{23} = \sigma_{31} = \sigma_{32} = 0$. Next consider σ_{33} where it can be seen that the second term vanishes, and by using an integral given in appendix E

$$\sigma_{33} = 4\pi i\omega_p^2 \epsilon_0 \int_0^\infty \frac{v^3 f_0'}{\omega_\nu}\left\{\frac{1}{3} + S\left[\frac{1}{(2l+1)(2l+3)}\right]\right\}dv \tag{D3}$$

is obtained. For σ_{12} and σ_{21} again integrals worked out in appendix E are used to find

$$\sigma_{12} = -\sigma_{21} = -\frac{4\pi\omega\epsilon_0\omega_p^2\omega_c}{k^2}\int_0^\infty \frac{v f_0' S\left(\frac{l}{2l+1}\right)}{\omega + i\nu S\left(\frac{1}{2l+1}\right)}dv \tag{D4}$$

For σ_{22},

$$\sigma_{22} = 4\pi i\omega_p^2\epsilon_0 \int_0^\infty \frac{v^3 f_0'}{\omega_\nu}\left\{\frac{1}{3} + S\left[\frac{1}{(2l+1)(2l+3)}\right]\right.$$

$$\left. + \left(\frac{\omega_c}{kv}\right)^2\left[S\left(\frac{l^2}{2l+1}\right) - \frac{i\nu S^2\left(\frac{l}{2l+1}\right)}{\omega + i\nu S\left(\frac{1}{2l+1}\right)}\right]\right\} dv \qquad \text{(D5)}$$

Finally, for σ_{11},

$$\sigma_{11} = \frac{4\pi i\omega_p^2\epsilon_0}{k^2}\int_0^\infty \frac{vf_0'}{\omega_\nu}\left[\frac{1}{3}\left(\frac{kv}{\omega_c}\right)^2 + \left(\frac{kv}{\omega_c}\right)^2 S\left(\frac{1}{2l+3}\right)\right.$$

$$\left. + S\left(\frac{l^2}{2l+1}\right) - \frac{i\nu\eta^2 S^2\left(\frac{1}{2l+1}\right)}{\omega + i\nu S\left(\frac{1}{2l+1}\right)}\right] dv \qquad \text{(D6)}$$

but after rearranging one can obtain

$$\sigma_{11} = \frac{i\omega\epsilon_0 4\pi\omega_p^2}{k^2}\int_0^\infty \frac{vf_0'\omega_\nu S\left(\frac{1}{2l+1}\right)}{\omega + i\nu S\left(\frac{1}{2l+1}\right)} dv \qquad \text{(D7)}$$

The algebra necessary to derive these equations is quite extensive but generally straightforward. One can show the equality of equations (D6) and (D7) most easily by subtracting the two and showing that zero is obtained. At one point it is helpful to make use of the identity

$$\overline{D} \cdot (\vec{k} \cdot \overline{L}) \equiv \overline{L} \cdot \vec{k} \qquad \text{(D8)}$$

This equation can easily be proved by using equations (29) and (30) for the tensors and showing that both sides yield the same result.

APPENDIX E

THE EVALUATION OF SEVERAL PERTINENT INTEGRALS

In this appendix several integrals used in appendixes D and F are evaluated and the rest are stated without proof as they are all done in a similar manner.

Consider first the integral

$$I_1 = \int e^{-\Phi(\varphi,\vec{v})} d\Omega \tag{E1}$$

where

$$\Phi(\varphi,\vec{v}) = i\eta\varphi - \frac{\vec{k} \cdot \overline{L} \cdot \vec{v}}{\omega_c}$$

and

$$\eta = \frac{\omega_\nu}{\omega_c}$$

Let $\vec{F} = \frac{\vec{k} \cdot \overline{L}}{\omega_c}$ and rewrite equation (E1) to obtain

$$I_1 = e^{-i\eta\varphi} \int e^{i\vec{F} \cdot \vec{v}} d\Omega \tag{E2}$$

This integral is easily evaluated and yields

$$I_1 = \int e^{-\Phi(\varphi,\vec{v})} d\Omega = e^{-i\eta\varphi} 4\pi j_0(Fv) \tag{E3}$$

where $j_0(Fv)$ is a spherical Bessel function of the first kind given in terms of the ordinary Bessel function of the first kind by

$$j_n(z) = \sqrt{\frac{\pi}{2z}} J_{n+\frac{1}{2}}(z)$$

Next consider the integral

$$I_2 = \int \vec{v}\, e^{-\Phi(\varphi,\vec{v})} d\Omega \tag{E4}$$

which can be written as

$$I_2 = -i \frac{\partial}{\partial \vec{F}} \int e^{-\Phi(\varphi,\vec{v})}\, d\Omega = -i \frac{\partial}{\partial \vec{F}} I_1 \tag{E5}$$

Then the following equation is easily obtained:

$$I_2 = \int \vec{v} e^{-\Phi(\varphi,\vec{v})}\, d\Omega = 4\pi v i e^{-i\eta\varphi} j_1(Fv) \frac{\vec{F}}{F} \tag{E6}$$

In a similar manner, it can be shown that

$$\int v_j v_l e^{-\Phi(\varphi,\vec{v})}\, d\Omega = 4\pi e^{-i\eta\varphi} \left[\delta_{l,j} \frac{v j_1(Fv)}{F} - \frac{F_l F_j}{F^2} v^2 j_2(Fv) \right] \tag{E7}$$

Now investigate integrals of the type

$$\int_0^\infty e^{-i\eta\varphi} F(\varphi) d\varphi \tag{E8}$$

In all the integrals of this type needed in appendixes D and F, it is possible to expand the $F(\varphi)$ in powers of $\sin(\varphi/2)$ and then to evaluate the integral in terms of a series. To demonstrate, consider

$$I_3 = \int \int_0^\infty e^{-\Phi(\varphi,\vec{v})}\, d\varphi\, d\Omega \tag{E9}$$

After using equation (E3), equation (E9) becomes

$$I_3 = \int_0^\infty e^{-i\eta\varphi} 4\pi j_0(Fv) d\varphi \tag{E10}$$

But for the case being considered, that is, $\vec{k} = k\hat{e}_1$, one can show $F = \left(2k/\omega_c\right)\sin(\varphi/2)$. After expanding $j_0(Fv)$ in its series representation, equation (E10) becomes

$$I_3 = 4\pi \sum_{l=0}^{\infty} \frac{(-)^l}{(2l+1)!} \left(\frac{2kv}{\omega_c}\right)^{2l} \left(\int_0^\infty e^{-i\eta\varphi} \sin^{2l} \frac{\varphi}{2}\, d\varphi \right) \tag{E11}$$

The integrals in equation (E11) are Laplace transforms and were evaluated by Bateman (ref. 52). Using his results yields

$$I_3 = \int \int_0^{\infty} e^{-\Phi(\varphi,\vec{v})}\, d\varphi\, d\Omega = \frac{4\pi\omega_c}{i\omega_\nu}\left[1 + S\left(\frac{1}{2l+1}\right)\right] \tag{E12}$$

where, for convenience, the symbolic notation

$$S(a_l) = \sum_{l=1}^{\infty} \frac{(kv/\omega_c)^{2l} a_l}{(\eta^2 - 1)\ldots(\eta^2 - l^2)} \tag{E13}$$

has been used where

$$\eta = \frac{\omega - i\nu(v)}{\omega_c}$$

The remaining integrals are solved in a similar manner; therefore, they will be given here without proof. The list of integrals follows:

$$\int e^{-\Phi}\, d\Omega = 4\pi j_0(Fv) e^{-i\eta\varphi} \tag{E14}$$

$$\int \vec{v} e^{-\Phi}\, d\Omega = 4\pi i v j_1(Fv) e^{-i\eta\varphi}\, \frac{\vec{F}}{F} \tag{E15}$$

$$\int v_j v_l e^{-\Phi}\, d\Omega = 4\pi\left[\delta_{l,j} v\, \frac{j_1(Fv)}{F} - \frac{F_l F_j}{F^2} v^2 j_2(Fv)\right] e^{-i\eta\varphi} \tag{E16}$$

$$\int \int_0^{\infty} e^{-\Phi}\, d\varphi\, d\Omega = \frac{4\pi\omega_c}{i\omega_\nu}\left[1 + S\left(\frac{1}{2l+1}\right)\right] \tag{E17}$$

$$\int_0^{\infty} e^{-i\eta\varphi} \cos\frac{\varphi}{2}\, j_1(Fv)\, d\varphi = -\frac{\omega_c}{kv}\, S\left(\frac{1}{2l+1}\right) \tag{E18}$$

$$\int_0^{\infty} e^{-i\eta\varphi} \sin\frac{\varphi}{2}\, j_1(Fv)\, d\varphi = -\frac{1}{i\eta}\frac{\omega_c}{kv}\, S\left(\frac{l}{2l+1}\right) \tag{E19}$$

$$\int_0^{\infty} e^{-i\eta\varphi}\, \frac{j_1(Fv)}{F}\, d\varphi = \frac{v}{i\eta}\left\{\frac{1}{3} + S\left[\frac{1}{(2l+1)(2l+3)}\right]\right\} \tag{E20}$$

$$\int_0^{\infty} e^{-i\eta\varphi} j_2(Fv)\, d\varphi = -\frac{1}{i\eta}\, S\left[\frac{2l}{(2l+1)(2l+3)}\right] \tag{E21}$$

$$\int_0^\infty e^{-i\eta\varphi} \sin^2\frac{\varphi}{2}\, j_2(Fv)\,d\varphi = \frac{1}{i\eta}\left(\frac{\omega_c}{kv}\right)^2 S\left[\frac{l(l-1)}{2l+1}\right] \tag{E22}$$

$$\int_0^\infty e^{-i\eta\varphi} \sin\frac{\varphi}{2}\cos\frac{\varphi}{2}\, j_2(Fv)\,d\varphi = \left(\frac{\omega_c}{kv}\right)^2 S\left(\frac{l-1}{2l+1}\right) \tag{E23}$$

$$\int_0^\infty e^{-i\eta\varphi} \cos^2\frac{\varphi}{2}\, j_2(Fv)\,d\varphi = -\frac{1}{i\eta}\left\{S\left[\frac{2l}{(2l+1)(2l+3)}\right] + \left(\frac{\omega_c}{kv}\right)^2 S\left[\frac{l(l-1)}{2l+1}\right]\right\} \tag{E24}$$

$$\int_0^\infty e^{-i\eta\varphi} \frac{\cos\varphi}{F}\, j_1(Fv)\,d\varphi = \frac{v}{i\eta}\left\{\frac{1}{3} + S\left[\frac{1}{(2l+1)(2l+3)}\right] + \left(\frac{\omega_c}{kv}\right)^2 S\left(\frac{l}{2l+1}\right)\right\} \tag{E25}$$

APPENDIX F

COLLISIONAL CYCLOTRON DISPERSION RELATION FROM ELECTROSTATIC APPROXIMATION

In appendix C it is shown that for waves that are nearly longitudinal, the electrostatic approximation yields the dispersion relation

$$D(\omega,k) = 1 + \frac{\pi_{11}}{\epsilon_0} = 0 \tag{F1}$$

where

$$\rho = -en \int \hat{f}_1(\vec{v}) d^3v = i\vec{k} \cdot \bar{\pi} \cdot \vec{E} \tag{F2}$$

From equation (26), an equation for the first-order distribution function $\hat{f}_1$ is obtained which when used in equation (F2) yields

$$\rho = -\frac{\omega_p^2 \epsilon_0}{\omega_c} \int \frac{\int_0^\infty e^{-\Phi(\varphi,\vec{v})} \vec{E}_1 \cdot \bar{D} \cdot \vec{v} \frac{f_0'}{v} d\varphi}{1 - \frac{\nu}{4\pi\omega_c} \int\int_0^\infty e^{-\Phi(\varphi,\vec{v}')} d\varphi \, d\Omega'} d^3v \tag{F3}$$

Recalling that $\vec{B} = B\hat{e}_3$ and $\vec{k} = k\hat{e}_1$ and using the integrals given in appendix E results in

$$\pi_{11} = 4\pi\epsilon_0 \left(\frac{\omega_p}{k}\right)^2 \int_0^\infty \frac{v f_0' G(v)(\omega - i\nu)}{\omega + i\nu G(v)} dv \tag{F4}$$

where

$$G(v) = \sum_{l=1}^{\infty} \frac{(kv/\omega_c)^{2l}}{(2l+1)(\eta^2 - 1) \ldots (\eta^2 - l^2)}$$

and

$$\eta = \frac{\omega_\nu}{\omega_c}$$

Substituting equation (F4) into equation (F1) yields

$$D(\omega,k) = 1 + 4\pi\left(\frac{\omega_p}{k}\right)^2 \int_0^\infty \frac{v f_0' G(v)\omega_\nu}{\omega + i\nu G(v)}\, dv \tag{F5}$$

and the dispersion relation given in equation (51) has been found but in a much simpler manner. The more complicated derivation was used earlier to show how the electrostatic dispersion relation could be obtained from the more complete theory.

APPENDIX G

QUADRATURE RULE FOR WEIGHT FUNCTION $\exp(-x^2)$ ON $[0,\infty]$

In several of the dispersion relations solved in this report, it was necessary to evaluate integrals numerically. These integrals were all of the form

$$\int_0^\infty e^{-x^2} f(x)\,dx \tag{G1}$$

and were performed by a Gauss quadrature rule. This rule enables us to write

$$\int_0^\infty e^{-x^2} f(x)\,dx \approx \frac{\sqrt{\pi}}{2} \sum_{l=1}^{N} w_l f(x_l) \tag{G2}$$

It is easily shown that if w_l and x_l have been chosen correctly, this equation is exact if $f(x)$ is a polynomial of order less than $2N$. From Gallant (ref. 53) and Wilensky (ref. 18) the weights w_l and the nodes x_l are used for $N = 20$ and 40. These values are given in table II.

TABLE II.- WEIGHTS AND NODES FOR THE QUADRATURE RULE USING THE WEIGHT FUNCTION $\frac{2}{\sqrt{\pi}} \exp(-x^2)$ ON $[0,\infty]$

(a) 20-point rule

x_l	w_l
0.1427950969991826E-01	0.4126248095354063E-01
0.7463130039219270E-01	0.9401377007261654E-01
0.18086156305803 97E 00	0.1398673127403206E 00
0.3294333560642905E 00	0.1704175033159441E 00
0.5160505430615322E 00	0.1764948260002838E 00
0.7362554575808914E 00	0.1545791839772282E 00
0.9858735750375285E 00	0.1123067291104619E 00
0.1261289016102767E 01	0.6604828742706440E-01
0.1559579645209661E 01	0.3061944925866195E-01
0.1878561919302981E 01	0.1088291653324355E-01
0.2216794165387664E 01	0.2879302149689494E-02
0.2573577820826277E 01	0.5488989148150679E-03
0.2948989746787235E 01	0.7261283758335416E-04
0.3343981379861640E 01	0.6366757009378284E-05
0.3760599932910770E 01	0.3487635540692594E-06
0.4202442600421132E 01	0.1100893097830079E-07
0.4675608847794480E 01	0.1778423417441857E-09
0.5190901686974998E 01	0.1214074765543346E-11
0.5769851655677 62E 01	0.2448428821057576E-14
0.6470558387064574E 01	0.5993073454594019E-18

TABLE II.- WEIGHTS AND NODES FOR THE QUADRATURE RULE USING THE WEIGHT FUNCTION $\frac{2}{\sqrt{\pi}} \exp\left(-x^2\right)$ ON $[0,\infty]$ - Concluded

(b) 40-point rule

x_l	w_l
0.5150010356393314E-02	0.1490554725118071E-01
0.2707802494829413E-01	0.3452733473086753E-01
0.6629858021142996E-01	0.5365120033130722E-01
0.1224396015988346E 00	0.7162848482763389E-01
0.1949786809306882E 00	0.8748201803249430E-01
0.2832755895057396E 00	0.9990783959338579E-01
0.3866018422176653E 00	0.1074557174139692E 00
0.5041705134328489E 00	0.1088800688850989E 00
0.6351645938060005E 00	0.1035938920774140E 00
0.7787623792828677E 00	0.9206274103552843E-01
0.9341589652282645E 00	0.7592560230950505E-01
0.1100583488138671E 01	0.5769699113930270E-01
0.1277312213015507E 01	0.4009918101795804E-01
0.1463677876957118E 01	0.2529440279616882E-01
0.1659075877002548E 01	0.1437098784698673E-01
0.1862967959865027E 01	0.7297696263942531E-02
0.2074884066030345E 01	0.3286876449615393E-02
0.2294422931706635E 01	0.1302941977664821E-02
0.2521251984268593E 01	0.4510407826591482E-03
0.2755106998376953E 01	0.1352649280556334E-03
0.2995791923381212E 01	0.3485330737193931E-04
0.3243179256519709E 01	0.7649469079803097E-05
0.3497211327571455E 01	0.1416940072635054E-05
0.3757902886114078E 01	0.2193302752467988E-06
0.4025345452403971E 01	0.2806496911831388E-07
0.4299714023322116E 01	0.2933096982986261E-08
0.4581276943399332E 01	0.2470041550273338E-09
0.4870410105599751E 01	0.1650361609485315E-10
0.5167617222469367E 01	0.8593168390112723E-12
0.5473558861103993E 01	0.3413713673581817E-13
0.5789094560417860E 01	0.1008670314083280E-14
0.6115345232898952E 01	0.2148684677740992E-16
0.6453788427291654E 01	0.3173178811113663E-18
0.6806409661424949E 01	0.3088596815526213E-20
0.7175955680231676E 01	0.1851864065560540E-22
0.7566388429073037E 01	0.6221943052492195E-25
0.7983778287554144E 01	0.1017307376257966E-27
0.8438311541355173E 01	0.6430445279019888E-31
0.8949841355010714E 01	0.1017466944507922E-34
0.9570481178890405E 01	0.1349404569685499E-39

APPENDIX H

ASYMPTOTIC EXPANSION OF G(v)

It has been pointed out that one can write

$$G(v) = -1 + {}_2F_3\left[1,\ 1/2;\ 3/2,\ 1 - \eta,\ 1 + \eta;\ -\left(\frac{kv}{\omega_c}\right)^2\right] \tag{H1}$$

Meijer (ref. 31) gives the theory of the asymptotic expansion of the generalized hypergeometric series ${}_pF_q$, and after specializing his results to the ${}_2F_3$ in equation (H1), one obtains

$$G(v) = \frac{\eta\sqrt{\pi}}{2p^{3/2}\sin \eta\pi}\left[A \cos\left(2p - \frac{3\pi}{4}\right) + B \sin\left(2p - \frac{3\pi}{4}\right)\right]$$

$$+ \left(\frac{\eta}{p}\right)^2 \sum_{l=0}^{\infty} \frac{\left(\eta^2 - 1\right) \ldots \left(\eta^2 - l^2\right)}{(2l + 1)p^{2l}} + \frac{\eta\pi}{2p} \cot \pi\eta - 1 \tag{H2}$$

where

$$p = \frac{kv}{\omega_c} \tag{H3}$$

$$\eta = \frac{\omega - i\nu(v)}{\omega_c} \tag{H4}$$

$$A = 1 - \frac{h_2}{p^2} + \frac{h_4}{p^4} - \frac{h_6}{p^6} + \frac{h_8}{p^8} + \ldots \tag{H5}$$

$$B = \frac{h_1}{p} - \frac{h_3}{p^3} + \frac{h_5}{p^5} - \frac{h_7}{p^7} + \ldots \tag{H6}$$

The h terms are given by the recurrence relation

$$h_\alpha = \frac{1}{1 - \alpha} \sum_{l=1}^{\alpha-1} \frac{(-1)^l V_l h_{\alpha-l}}{l + 1} \tag{H7}$$

where

$$h_1 = 1 \tag{H8}$$

$$V_l = -\frac{l+1}{2^l} - (l+1)\eta^l - 2H_l B_{l+1}(\eta) + B_{l+1}\left(\frac{l}{2} + \frac{3}{4}\right) + B_{l+1}\left(\frac{l}{2} + \frac{5}{4}\right) \tag{H9}$$

$$H_l = \begin{cases} 1 & (l \text{ odd}) \\ 0 & (l \text{ even}) \end{cases} \tag{H10}$$

and $B_l(x)$ are the Bernoulli polynomials.

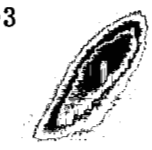

APPENDIX I

NUMERICAL CONTOUR INTEGRATION

Let us consider the contour integral of some function F

$$I = \int_c F(z)e^{-z^2}\,dz \tag{I1}$$

with the contour given by

$$z = x\left(1 + \frac{2i\gamma x_m^2}{x_m^2 + x^2}\right) \tag{I2}$$

where

$$\left.\begin{aligned} \gamma &= \frac{y_m}{x_m} \\ 0 &\leq x < \infty \end{aligned}\right\} \tag{I3}$$

Note that x is real, and one can easily show that $\text{Max}\left[\text{Im}(z)\right] = y_m$ at $x = x_m$. A plot of this contour is shown in figure 28. Substituting equation (I2) into equation (I1) yields

$$\begin{aligned} I &= \int_c F(z)e^{-z^2}\,dz \\ &= \int_0^\infty F\left[x\left(1 + \frac{2i\gamma x_m^2}{x_m^2 + x^2}\right)\right]e^{-x^2} \cdot \exp\left[\frac{4\gamma x^2 x_m^2}{x^2 + x_m^2}\left(-i + \frac{\gamma x_m^2}{x^2 + x_m^2}\right)\right]\left[1 + \frac{2i\gamma x_m^2\left(x_m^2 - x^2\right)}{\left(x_m^2 + x^2\right)^2}\right]dx \end{aligned} \tag{I4}$$

From appendix G, the Gauss quadrature rule is

$$\int_0^\infty f(x)e^{-x^2}\,dx = \frac{\sqrt{\pi}}{2}\sum_{l=1}^{N} w_l f\left(x_l\right) \tag{I5}$$

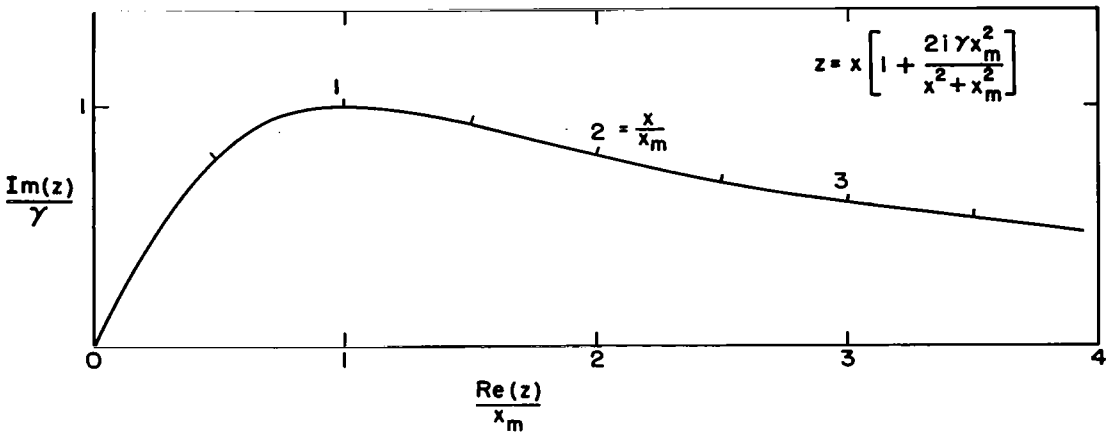

Figure 28.- Normalized mapping of contour in complex z plane. Note that Re(z) = x.

and applying this rule to equation (I4) yields

$$\int_c F(z)e^{-z^2}\,dz = \frac{\sqrt{\pi}}{2}\sum_{l=1}^{N} w_l' F(z_l) \tag{I6}$$

where

$$z_l = x_l\left(1 + \frac{2i\gamma x_m^2}{x_m^2 + x_l^2}\right) \tag{I7}$$

$$w_l' = w_l\left[1 + \frac{2i\gamma x_m^2\left(x_m^2 - x_l^2\right)}{\left(x_m^2 + x_l^2\right)^2}\right]\exp\left[\frac{4\gamma x_l^2 x_m^2}{x_m^2 + x_l^2}\left(-i + \frac{\gamma x_m^2}{x_m^2 + x_l^2}\right)\right] \tag{I8}$$

By using the technique described, it is possible to do very accurate numerical contour integration by means of the Gauss quadrature rule. Note that no rapidly oscillating terms are introduced in the integrand of equation (I4). For best results it was found that γ should be kept small, for example, $\gamma < 0.5$.

APPENDIX J

DERIVATION OF TRANSFER COLLISION CROSS SECTION $Q_\ell(v)$

From the definition,

$$Q_{\ell m}(v) = \int \sigma(v,\chi)\left[1 - \frac{Y_{\ell m}(\theta',\varphi')}{Y_{\ell m}(\theta,\varphi)}\right]d\Omega' \tag{J1}$$

and use of the Legendre polynomial expansion

$$\sigma(v,\chi) = \sum_{n=0}^{\infty} \sigma_n(v)\, P_n(\cos\chi) \tag{J2}$$

yields

$$Q_{\ell m} = \sum_{n} \sigma_n(v) \int P_n(\cos\chi)\left[1 - \frac{Y_{\ell m}(\theta',\varphi')}{Y_{\ell m}(\theta,\varphi)}\right]d\Omega' \tag{J3}$$

From figure 29 it can be seen that

$$\cos\chi = \cos\theta' \cos\theta + \sin\theta' \sin\theta \cos(\varphi' - \varphi) \tag{J4}$$

which allows the use of the addition formula

$$P_n(\cos\chi) = \sum_{k=-n}^{n} (-)^k P_n^k(\cos\theta')\, P_n^{-k}(\cos\theta)\, e^{im(\varphi'-\varphi)} \tag{J5}$$

Then evaluate the integrals in equation (J3) and obtain

$$Q_{\ell m} = 4\pi\left(\sigma_0 - \frac{\sigma_\ell}{2\ell + 1}\right) \tag{J6}$$

This equation is identical to that obtained from substituting equation (J2) into Allis' transfer collision cross section

$$Q_\ell(v) = 2\pi \int_0^{\pi} \sigma(\chi,v)\left[1 - P_\ell(\cos\chi)\right]\sin\chi\, d\chi \tag{J7}$$

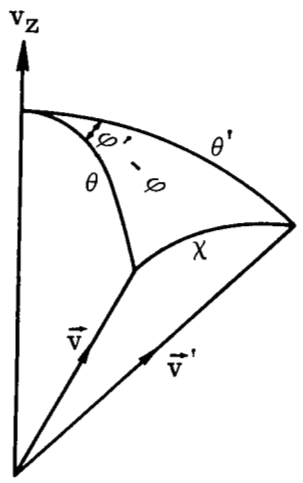

Figure 29.- Geometry of collision velocities $\vec{v}$ and $\vec{v}'$ before and after impact, respectively.

Thus it is concluded that

$$Q_{l\,m}(v) = Q_l(v) \tag{J8}$$

for all m as claimed in the text.

APPENDIX K

CONDUCTIVITY TENSOR FOR $\vec{k} \parallel \vec{B}$ WITH ISOTROPIC SCATTERING

In this appendix the conductivity tensor from equation (34) will be obtained for the case of propagation parallel to the magnetic field. By taking $\vec{k} \parallel \vec{B}$, that is, $\vec{k} = k\hat{e}_3$, equation (38) yields

$$\Phi(\varphi,\vec{v}) = i\,\frac{\omega_\nu - kv_3}{\omega_c}\,\varphi \tag{K1}$$

Substituting equation (K1) into equation (34) yields

$$\sigma_{13} = \sigma_{23} = \sigma_{31} = \sigma_{32} = 0 \tag{K2}$$

$$\sigma_{11} = \sigma_{22} = -\frac{\omega_p^2 \epsilon_0}{\omega_c} \int \frac{f_0' v_1^2}{v} \left(\int_0^\infty e^{-\Phi} \cos\varphi \, d\varphi \right) d^3v \tag{K3}$$

$$\sigma_{12} = -\sigma_{21} = \frac{\omega_p^2 \epsilon_0}{\omega_c} \int \frac{f_0' v_2^2}{v} \left(\int_0^\infty e^{-\Phi} \sin\varphi \, d\varphi \right) d^3v \tag{K4}$$

$$\sigma_{33} = -\frac{\omega_p^2 \epsilon_0}{\omega_c} \int_0^\infty v f_0'(v) \left\{ \int v_3^2 \int_0^\infty e^{-\Phi(\varphi,\vec{v})} \, d\varphi \, d\Omega \right.$$

$$\left. + \frac{\nu}{4\pi\omega_c} \frac{\left[\int \int_0^\infty e^{-\Phi(\varphi,\vec{v})} v_3 \, d\varphi \, d\Omega \right]^2}{1 - \frac{\nu}{4\pi\omega_c} \int \int_0^\infty e^{-\Phi(\varphi,\vec{v}')} \, d\varphi \, d\Omega'} \right\} dv \tag{K5}$$

Upon evaluating the integrals in equations (K3) to (K5), one finds

$$\sigma_{11} = \sigma_{22} = -i\omega_p^2 \epsilon_0 \int \frac{f_0' v_1^2}{v} \frac{\omega_\nu - kv_3}{\omega_c^2 - (\omega_\nu - kv_3)^2} \, d^3v \tag{K6}$$

$$\sigma_{12} = -\sigma_{21} = \omega_p^2 \epsilon_0 \int \frac{f_0' v_1^2}{v} \frac{\omega_c}{\omega_c^2 - (\omega_\nu - k v_3)^2} d^3v \tag{K7}$$

$$\sigma_{33} = -\frac{4\pi i \omega_p^2 \epsilon_0 \omega}{k^2} \int_0^\infty v f_0' \frac{1 - \lambda \coth^{-1}\lambda}{1 + \frac{i\nu}{kv} \coth^{-1}\lambda} dv \tag{K8}$$

where

$$\lambda = \frac{\omega_\nu}{kv}$$

The angular part of the integrals in equations (K6) and (K7) can be easily evaluated but will not be needed at this time.

APPENDIX L

PROOF THAT THE ANISOTROPIC DISPERSION RELATION YIELDS THE ISOTROPIC DISPERSION RELATION IN THE LIMIT OF ISOTROPIC SCATTERING

In this appendix the dispersion relation expressed by equation (108) is reduced to the one in equation (116) in the limit of isotropic collisions. For isotropic collisions, that is, $\sigma = \sigma(v)$, it can be seen from equation (88) that all the ν_l terms are equal. Hence let $\nu_l = \nu(v)$ for all l and equation (108) then yields

$$D_{\bullet}(\omega,k) = 1 - \left(\frac{ck}{\omega}\right)^2 + \frac{2\pi\omega_p^2}{\omega k}\int_0^{\infty} g_{\pm}(v)\, v^2 f_0'(v)\, dv \tag{L1}$$

where

$$g_{\pm} = \frac{2}{3\lambda_{\pm}} - \frac{3}{5\lambda_{\pm}} - \frac{8}{7\lambda_{\pm}} - \cdots - \frac{n^2 - 1}{(2n+1)\lambda_{\pm}} - \cdots$$

and

$$\lambda_{\pm} \equiv \frac{\omega_{\nu} \pm \omega_c}{kv}$$

Take now the part of the integrand in brackets in equation (116) and expand it in a series in powers of $\lambda_{\pm}^{-1}$ to obtain

$$\lambda_{\pm} + \left(1 - \lambda_{\pm}^2\right)\coth^{-1}\lambda_{\pm} = \frac{2}{\lambda_{\pm}}\left[\frac{1}{3} + \frac{\lambda_{\pm}^{-2}}{3\cdot 5} + \frac{\lambda_{\pm}^{-4}}{5\cdot 7} + \cdots + \frac{\lambda_{\pm}^{-2n}}{(2n+1)(2n+3)} + \cdots\right] \tag{L2}$$

Convert this asymptotic series into a continued fraction by the method of Viskovatoff as described by Khovanskii (ref. 43) to obtain

$$\lambda_{\pm} + \left(1 - \lambda_{\pm}^2\right)\coth^{-1}\lambda_{\pm} = \frac{2}{3\lambda_{\pm}} - \frac{3}{5\lambda_{\pm}} - \frac{8}{7\lambda_{\pm}} - \cdots - \frac{n^2 - 1}{(2n+1)\lambda_{\pm}} - \cdots \tag{L3}$$

Hence equation (116) yields an equation identical with equation (L1). It has therefore been shown that equations (108) and (116) are identical in the limit of isotropic collisions.

APPENDIX M

SIMPLE DERIVATION OF DISPERSION RELATION FOR WAVES WITH $\vec{k} \parallel \vec{B}$

In this appendix the dispersion relation for propagation parallel to the magnetic field is derived in a simpler but less rigorous manner (ref. 45) than was used earlier. The assumption is made that the waves are transverse in the course of the derivation; therefore, only the dispersion relation for the transverse electric waves is obtained. For isotropic collisions in a Lorentz gas, the Boltzmann equation is written as

$$\frac{\partial f}{\partial t} + \vec{v} \cdot \frac{\partial f}{\partial \vec{r}} - \frac{e}{m}\left(\vec{E} + \vec{v} \times \vec{B}\right) \cdot \frac{\partial f}{\partial \vec{v}} = -\nu f + \frac{\nu}{4\pi} \int f(\vec{v}')\, d\Omega' \tag{M1}$$

The ansatz is made

$$\left.\begin{aligned} f(\vec{v}) &= f_0(\vec{v}) + f_1(\vec{v}) \\ \vec{E} &= 0 + \vec{E}_1 \\ \vec{B} &= \vec{B}_0 + \vec{B}_1 \end{aligned}\right\} \tag{M2}$$

and the zero- and first-order equations for f_0 and f_1 are obtained. The zero-order equation has as its solution any isotropic $f_0\left(|\vec{v}|\right)$ (appendix A), and the first-order equation is solved by means of Fourier and Laplace transforms in space and time based on the wave representation $\exp(i\omega t - i\vec{k} \cdot \vec{r})$. Taking $\vec{B}_0 = B_0 \hat{e}_3$ and writing the first-order equation in spherical coordinates then yields

$$i\left(\omega_\nu - kv \cos\theta\right)\hat{f}_1 + \omega_c \frac{\partial \hat{f}_1}{\partial \varphi} = \frac{\nu(v)}{4\pi} \int \hat{f}_1(\vec{v}')\, d\Omega' + \frac{e}{m} \vec{E}_1 \cdot \frac{\partial f_0}{\partial \vec{v}} \tag{M3}$$

Expanding the dot product in component form results in

$$\vec{E}_1 \cdot \frac{\partial f_0}{\partial \vec{v}} = \frac{f_0' \sin\theta}{2}\left(e^{i\varphi} E_- + e^{-i\varphi} E_+\right) \tag{M4}$$

where $E_\pm = E_x \pm iE_y$ are the fields of the right- and left-hand polarized waves, respectively. Now the solution

$$f_1 = f_-\, e^{i\varphi} + f_+\, e^{-i\varphi} \tag{M5}$$

is assumed and from equation (M3)

$$f_{\pm} = -\frac{ie}{2m}\frac{E_{\pm}f_0' \sin\theta}{\omega_\nu \mp \omega_c - kv\cos\theta} \tag{M6}$$

is easily obtained. From Maxwell's equations of electrodynamics, the current density is

$$\vec{j} = -en\int \vec{v}\,\hat{f}_1\,d^3v = \left[\left(\frac{ck}{\omega}\right)^2 - 1\right]i\omega\epsilon_0\vec{E}_1 \tag{M7}$$

which yields

$$j_{\pm} = -2\pi\, en\int v^3 \sin^2\theta f_{\pm}\,d\theta\,dv = \left[\left(\frac{ck}{\omega}\right)^2 - 1\right]i\omega\epsilon_0 E_{\pm} \tag{M8}$$

Then, substituting equation (M6) into equation (M8) yields

$$\frac{\pi ine^2 E_{\pm}}{m}\int_0^{\infty}\int_0^{\pi}\frac{v^3\sin^3\theta f_0'\,d\theta\,dv}{\omega_\nu \mp \omega_c - kv\cos\theta} = \left[\left(\frac{ck}{\omega}\right)^2 - 1\right]i\omega\epsilon_0 E_{\pm} \tag{M9}$$

Equation (M9) then gives the dispersion relation

$$D_{\pm}(\omega,k) = 1 - \left(\frac{ck}{\omega}\right)^2 + \frac{\pi\omega_p^2}{\omega}\int_0^{\infty}\int_0^{\pi}\frac{v^3\sin^3\theta f_0'}{\omega_\nu \pm \omega_c - kv\cos\theta}\,d\theta\,dv = 0 \tag{M10}$$

where

$$\omega_p^2 = \frac{ne^2}{m\epsilon_0}$$

Evaluating the integral over θ then yields

$$D_{\pm}(\omega,k) = 1 - \left(\frac{ck}{\omega}\right)^2 + \frac{2\pi\omega_p^2}{\omega k}\int_0^{\infty} v^2 f_0'\left[\lambda_{\pm} + \left(1 - \lambda_{\pm}^2\right)\coth^{-1}\lambda_{\pm}\right]dv \tag{M11}$$

where

$$\lambda_{\pm} = \frac{\omega_\nu \pm \omega_c}{kv}$$

which is the same as equation (116). This derivation demonstrates that the integral term in the Boltzmann equation (eq. (79)) does not contribute to the dispersion relation for transverse waves propagating parallel to the magnetic field. Note the integral vanishes when obtaining equation (M6). From equation (M10) it can also be seen how $D_-(\omega,k)$ and $D_+(\omega,k)$ are associated with right- and left-hand polarized waves, respectively.

APPENDIX N

REDUCTION OF EQUATION (116) TO FRIED FUNCTION REPRESENTATION IN THE APPROPRIATE LIMIT

In this appendix the Fried function representation of the dispersion relation (eq. (119)) is obtained from equation (116) under the assumption of (1) a constant collision frequency and (2) a Maxwellian electron distribution. Integrating equation (116) by parts yields

$$D_{\pm}(\omega,k) = 1 - \left(\frac{ck}{\omega}\right)^2 - \frac{4\pi\omega_p^2}{\omega k}\int_0^{\infty} vf_0 \coth^{-1}\lambda_{\pm}\, dv \tag{N1}$$

If f_0 is Maxwellian,

$$vf_0 = -\frac{v_0^2}{2} f_0' \tag{N2}$$

and the integral in equation (N1) becomes

$$I \equiv \int_0^{\infty} vf_0 \coth^{-1}\lambda_{\pm}\, dv = -\frac{v_0^2}{2}\int_0^{\infty} f_0' \coth^{-1}\lambda_{\pm}\, dv \tag{N3}$$

Doing a second integration by parts and substituting equation (75) for f_0 results in

$$I = -\frac{\lambda_0}{2\pi^{3/2} v_0}\int_0^{\infty} \frac{e^{-x^2}}{x^2 - \lambda_0^2}\, dx \tag{N4}$$

where

$$x = \frac{v}{v_0}$$

$$\lambda_0 = \frac{\omega_\nu \pm \omega_c}{kv_0}$$

The integrand is an even function; thus,

$$I = -\frac{\lambda_0}{4\pi^{3/2} v_0}\int_{-\infty}^{\infty} \frac{e^{-x^2}}{x^2 - \lambda_0^2}\, dx \tag{N5}$$

Expand equation (N5) in partial fractions to obtain

$$I = -\frac{1}{8\pi^{3/2} v_0}\left(\int_{-\infty}^{\infty} \frac{e^{-x^2}}{x - \lambda_0}\, dx - \int_{-\infty}^{\infty} \frac{e^{-x^2}}{x + \lambda_0}\, dx\right) \tag{N6}$$

Putting $x \rightarrow -x$ in the second integral yields

$$I = -\frac{1}{4\pi^{3/2} v_0} \int_{-\infty}^{\infty} \frac{e^{-x^2}}{x - \lambda_0}\, dx \tag{N7}$$

Since the dispersion relation is defined for k real and ω on a Laplace integral path, equation (N7) is the proper equation for $\mathrm{Im}(\lambda_0) < 0$. For other values of λ_0, the analytic continuation is used. Hence define

$$Z(\lambda_0) = \frac{1}{\sqrt{\pi}} \int_{-\infty}^{\infty} \frac{e^{-x^2}}{x - \lambda_0}\, dx \qquad \left(\mathrm{Im}(\lambda_0) < 0\right) \tag{N8}$$

and equation (N7) then becomes

$$I = -\frac{Z(\lambda_0)}{4\pi v_0} \tag{N9}$$

Substituting equation (N9) into equation (N1) yields

$$D_{\pm}(\omega, k) = 1 - \left(\frac{ck}{\omega}\right)^2 + \frac{\omega_p^2}{\omega k v_0} Z \frac{\omega_\nu \bullet \omega_c}{kv} \tag{N10}$$

and hence gives equation (119). Fried and Conte (ref. 35) define

$$Z_F(\xi) = \frac{1}{\sqrt{\pi}} \int_{-\infty}^{\infty} \frac{e^{-x^2}}{x - \xi}\, dx \qquad (\mathrm{Im}(\xi) > 0) \tag{N11}$$

and by using equation (N8) one can show

$$Z(\lambda_0) = Z_F^*(\lambda_0^*) \tag{N12}$$

Equation (N10) can then be written in terms of the Fried function (plasma dispersion function) if desired.

REFERENCES

1. Twiss, R. Q.: Radiation Transfer and the Possibility of Negative Absorption in Radio Astronomy. Aust. J. Phys., vol. II, no. 4, Dec. 1958, pp. 564-579.

2. Bekefi, G.; Hirshfield, Jay L.; and Brown, Sanborn C.: Kirchhoff's Radiation Law for Plasmas With Non-Maxwellian Distributions. Phys. Fluids, vol. 4, no. 2, Feb. 1961, pp. 173-176.

3. Fields, H.; Bekefi, G.; and Brown, Sanborn C.: Microwave Emission From Non-Maxwellian Plasmas. Phys. Rev., Second ser., vol. 129, no. 2, Jan. 15, 1963, pp. 506-515.

4. Oddou, C.: Collisional Cyclotron Instability in a Xenon Plasma. Quart. Progr. Rep. No. 93, Res. Lab. Electron., Massachusetts Inst. Technol., Apr. 15, 1969, pp. 93-101.

5. Tanaka, Shigetoshi; and Takayama, Kazuo: Anomalous Radio-Frequency Emission at Electron Cyclotron Frequency in Partially Ionized Plasmas. J. Phys. Soc. Jap., vol. 21, no. 11, Nov. 1966, pp. 2372-2380.

6. Tanaka, Shigetoshi; Mitani, Kenji; and Kubo, Hiroshi: Experiments on Negative Radiation Temperature at Cyclotron Resonance in Cold Plasmas. J. Phys. Soc. Jap., vol. 17, no. 11, Nov. 1962, p. 1800.

7. Idehara, Toshitaka; Sugaya, Reiji; Terumichi, Yasushi; Tanaka, Shigetoshi; and Takahashi, Isao: Negative Absorption at Harmonics of the Electron Cyclotron Frequency in Weakly Ionized Plasma. J. Phys. Soc. Jap., vol. 22, no. 2, Feb. 1967, p. 671.

8. Wachtel, J. M.; and Hirshfield, J. L.: Negative Electron Cyclotron Resonance Absorption Due to Collisions. Phys. Rev. Lett., vol. 19, no. 6, Aug. 7, 1967, pp. 293-295.

9. Oddou, C.: Anomalous Cyclotron Radiation. Quart. Progr. Rep. No. 95, Res. Lab. Electron., Massachusetts Inst. Technol., Oct. 15, 1969, pp. 57-63. (Available from DDC as AD 696 281.)

10. Reisz, A. C.; and Wright, B. L.: Radiation Temperature of Extraordinary Waves. Quart. Progr. Rep. No. 94, Res. Lab. Electron., Massachusetts Inst. Technol., July 15, 1969, pp. 122-129. (Available from DDC as AD 692 201.)

11. Tanaka, Shigetoshi; and Mitani, Kenji: Negative Absorption at the Cyclotron Frequency in Weakly Ionized Gases. J. Phys. Soc. Jap., vol. 19, no. 8, Aug. 1964, pp. 1376-1384.

12. Ďurček, J.: A Note on the Negative Absorption of Electromagnetic Waves at the Cyclotron Resonance of Plasma Electrons. Czech. J. Phys., sect. B, vol. 17, no. 11, 1967, pp. 1005-1011.

13. Drummond, J. E.; Nelson, D. J.; and Hirshfield, J. L.: Collision-Induced Instability in a Plasma With an Isotropic Velocity-Space Distribution. Comptes Rendus de la VI^{e} Conférence Internationale sur les Phénomènes d'Ionisation dans les Gaz (Paris), Vol. III, P. Hubert and E. Crêmieu-Alcan, eds., 1963, pp. 23-27.

14. Derfler, Heinrich: Electrostatic Relaxation Waves in an Isotropic Lorentz Gas. Phys. Fluids, vol. 10, no. 8, Aug. 1967, pp. 1636-1646.

15. Suzuki, Kunihiro: Linear Theory of Collision-Induced Instability of Partially Ionized Gases in External Magnetic Field. J. Phys. Soc. Jap., vol. 22, no. 6, June 1967, pp. 1454-1460.

16. Idehara, Toshitaka; and Sugaya, Reiji: Collision-Induced Instabilities Near Electron Cyclotron Harmonics in Plasma. J. Phys. Soc. Jap., vol. 23, no. 5, Nov. 1967, pp. 1122-1131.

17. Shimomura, Noboru; and Mitani, Kenji: Collision-Induced Instability at Cyclotron Harmonics. J. Phys. Soc. Jap., vol. 25, no. 5, Nov. 1968, pp. 1467-1474.

18. Wilensky, R.: Collisional Effects on Electrostatic Waves in an Isotropic Plasma. SUIPR Rep. 368, Stanford Univ., June 1970.

19. Dougherty, J. P.: Model Fokker-Planck Equation for a Plasma and Its Solution. Phys. Fluids, vol. 7, no. 11, Nov. 1964, pp. 1788-1799.

20. Holt, E. H.; and Haskell, R. E.: Foundations of Plasma Dynamics. Macmillan Co., c.1965, p. 257.

21. Bhatnagar, P. L.; Gross, E. P.; and Krook, M.: A Model for Collision Processes in Gases. I. Small Amplitude Processes in Charged and Neutral One-Component Systems. Phys. Rev., Second ser., vol. 94, no. 3, May 1, 1954, pp. 511-525.

22. Allis, William P.; Buchsbaum, Solomon J.; and Bers, Abraham: Waves in Anisotropic Plasmas. M.I.T. Press, 1963, p. 88.

23. Derfler, Heinrich: Growing Wave and Instability Criteria for Hot Plasmas. 8th International Conference on Phenomena in Ionized Gases, Contributed Papers, Springer-Verlag, 1967, p. 294.

24. Derfler, Heinrich: The Frequency Cusp, a New Means for Discriminating Between Growing Waves and Instabilities in Hot Plasmas. Stanford Univ. paper presented at 9th International Conference on Phenomena in Ionized Gases (Bucharest, Romania), Sept. 1969.

25. Derfler, H.; Burger, P.; and Holmstrom, F. R.: Stationary Non-Equilibrium Plasmas. Consolidated Quart. Status Rep. No. 18, Stanford Electron. Lab., Stanford Univ., 1961, pp. 17-42.

26. Derfler, Heinrich: Frequency Cusp, a Means for Discriminating Between Convective and Nonconvective Instability. Phys. Rev. A, Third ser., vol. 1, no. 5, May 1970, pp. 1467-1471.

27. Omura, Masayuki: Electrostatic Waves in Bounded Hot Plasmas. Tech. Rep. ECOM-00482-11, U.S. Army, June 1967.

28. Stix, Thomas Howard: The Theory of Plasma Waves. McGraw-Hill Book Co., Inc., c.1962.

29. Bernstein, Ira B.: Waves in a Plasma in a Magnetic Field. Phys. Rev., Second ser., vol. 109, no. 1, Jan. 1, 1958, pp. 10-21.

30. Crawford, F. W.: Cyclotron Harmonic Wave Phenomena in Plasmas. A Survey of Phenomena in Ionized Gases, International Atomic Energy Agency, 1968, pp. 109-127.

31. Meijer, C. S.: On the G-Function. Proc. Ned. Akad. Wetensch., vol. 49, 1946, pp. 344-356, 457-469, 632-641, 765-772, 936-943, 1063-1072, 1165-1175; also, Ned. Akad. Wetensch. Indagationes Math., vol. 8, 1946, pp. 213-225, 312-324, 391-400, 468-475, 595-602, 661-670, 713-723.

32. Landau, L.: On the Vibrations of the Electronic Plasma. J. Phys. (USSR), vol. X, no. 1, 1946, pp. 25-34.

33. Simonen, Thomas C.: Landau Waves. SUIPR Rep. No. 100 (Contract AF 33(615)1504), Stanford Univ., Dec. 1966.

34. Baldwin, D. E.; and Rowlands, G.: Plasma Oscillations Perpendicular to a Weak Magnetic Field. Phys. Fluids, vol. 9, no. 12, Dec. 1966, pp. 2444-2453.

35. Fried, Burton D.; and Conte, Samuel D.: The Plasma Dispersion Function. Academic Press, Inc., 1961.

36. Tataronis, J. A.: Cyclotron Harmonic Wave Propagation and Instabilities. SUIPR Rep. No. 205 (NASA Grant NGR 05-020-077 and AEC Contract AT(04-3)-326), Stanford Univ., Dec. 1967.

37. Landau, L. D., and Lifshitz, E. M.: Electrodynamics of Continuous Media. Pergamon Press, 1960, p. 259.

38. Brode, Robert B.: The Quantitative Study of the Collisions of Electrons With Atoms. Rev. Mod. Phys., vol. 5, Oct. 1933, pp. 257-279.

39. Brown, Sanborn C.: Basic Data of Plasma Physics, 1966. Second ed., M.I.T. Press, c.1967.

40. McCutchen, C. W.: Drift Velocity of Electrons in Mercury Vapor and Mercury Vapor-CO_2 Mixtures. Phys. Rev., Second ser., vol. 112, no. 6, Dec. 15, 1958, pp. 1848-1851.

41. Bekefi, G.; Hirshfield, Jay L.; and Brown, Sanforn C.: Cyclotron Emission From Plasmas With Non-Maxwellian Distributions. Phys. Rev., Second ser., vol. 122, no. 4, May 15, 1961, pp. 1037-1042.

42. Allis, W. P.: Motions of Ions and Electrons. Encyclopedia of Physics, Vol. XXI, Springer-Verlag (Berlin), 1956, pp. 383-444.

43. Khovanskii, Alexey Nikolaevitch (Peter Wynn, transl.): The Application of Continued Fractions and Their Generalizations to Problems in Approximation Theory. P. Noordhoff, Ltd. (Groningen), c.1963, p. 27.

44. Abramowitz, Milton; and Stegun, Irene A., eds.: Handbook of Mathematical Functions With Formulas, Graphs, and Mathematical Tables. Nat. Bur. Stand., Appl. Math. Ser. 55, U.S. Dep. Com., June 1964.

45. Derfler, Heinrich; and Howell, John Q.: Collisional Whistler Instabilities. Stanford Univ. paper presented at 9th International Conference on Phenomena in Ionized Gases (Bucharest, Romania), Sept. 1969.

46. Scarf, F. L.: Landau Damping and the Attenuation of Whistlers. Phys. Fluids, vol. 5, no. 1, Jan. 1962, pp. 6-13.

47. Lee, Joseph C.: Whistler Propagation and Instability Characteristics. SUIPR Rep. No. 312 (NASA Grant NGR 05-020-176), Stanford Univ., May 1969.

48. Howell, John Q.; and Derfler, Heinrich: Collisional Instabilities in a Magnetoplasma. Paper presented at 1969 Annual Meeting, Div. Plasma Phys., Amer. Phys. Soc. (Los Angeles), Nov. 1969.

49. Perkins, F. W.; Salpeter, E. E.; and Yngvesson, K. O.: Incoherent Scatter From Plasma Oscillations in the Ionosphere. Phys. Rev. Lett., vol. 14, no. 15, Apr. 12, 1965, pp. 579-581.

50. Dalgarno, A.; and Henry, R. J. W.: Electron Temperatures in the D Region. Proc. Roy. Soc. (London), ser. A., vol. 288, no. 1415, Nov. 30, 1965, pp. 521-530.

51. Derfler, Heinrich; and Simonen, Thomas C.: Higher-Order Landau Modes. Phys. Fluids, vol. 12, no. 2, Feb. 1969, pp. 269-278.

52. Staff of Bateman Manuscript Project, compiler: Tables of Integral Transforms. Vol. II. McGraw-Hill Book Co., Inc., 1954.

53. Galant, D.: Gauss Quadrature Rules for the Evaluation of $2\pi^{-\frac{1}{2}} \int_0^\infty \exp(-x^2) f(x)dx$. Math. Comput., vol. 23, July 1969, p. 674.

NASA-Langley, 1971 —— 25 L-7531

020 001 C1 U 25 710903 S00903DS
DEPT OF THE AIR FORCE
AF SYSTEMS COMMAND
AF WEAPONS LAB (WLOL)
ATTN: E LOU BOWMAN, CHIEF TECH LIBRARY
KIRTLAND AFB NM 87117

"The aeronautical and space activities of the United States shall be conducted so as to contribute . . . to the expansion of human knowledge of phenomena in the atmosphere and space. The Administration shall provide for the widest practicable and appropriate dissemination of information concerning its activities and the results thereof."

—NATIONAL AERONAUTICS AND SPACE ACT OF 1958

NASA SCIENTIFIC AND TECHNICAL PUBLICATIONS

TECHNICAL REPORTS: Scientific and technical information considered important, complete, and a lasting contribution to existing knowledge.

TECHNICAL NOTES: Information less broad in scope but nevertheless of importance as a contribution to existing knowledge.

TECHNICAL MEMORANDUMS: Information receiving limited distribution because of preliminary data, security classification, or other reasons.

CONTRACTOR REPORTS: Scientific and technical information generated under a NASA contract or grant and considered an important contribution to existing knowledge.

TECHNICAL TRANSLATIONS: Information published in a foreign language considered to merit NASA distribution in English.

SPECIAL PUBLICATIONS: Information derived from or of value to NASA activities. Publications include conference proceedings, monographs, data compilations, handbooks, sourcebooks, and special bibliographies.

TECHNOLOGY UTILIZATION PUBLICATIONS: Information on technology used by NASA that may be of particular interest in commercial and other non-aerospace applications. Publications include Tech Briefs, Technology Utilization Reports and Technology Surveys.

Details on the availability of these publications may be obtained from:

SCIENTIFIC AND TECHNICAL INFORMATION OFFICE

NATIONAL AERONAUTICS AND SPACE ADMINISTRATION

Washington, D.C. 20546